propagation of relativistic jets

Manel Perucho-Pla

Dublin Summer School on High Energy Astrophysics
Dublin, July 6th 2011

Outline of the first part
(magneto-)hydrodynamics of jets

- Introduction.
- Basic equations.
  - Relativistic (magneto-)hydrodynamics.
  - Shocks.
- Large-scale morphology and long-term evolution.
- Instabilities

Introduction

jet power

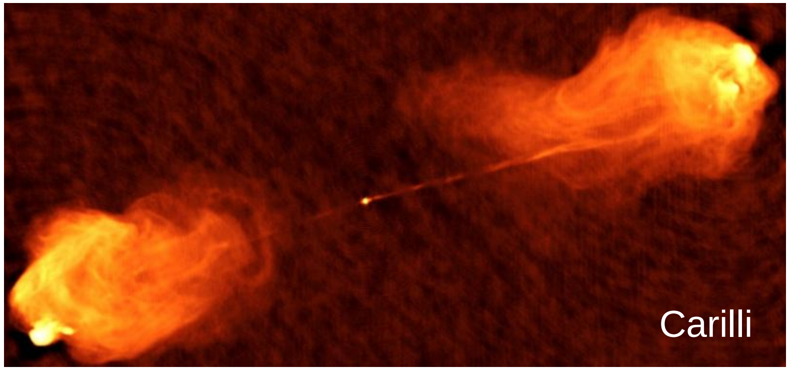

AGN

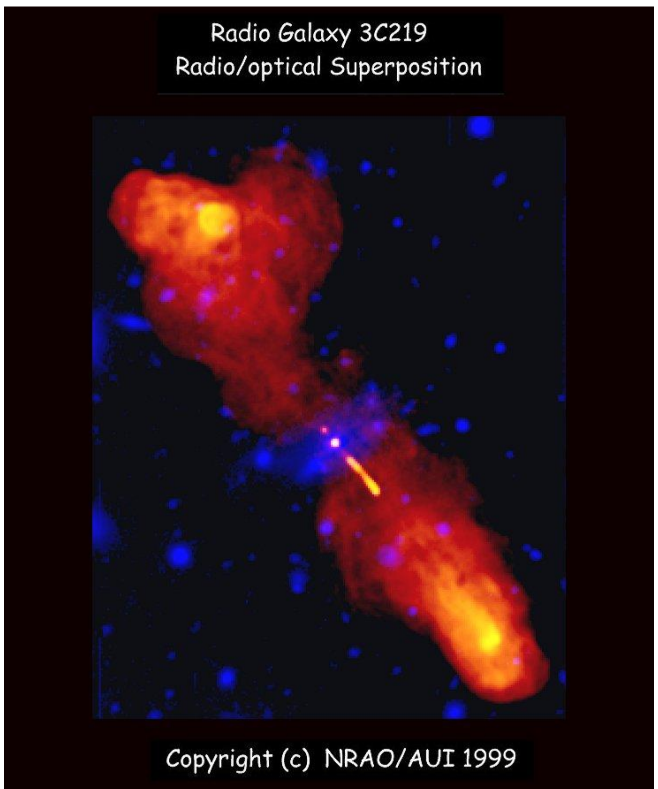

FRII

FRI

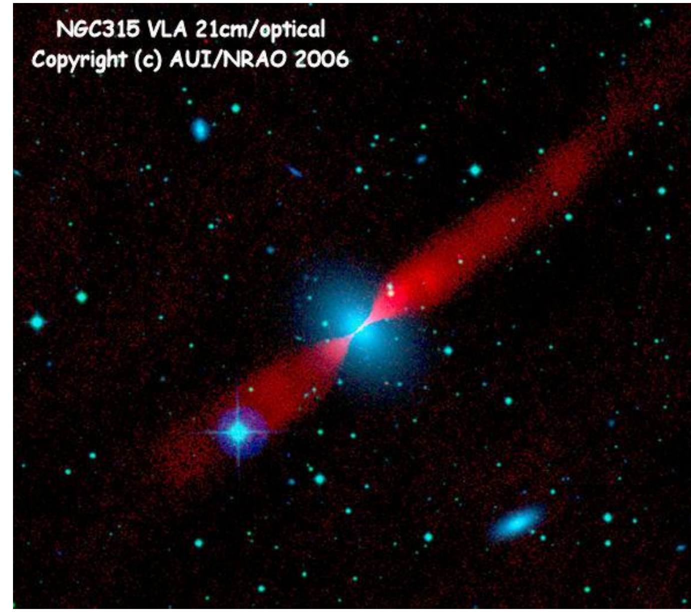

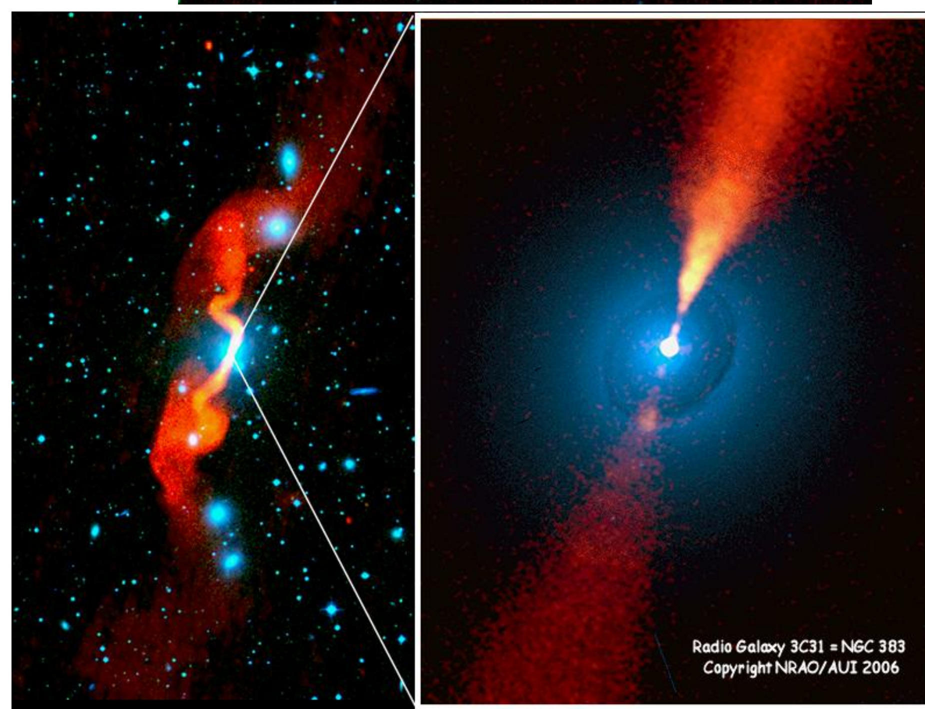

A. Bridle's gallery

Introduction

NGC 326

(Murgia et al. 2001)

Hercules A: (Dreher & Feigelson 1984)

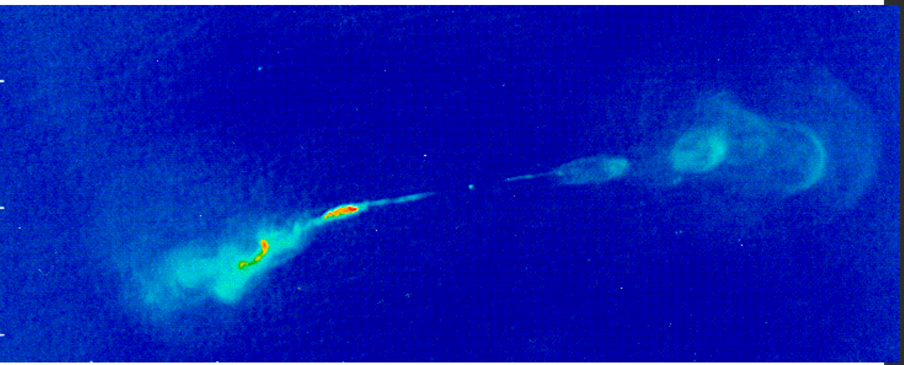

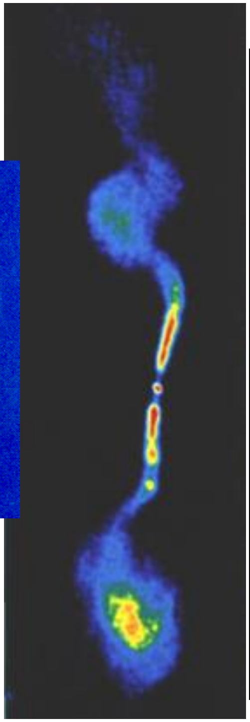

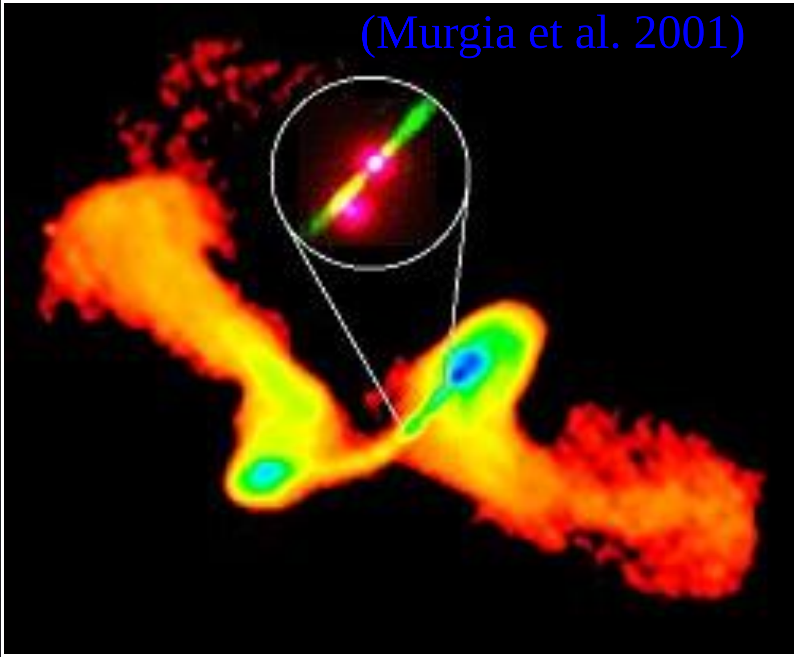

3C449

Hardcastle et al. (1998)

Cygnus A: FR II (Carilli, Perley, Barthel, Dreher 1996)

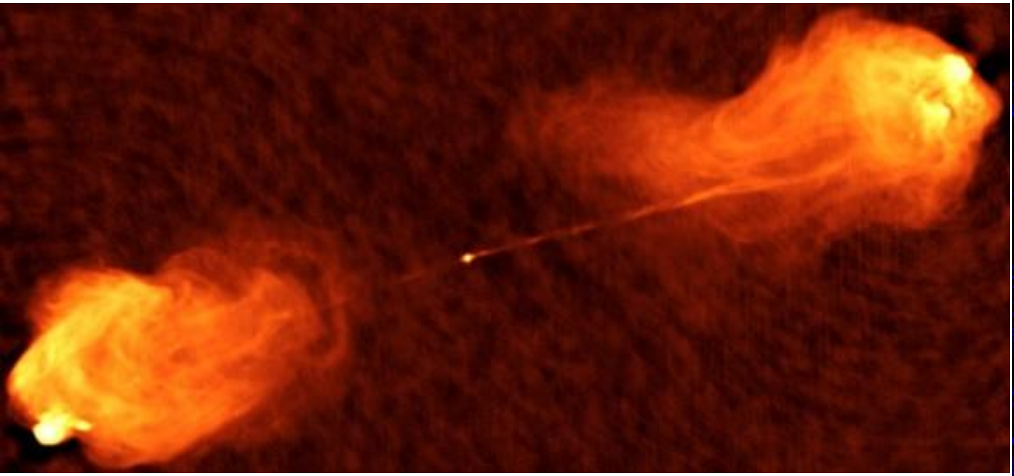

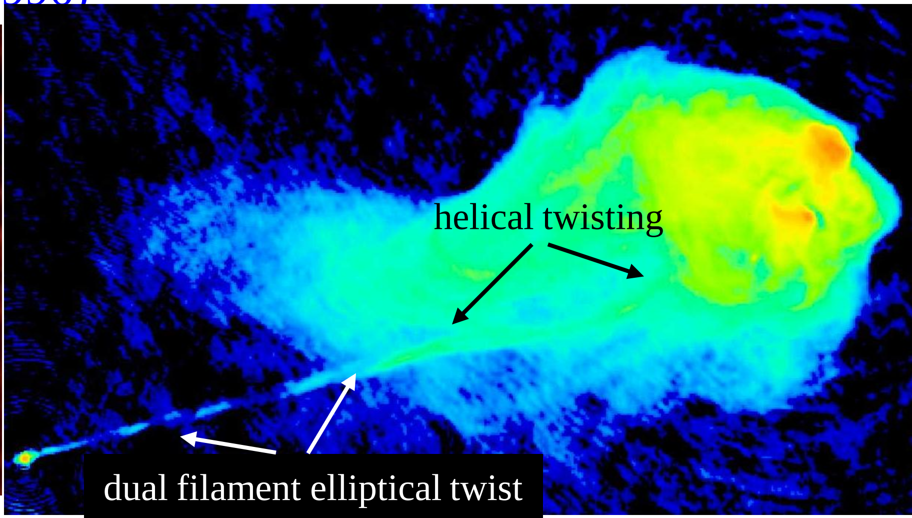

Introduction

Quasar 3C215 (Bridle et al. 1994)

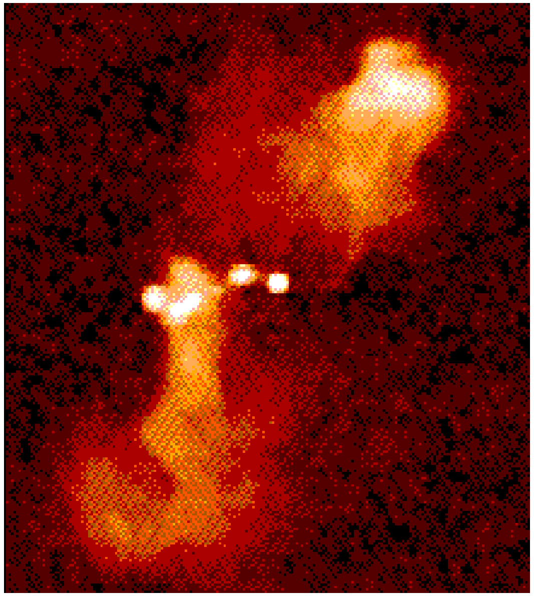

Quasar 3C175 (Bridle et al. 1994)

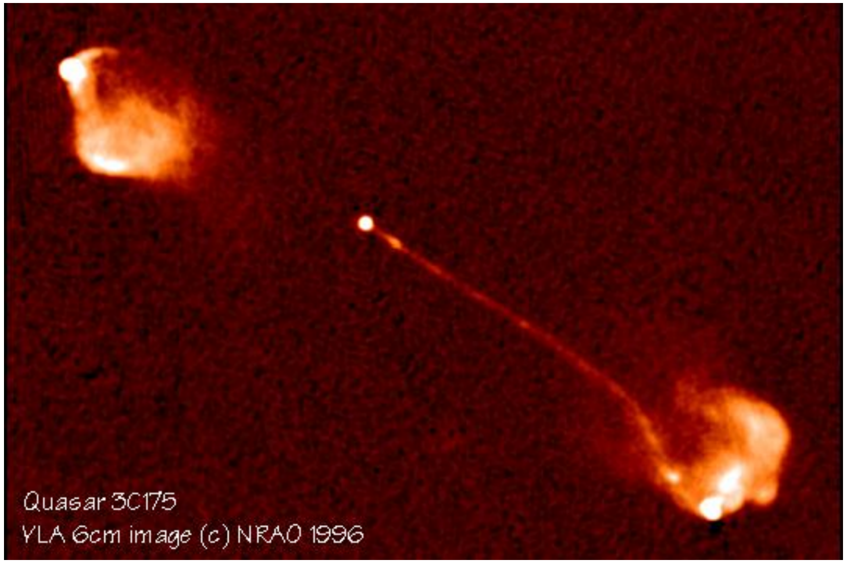

3C31 (Laing et al. 2002)

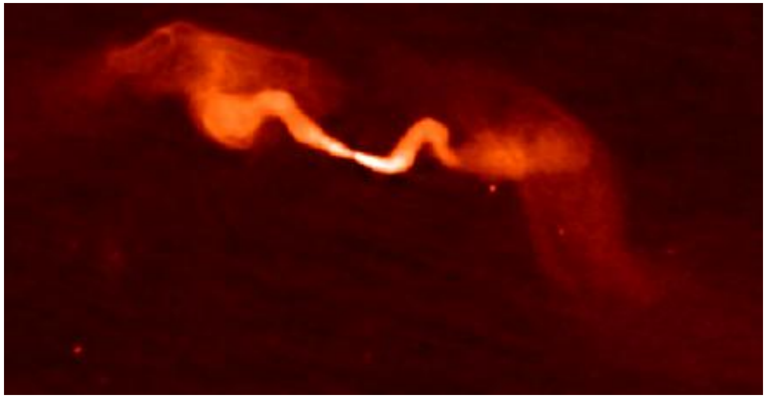

3C353 (Swan, Bridle & Baum 1998)

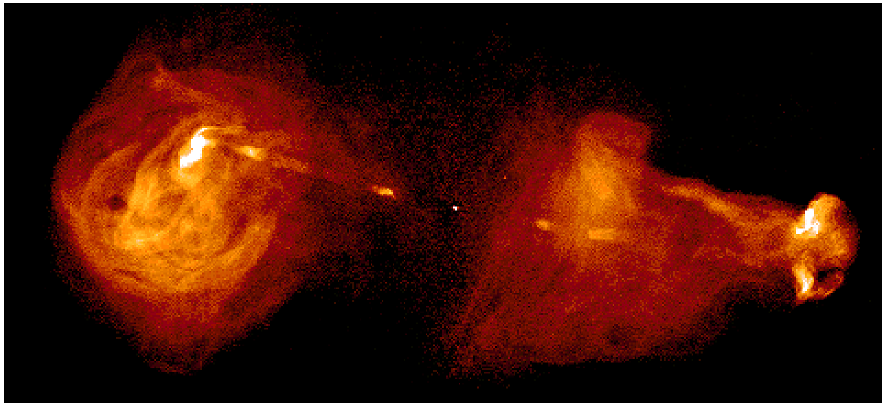

Introduction

M87: Virgo Cluster
(Owen, Biretta, & Eilek)

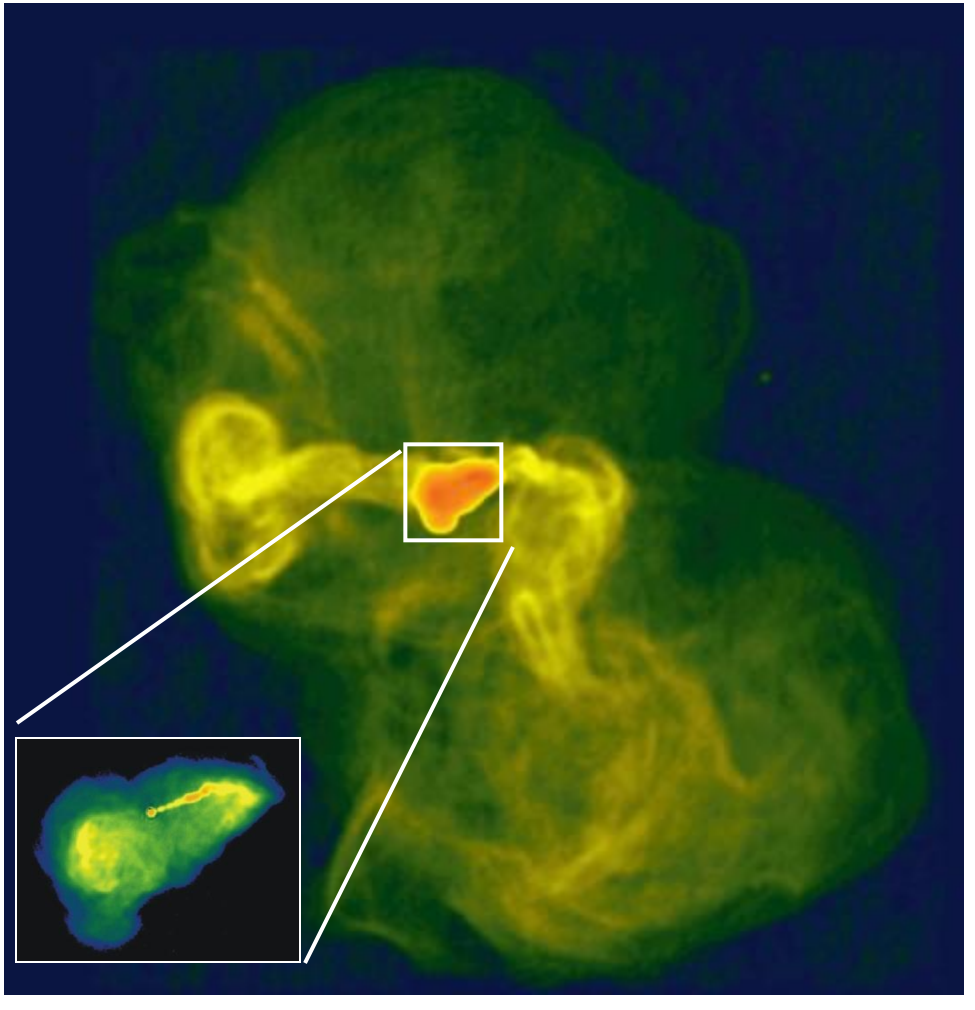

NGC 1265: Perseus Cluster
(O’Dea & Owen)

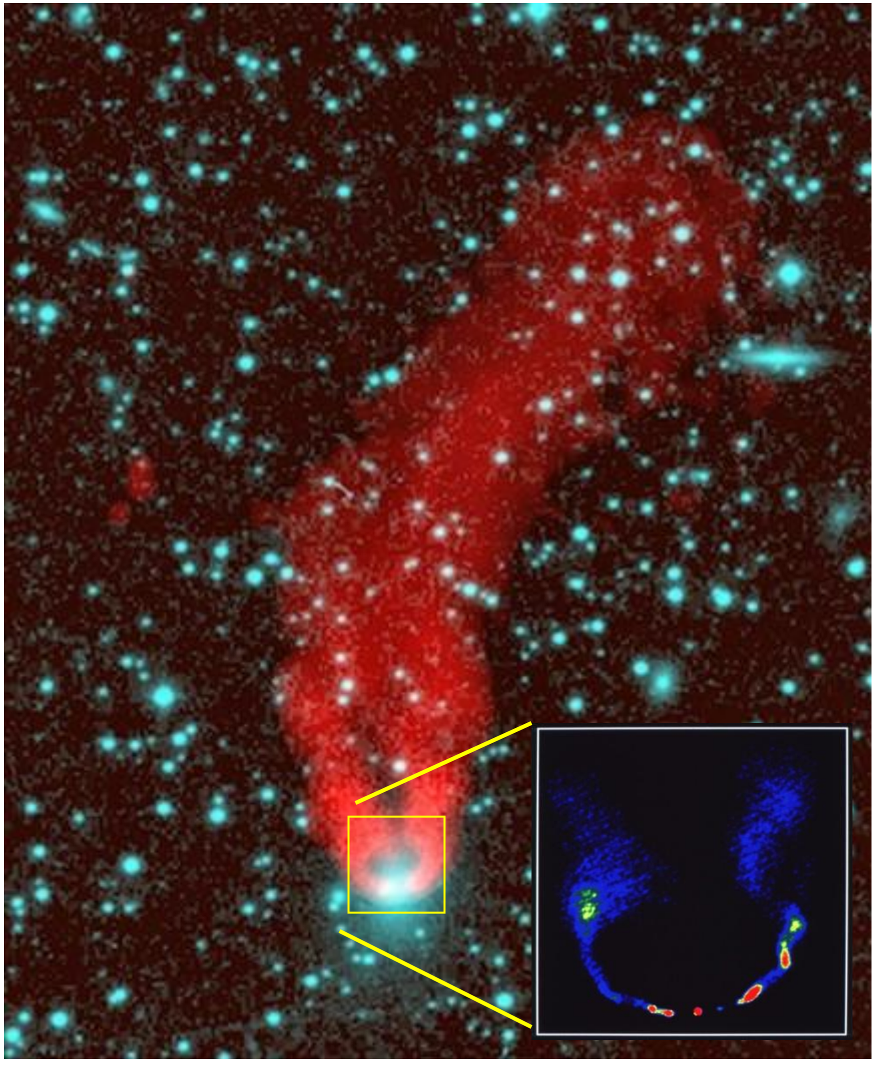

Introduction

Pc scales: Superluminal motion, one-sidedness

Subpc scale: Collimation and acceleration

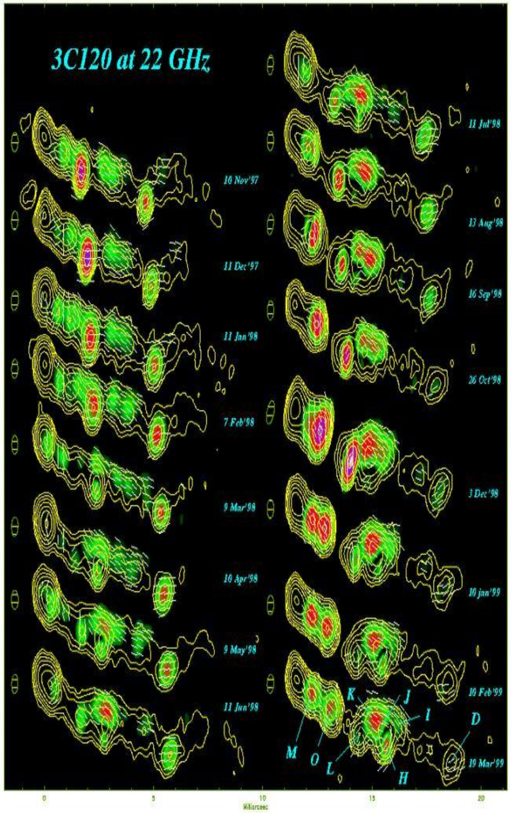

3C120, VLBA
Gómez et al. 2000

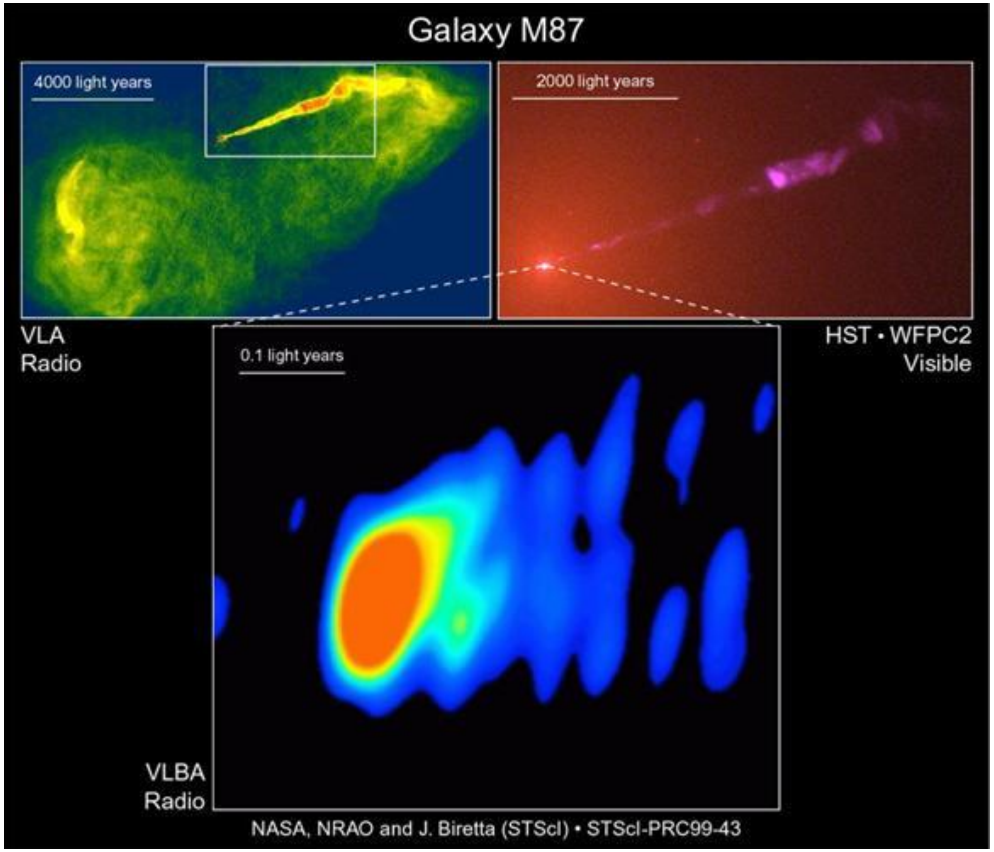

M87, VLA/VLBA
Junor et al. 1999

Introduction

Very frequent observations can give deep insight into jet dynamics:

3C 120 – Gómez et al.

3C 111 – MOJAVE

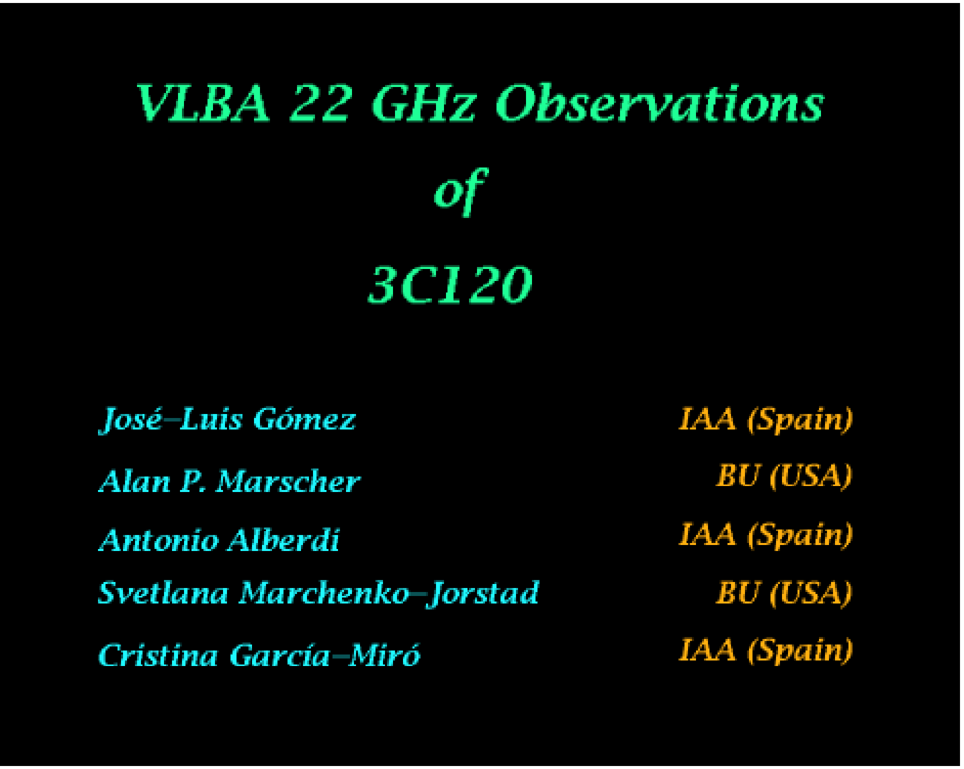

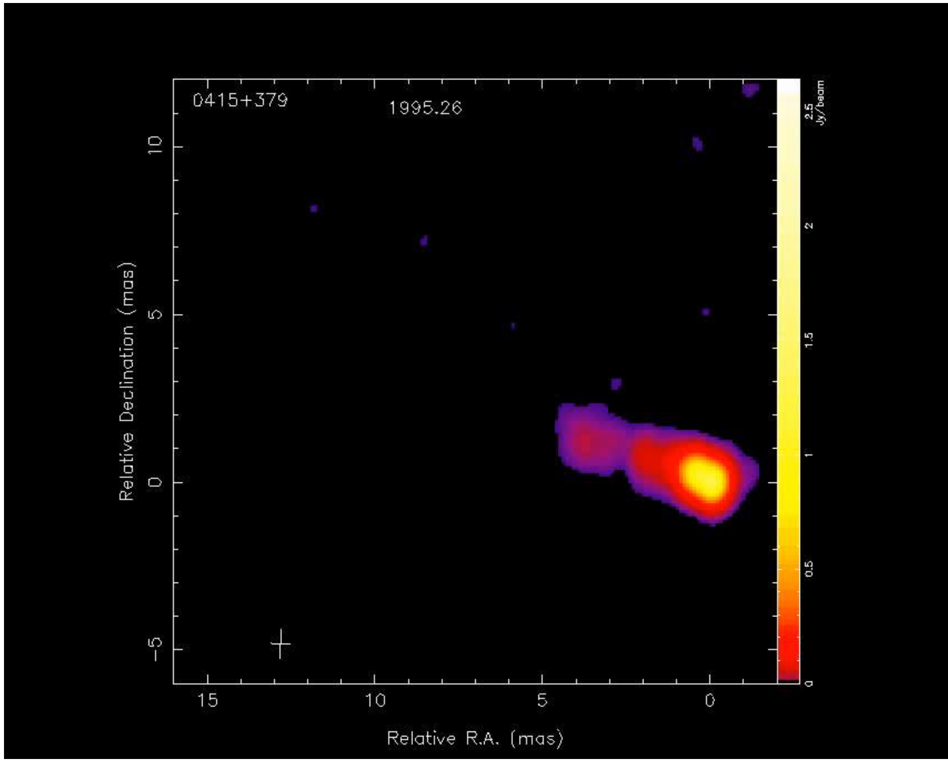

Gómez et al. 2000

Kadler et al. 2008

http://www.physics.purdue.edu/astro/MOJAVE/index.html

Galaxy Cluster MS 0735.6+7421

CXO ▪ HST ▪ VLA

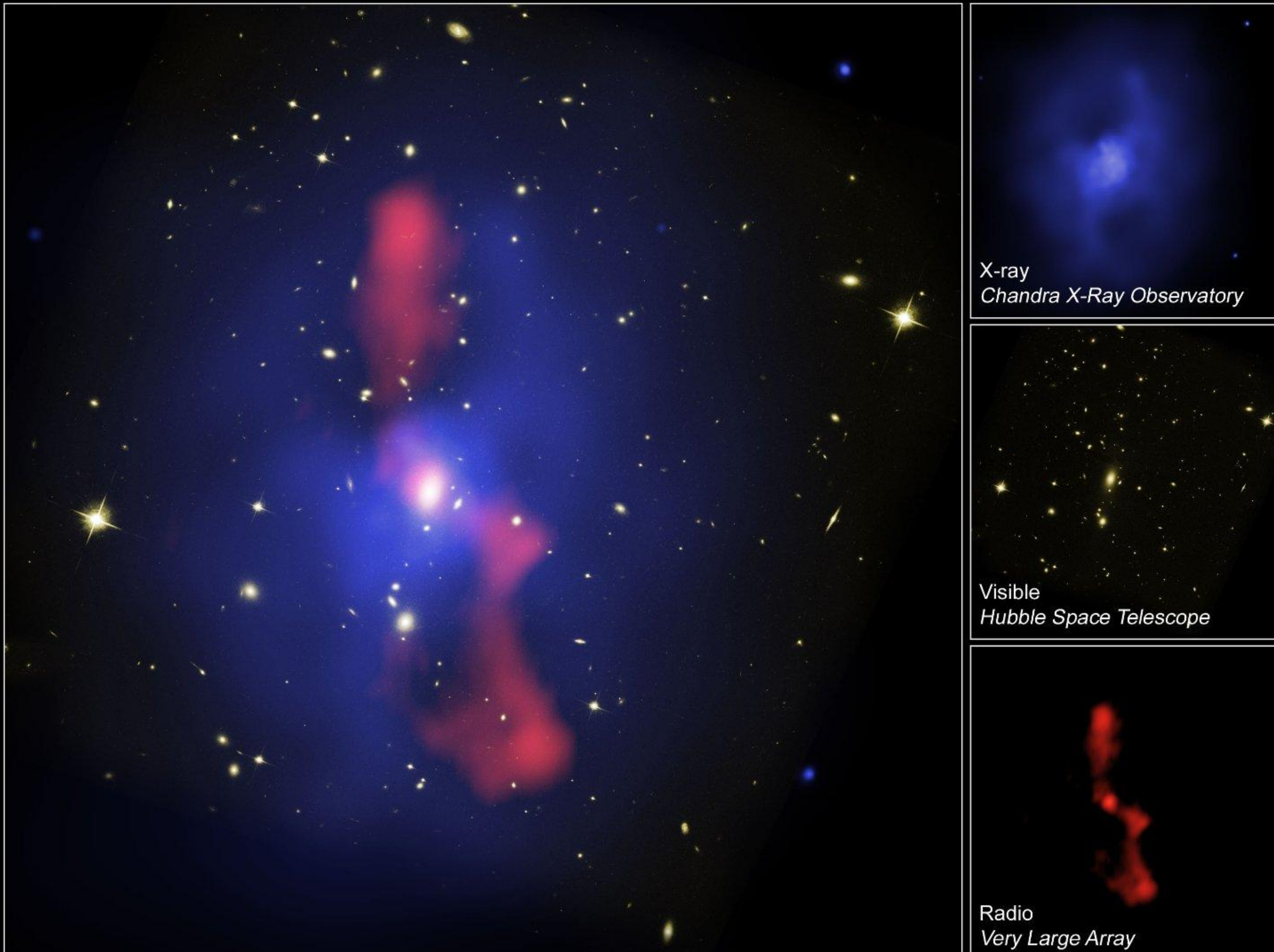

NASA, ESA, CXC/NRAO/STScI, B. McNamara (University of Waterloo and Ohio University)

STScI-PRC06-51

Introduction

MICROQUASARS

~20 sources with detected jetsin the galaxy (Massi '05, Ribó '05).

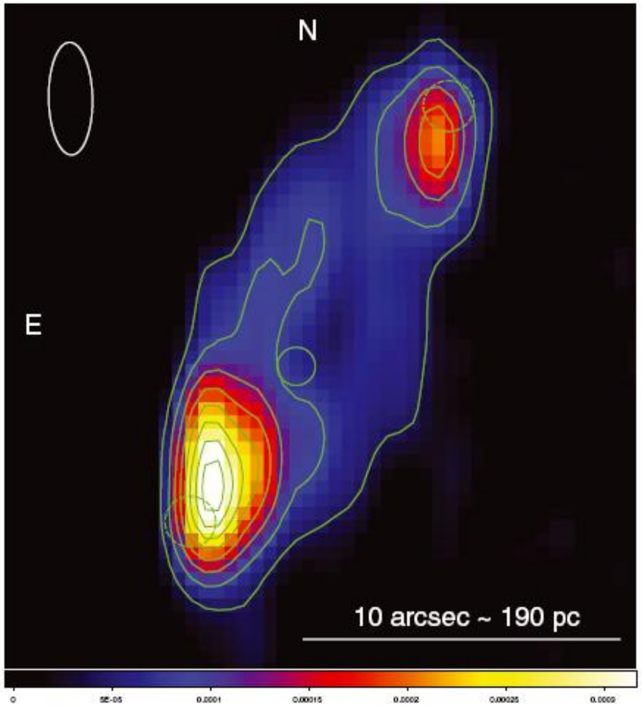

S6 in NGC 7793
Pakull et al.,
Soria et al. 2010

Cygnus X-1
Gallo et al. 2005

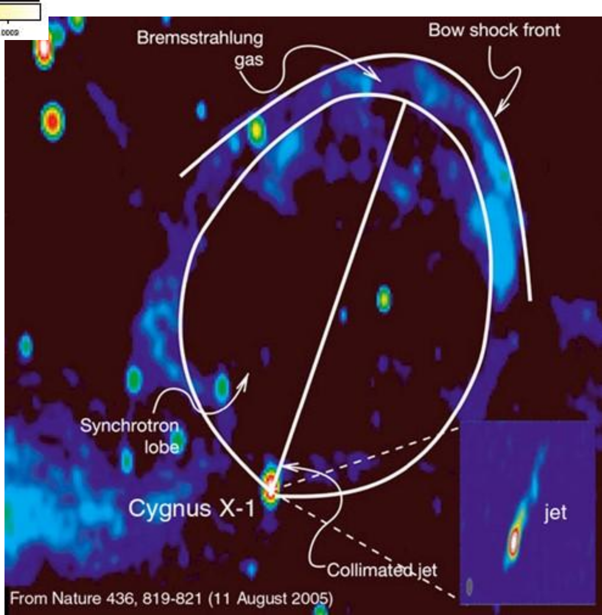

Migliari et al.

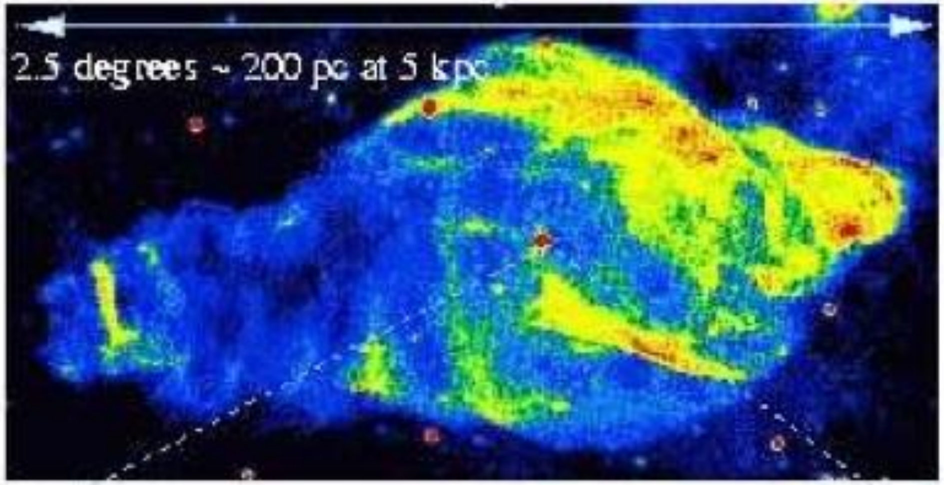

extragalactic jets – the standard model

The production of jets is connected with the process of accretion on supermassive black holes at the core of AGNs

- **Hydromagnetic acceleration** (Blandford-Payne)
- **Extraction of rotational energy from Kerr BH** by magnetic processes (Blandford-Znajek, Penrose)

3C273 HST – CHANDRA - MERLIN

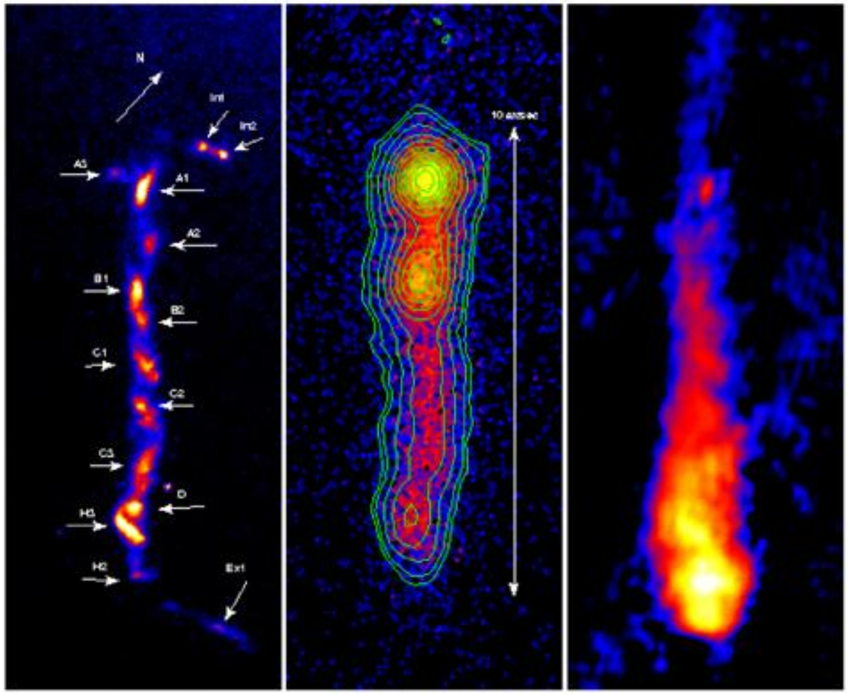

Emission: **synchrotron** (from radio to X-rays) **and inverse Compton** (γ-ray emission) from a relativistic (e+/e-, ep) jet (e.g., Ghisellini et al. 1998). Seed photons for the IC process:

- Self Compton: synchrotron photons
- External Compton: disk, BLR, dusty torus, CMB

Jets are relativistic, as indicated by:

- Superluminal motion at pc scales.
- One-sidedness of pc scale jets and brigthness asymmetries between jets and counterjets at kpc scales (due to Doppler boosting of the emitted radiation).

Jets: Relativistic collimated ejections of thermal (e+/e-, ep) plasma + ultrarelativistic electrons/positrons + magnetic fields + radiation, generated in the vicinity of SMBH

↓

(GENERAL) RELATIVISTIC MHD + ELECTRON TRANSPORT + RADIATION TRANSFER

Introduction

Can astrophysical jets be treated as flows?

Blandford & Rees 1974

‡ Some justification is perhaps needed for treating the relativistic plasma as a fluid, even though the collisional mean-free-paths are very long. If a magnetic field B gauss were present, the Larmor radius for a proton of Lorentz factor γ would be $\sim 10^{-12}\gamma B^{-1}$ pc. The smallest length-scales of the flow patterns we should consider are 1–10 pc. Thus even a magnetic field whose dynamical effects were completely negligible could guarantee fluid-like behaviour. Collective processes in the plasma would also decrease the effective mean-free-path. (Similar arguments justify a fluid dynamical approach in discussing some aspects of—for instance—the solar wind.) The nature of the 'hot' fluid is discussed further in Sections 3 and 4. If the mean-free-paths are small, the path of a typical particle closely follows a stream-line of the bulk flow; also we are justified in assuming a sharp boundary between the two fluids—except in so far as instabilities occur.

Introduction

Can astrophysical jets be treated as flows?

CLASSICAL

$$\omega_L \equiv \frac{eB}{mc}$$

$$r_L = \frac{v_\perp}{\omega_L}$$

RELATIVISTIC

$$\omega_B \equiv \frac{qB}{\gamma mc} = \frac{\omega_L}{\gamma}$$

$$r_B = \gamma r_L$$

$r_L \ll L$

r_L is the Larmor radius

L is the scale of the problem

The magnetic field keeps the particles confined.

Basic equations

Relativistic flow

$$u^\mu = \frac{\mathrm{d}x^\mu}{c\mathrm{d}\tau}; \mu = 0, 1, 2, 3$$ four-velocity

$$T^{\mu\nu} = (e+p)u^\mu u^\nu + pg^{\mu\nu}$$ energy-momentum tensor $$T^{\mu\nu} = \rho h u^\mu u^\nu + pg^{\mu\nu}$$

$e = \rho c^2 + \rho\varepsilon$ total energy density $h \equiv c^2 + \varepsilon + p/\rho$ specific enthalpy

Conservation of particle number

$$J^\mu = \rho u^\mu \qquad \nabla_\mu J^\mu = 0$$

Conservation of energy and momentum

$$\nabla_\mu T^{\mu\nu} = 0$$

Covariant derivative

$$\nabla_\mu A^\nu \equiv A^\nu{}_{,\mu} + \Gamma^\mu_{\sigma\nu} A^\sigma$$

with $A^\nu_\mu \equiv \dfrac{\partial A^\nu}{\partial x^\mu}$ and $\Gamma^\nu_{\sigma\mu} = \dfrac{1}{2} g^{\nu\lambda}\left(\dfrac{\partial g_{\lambda\mu}}{\partial x^\sigma} + \dfrac{\partial g_{\lambda\sigma}}{\partial x^\mu} - \dfrac{\partial g_{\sigma\mu}}{\partial x^\lambda}\right)$

Basic equations

We work in Minkowski space-time

$$g^{\mu\nu} = \eta^{\mu\nu} = \begin{pmatrix} -1 & 0 & 0 & 0 \\ 0 & 1 & 0 & 0 \\ 0 & 0 & 1 & 0 \\ 0 & 0 & 0 & 1 \end{pmatrix} = \mathrm{diag}(-1,1,1,1) \longrightarrow \nabla_\mu \rightarrow \partial/(\partial x^\mu) \longrightarrow \begin{matrix} \dfrac{\partial(\rho u^\mu)}{\partial x^\mu} = 0 \\ \\ \dfrac{\partial T^{\mu\nu}}{\partial x^\mu} = 0 \end{matrix}$$

Continuity equation (lab frame)

$$W \equiv \frac{1}{\sqrt{1 - \frac{v^2}{c^2}}} \longrightarrow u^\mu = W\left(1, \frac{\mathbf{v}}{c}\right) \longrightarrow D \equiv \rho u^0 = \rho W\,. \longrightarrow \boxed{\frac{\partial D}{\partial t} + \boldsymbol{\nabla}(D\mathbf{v}) = 0}$$

Basic equations

Energy-momentum tensor in Minkowski space-time

$$T^{\mu\nu} = \begin{pmatrix} \rho h W^2 - p & \rho h W^2 \frac{v^1}{c} & \rho h W^2 \frac{v^2}{c} & \rho h W^2 \frac{v^3}{c} \\ \rho h W^2 \frac{v^1}{c} & \rho h W^2 \frac{(v^1)^2}{c^2} + p & \rho h W^2 \frac{v^1 v^2}{c^2} & \rho h W^2 \frac{v^1 v^3}{c^2} \\ \rho h W^2 \frac{v^2}{c} & \rho h W^2 \frac{v^1 v^2}{c^2} & \rho h W^2 \frac{(v^2)^2}{c^2} + p & \rho h W^2 \frac{v^2 v^3}{c^2} \\ \rho h W^2 \frac{v^3}{c} & \rho h W^2 \frac{v^1 v^3}{c^2} & \rho h W^2 \frac{v^2 v^3}{c^2} & \rho h W^2 \frac{(v^3)^2}{c^2} + p \end{pmatrix}$$

Conservation of energy and momentum

$$\boxed{\frac{\partial T^{0\nu}}{c\partial t} + \frac{\partial T^{i\nu}}{\partial x^i} = 0}$$

relativistic momentum

$$S^i \equiv \frac{T^{0i}}{c} = \frac{\rho h W^2 v^i}{c} \longrightarrow \frac{\partial S^i}{\partial t} + \boldsymbol{\nabla}(S^i \mathbf{v}) + (\boldsymbol{\nabla} p)^i = 0$$

relativistic energy-density

$$\tau \equiv T^{00} - \rho u^0 c^2 = \rho h W^2 - p - \rho W c^2 \longrightarrow \begin{cases} \frac{\partial \tau}{\partial t} + c^2 \boldsymbol{\nabla}(\mathbf{S} - D\mathbf{v}) = 0 \\ \frac{\partial \tau}{\partial t} + \boldsymbol{\nabla}[(\tau + p)\mathbf{v}] = 0 \end{cases}$$

Basic equations

classical		relativistic	
primitive	conserved	primitive	conserved
ρ	ρ	ρ	ρW
u	ρu	v	$\rho h W^2 v$
P	$\rho u^2/2 + P/(\gamma - 1)$	p	$\rho h W^2 - p - \rho W$

$$\frac{\partial}{\partial t}\rho + \frac{\partial}{\partial x}(\rho u) = 0$$

$$\frac{\partial}{\partial t}(\rho u) + \frac{\partial}{\partial x}(\rho u^2 + P) = 0$$

$$\frac{\partial}{\partial t}(\rho E) + \frac{\partial}{\partial x}[(\rho E + P)u] = 0$$

$$\rho E \equiv \frac{1}{2}\rho u^2 + \rho\varepsilon = \frac{1}{2}\rho u^2 + \frac{P}{\gamma - 1}$$

$$\frac{\partial D}{\partial t} + \nabla \cdot (D\mathbf{v}) = 0 \quad \text{(mass conservation)}$$

$$\frac{\partial \mathbf{S}}{\partial t} + \nabla \cdot (\mathbf{S} \otimes \mathbf{v} + p\mathbf{I}) = 0 \quad \text{(momentum conservation)}$$

$$\frac{\partial \tau}{\partial t} + \nabla \cdot (\mathbf{S} - D\mathbf{v}) = 0 \quad \text{(energy conservation)}$$

Relativistic hydrodynamics: SRHD equations

$$\frac{\partial D}{\partial t} + \nabla \cdot (D\mathbf{v}) = 0 \ \ \text{(mass conservation)}$$

$$\frac{\partial \mathbf{S}}{\partial t} + \nabla \cdot (\mathbf{S} \otimes \mathbf{v} + p\mathbf{I}) = 0 \ \ \text{(momentum conservation)}$$

$$\frac{\partial \tau}{\partial t} + \nabla \cdot (\mathbf{S} - D\mathbf{v}) = 0 \ \ \text{(energy conservation)}$$

STATE VECTOR

$$\mathbf{U} = (D, S^1, S^2, S^3, \tau)$$

FLUX VECTORS

$$\mathbf{F}^i = (Dv^i, S^1 v^i + \delta^{1i}, S^2 v^i + \delta^{2i}, S^3 v^i + \delta^{3i}, S^i - Dv^i)$$

DEFINITIONS

$D = \rho W$: relativistic rest-mass density.

$\mathbf{S} = \rho h W^2 \mathbf{v}$: relativistic momentum density.

$\tau = \rho h W^2 c^2 - p - \rho W c^2$: relativistic energy density.

$\mathbf{v}$: fluid flow velocity.

$W = 1/\sqrt{1 - \mathbf{v}^2/c^2}$: flow Lorentz factor.

FLUID REST FRAME QUANTITIES

ρ: proper rest-mass density.

$h = 1 + \varepsilon/c^2 + p/\rho c^2$: specific enthalpy.

ε: specific internal energy.

p: pressure.

RELATIVISTIC EFFECTS

$$h \geq 1 \ (\varepsilon \geq c^2)$$

$$W \geq 1 \ (v \rightarrow c)$$

Relativistic Magnetohydrodynamics

RMHD: Describes the dynamics of relativistic, electrically conducting fluids in the presence of magnetic fields.

Ideal RMHD: Absence of viscosity effects and heat conduction in the limit of infinite conductivity.

The relativistic description is easier in terms of the MAGNETIC FIELD FOUR-VECTOR IN THE LOCAL FLUID REST FRAME, $b^\mu = (b^0, \mathbf{b})$.

EQUATIONS

$$\frac{\partial D}{\partial t} + \nabla \cdot (D\mathbf{v}) = 0 \quad (\text{mass conservation})$$

$$\frac{\partial \mathbf{S}^*}{\partial t} + \nabla \cdot ((\mathbf{S}^* + b^0\mathbf{b}) \otimes \mathbf{v} + p^*\mathbf{I} - \mathbf{b} \otimes \mathbf{b}) = 0$$

$$(\text{momentum conservation})$$

$$\frac{\partial \tau^*}{\partial t} + \nabla \cdot (\mathbf{S}^* - D\mathbf{v}) = 0 \quad (\text{energy conservation})$$

$$\frac{\partial \mathbf{B}}{\partial t} - \nabla \times (\mathbf{v} \times \mathbf{B}) = 0 \quad (\text{induction equation})$$

$$\nabla \cdot \mathbf{B} = 0 \quad (\text{magnetic flux conservation})$$

$$b^0 = W(\boldsymbol{v} \cdot \boldsymbol{B}), \qquad b^i = \frac{B^i}{W} + v^i b^0.$$

$$\sigma \equiv \frac{|b|^2}{\rho} \left(= \frac{2p_{\rm mag}}{\rho} \right).$$

DEFINITIONS

$\mathbf{S}^* = \rho h^* W^2 \mathbf{v} - b^0\mathbf{b}$: relativistic momentum density.

$\tau^* = \rho h^* W^2 c^2 - p^* - (b^0)^2 - \rho W c^2$: relativistic energy density.

$\mathbf{B} = W(\mathbf{b} - b^0\mathbf{v}/c)$: *laboratory* magnetic field

FLUID REST FRAME QUANTITIES

$p^* = p(1+\beta)$; β: magnetization, magnetic to internal (gas) energy density ratio.

$h^* = h + \sigma$; σ: magnetic to rest mass energy density ratio.

RELATIVISTIC/MAGNETIC EFFECTS

$\beta \geq 1$

$\beta, \sigma \geq 1$: force-free magnetic field; Poynting flux dominated flow

Basic equations

steady flow, Bernoulli equations

$$\cancel{\frac{\partial D}{\partial t}} + \nabla(D\mathbf{v}) = 0 \qquad D \equiv \rho u^0 = \rho W\,. \longrightarrow \rho(z)W(z)v(z)\pi R(z)^2 = \rho_0 W_0 v_0 \pi R_0^2$$

$$\cancel{\frac{\partial \tau}{\partial t}} + \nabla[(\tau + p)\mathbf{v}] = 0 \qquad \tau \equiv T^{00} - \rho u^0 c^2 = \rho h W^2 - p - \rho W c^2 \longrightarrow h(z)W(z) = h_0 W_0$$

adiabatic expansion $\qquad p(z)\rho(z)^{-\gamma} = p_0\rho_0^{-\gamma}$

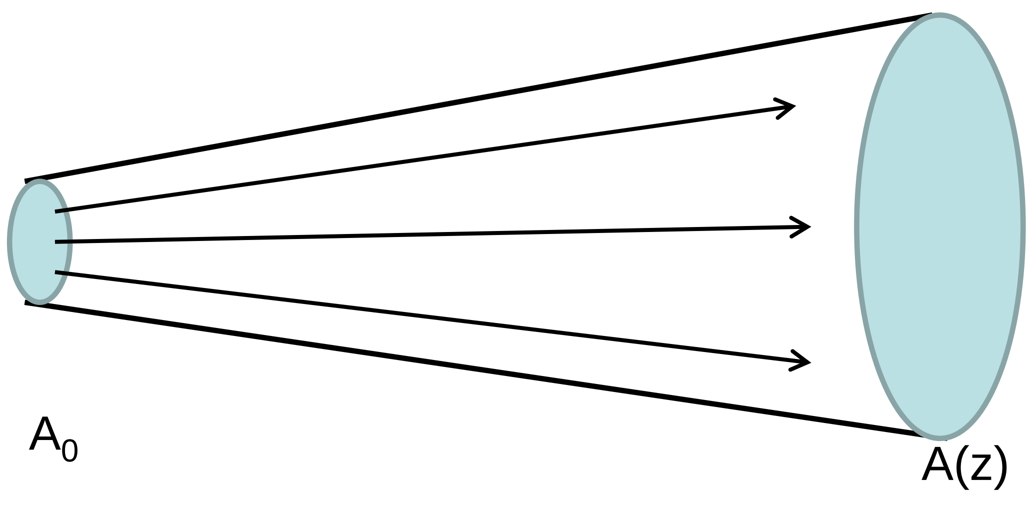

Basic equations

Internal beam structure: governed by the relativistic beam Mach number, $M_{b,R}$:

$$\boxed{M_{b,R} = \frac{W_b}{W_{cb}} \frac{v_b}{c_b} \quad (\sim W_b M_b)}$$

For models with same v_b, c_b, stronger internal shocks and hot spots in relativistic jets

Mean flow follows relativistic Bernoulli's law:

$$\boxed{h_b W_b = \text{constant}}$$

Hot jets: adiabatic expansion down the jet: $h_b \Downarrow\Downarrow$, $W_b \Uparrow\Uparrow$
Cold jets: $h_b \sim 1$, $W_b \sim$ constant

Large-scale evolution: dynamics governed by the momentum, Π_j, and energy, L_j, fluxes through the terminal shock (which are roughly proportional to $h_b W_b^2$); cocoon temperature depends also on the particle flux, J_j, through the ratio L_j / J_j (proportional to $h_b W_b$)

Basic equations

Equivalence between classical and relativistic models with the same values of:

- Inertial mass density contrast: $$\boxed{\eta = \frac{\rho_b}{\rho_a} \quad \Leftrightarrow \quad \eta_R = \frac{\rho_b h_b W_b^2}{\rho_a}}$$

- Internal beam Mach number: $$\boxed{M_b = \frac{v_b}{c_b} \quad \Leftrightarrow \quad M_{b,R} = \frac{W_b}{W_{cb}} \frac{v_b}{c_b}}$$

For equivalent models, classical and relativistic jet models:

- have almost the same power and thrust ⟶ Same jet advance speed (similar cocoon prominence) similar cocoon/cavity dynamics

- **BUT** different rest mass fluxes ⟶ Different cocoon temperature, particle number densities

- **AND** the velocity field of nonrelativistic jet simulations can not be scaled up to give the spatial distribution of Lorentz factors of the relativistic simulations ⟶ Relativistic simulations needed to compute Doppler factors

Komissarov & Falle 1996, 1998
Rosen et al. 1999

Shocks

the jet flow is supersonic $\Rightarrow$ it generates shocks.

Rankine-Hugoniot jump conditions

classical flow

$$\begin{aligned} \rho_1 u_1 &= \rho_2 u_2 \\ \rho_1 u_1^2 + P_1 &= \rho_2 u_2^2 + P_2 \\ \frac{1}{2} u_1^2 + h_1 &= \frac{1}{2} u_2^2 + h_2 \end{aligned}$$

$$h = 1 + \frac{\gamma P}{(\gamma - 1)\rho} = \frac{\gamma}{\gamma - 1} \frac{kT}{m}$$

relativistic flow

$$\begin{aligned} \rho_1 W_1 v_1 &= \rho_2 W_2 v_2 \\ \rho_1 h_1 W_1^2 v_1^2 + p_1 &= \rho_2 h_2 W_2^2 v_2^2 + p_2 \\ \rho_1 h_1 W_1^2 v_1 &= \rho_1 h_1 W_1^2 v_1 \end{aligned}$$

$$h \equiv c^2 + \varepsilon + p/\rho$$

Shocks

the jet flow is supersonic ⇨ it generates shocks.

Rankine-Hugoniot jump conditions

classical flow

$$\rho_1 u_1 = \rho_2 u_2$$

$$\rho_1 u_1^2 + P_1 = \rho_2 u_2^2 + P_2$$

$$\frac{1}{2}u_1^2 + h_1 = \frac{1}{2}u_2^2 + h_2$$

$$h = 1 + \frac{\gamma P}{(\gamma-1)\rho} = \frac{\gamma}{\gamma-1}\frac{kT}{m}$$

relativistic flow

$$\rho_1 W_1 v_1 = \rho_2 W_2 v_2$$

$$\rho_1 h_1 W_1^2 v_1^2 + p_1 = \rho_2 h_2 W_2^2 v_2^2 + p_2$$

$$\rho_1 h_1 W_1^2 v_1 = \rho_1 h_1 W_1^2 v_1$$

$$h \equiv c^2 + \varepsilon + p/\rho$$

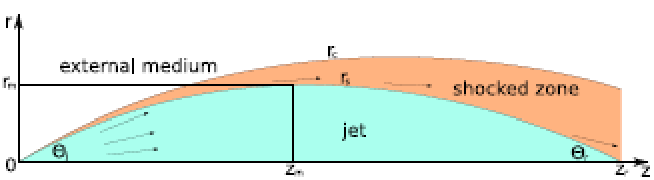

Figure 3.1: Structure of the reconfinement shock for static external medium.

Nalewajko 2011

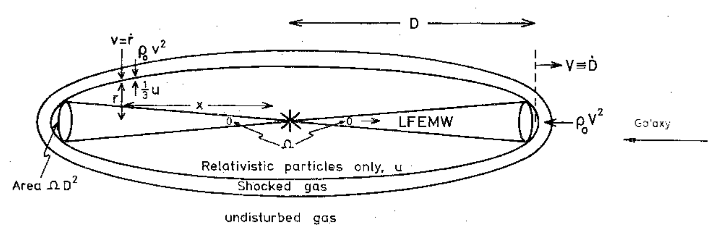

Scheuer 1974

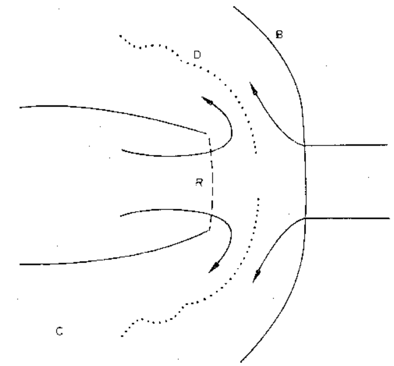

Blandford & Rees 1974

Shocks

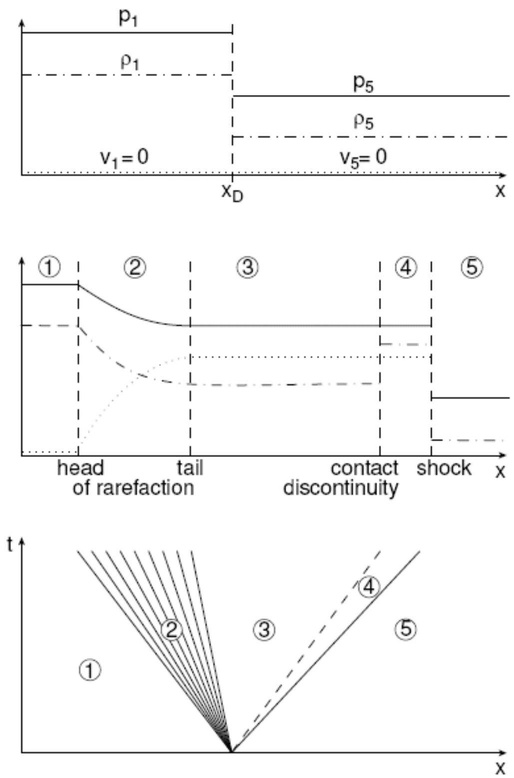

Figure 1: *Schematic solution of a Riemann problem in special relativistic hydrodynamics. The initial state at $t = 0$ (top figure) consists of two constant states 1 and 5 with $p_1 > p_5$, $\rho_1 > \rho_5$, and $v_1 = v_2 = 0$ separated by a diaphragm at x_D. The evolution of the flow pattern once the diaphragm is removed (middle figure) is illustrated in a spacetime diagram (bottom figure) with a shock wave (solid line) and a contact discontinuity (dashed line) moving to the right. The bundle of solid lines represents a rarefaction wave propagating to the left.*

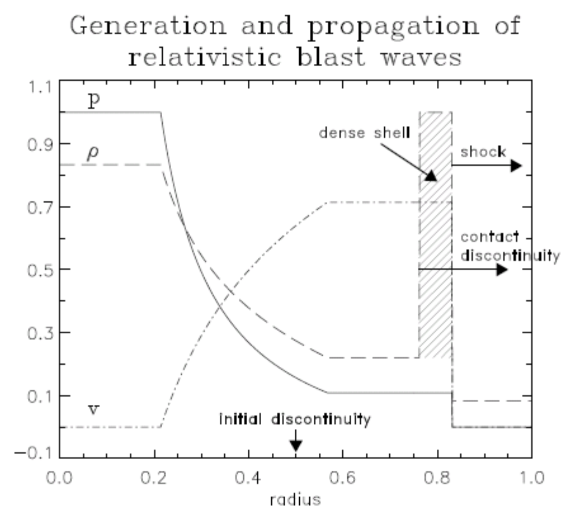

Figure 7: *Generation and propagation of a relativistic blast wave (schematic). The large pressure jump at a discontinuity initially located at $r = 0.5$ gives rise to a blast wave and a dense shell of material propagating at relativistic speeds. For appropriate initial conditions both the speed of the leading shock front and the velocity of the shell approach the speed of light, producing very narrow structures.*

Large-scale morphology and long-term evolution.

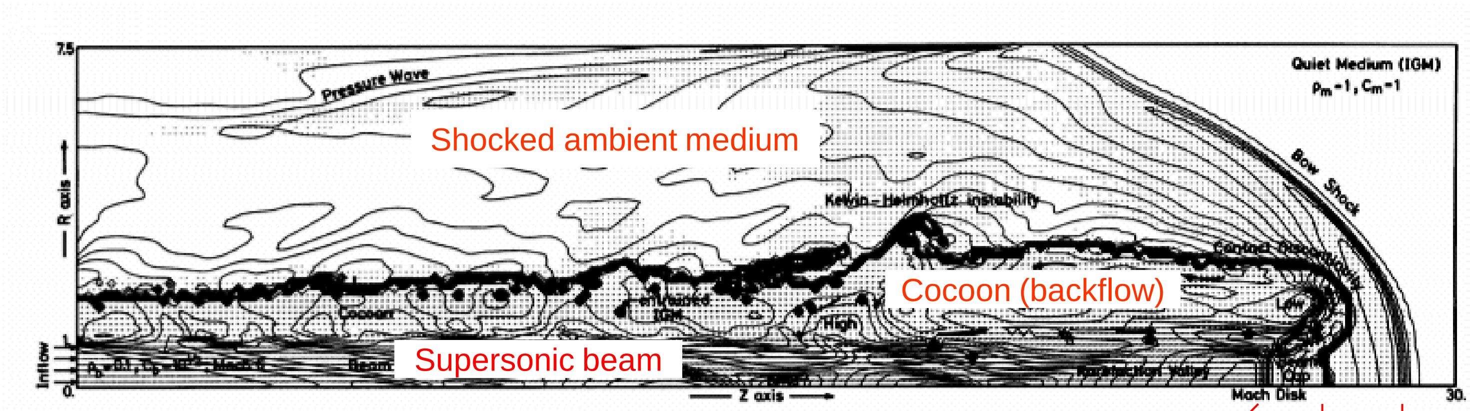

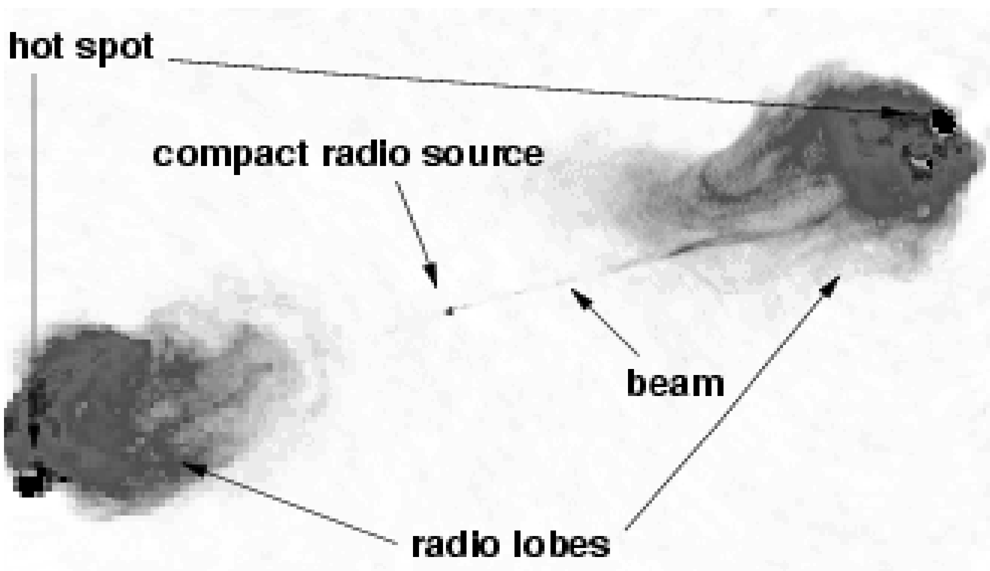

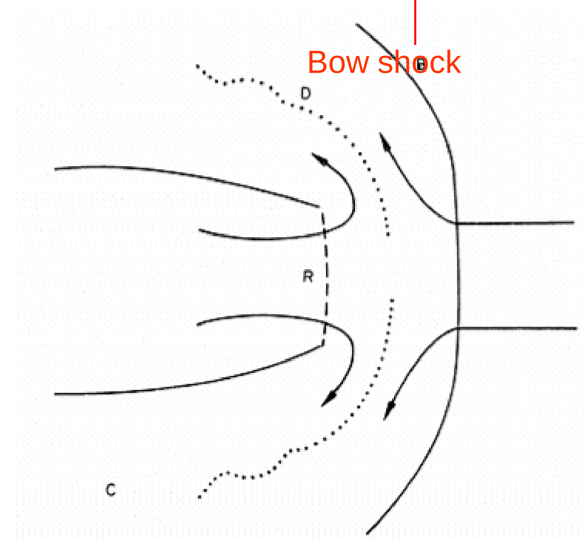

Morphology and dynamics governed by the interaction with the external medium.

Large-scale morphology and long-term evolution.

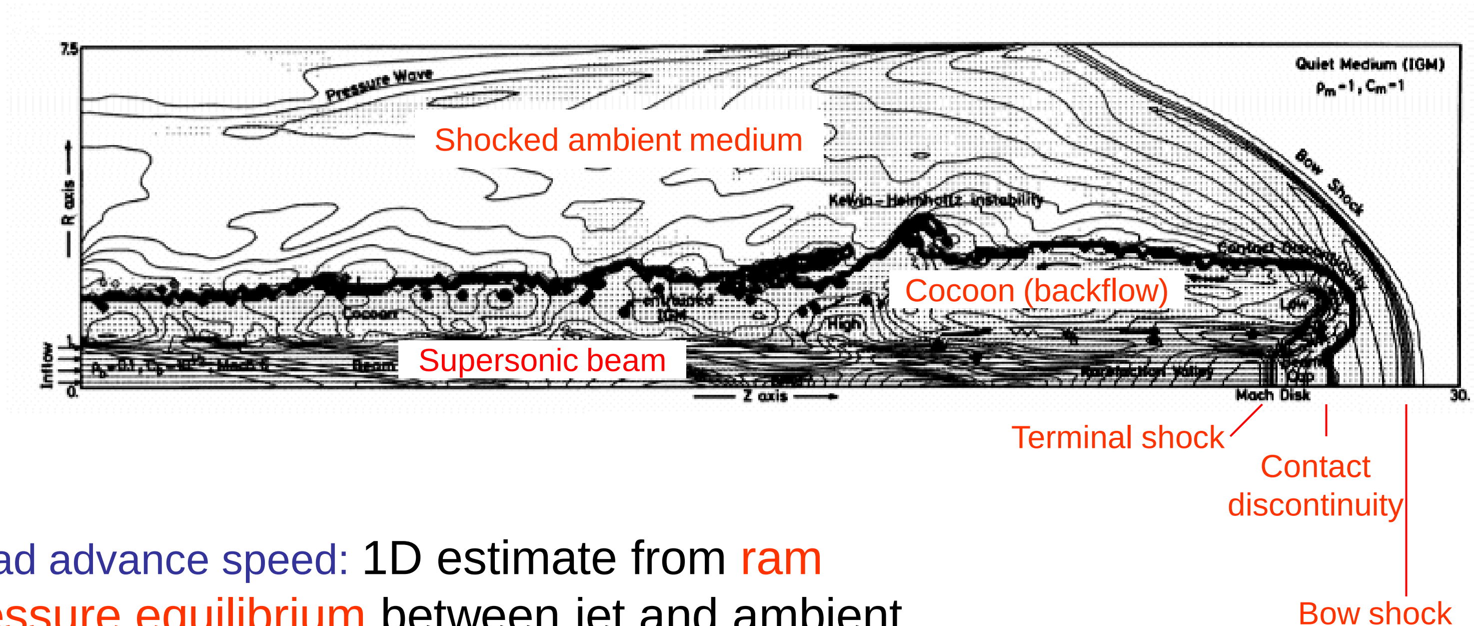

Head advance speed: 1D estimate from ram pressure equilibrium between jet and ambient in the rest frame of the jet working surface

classical jet

$$\rho_b(v_b - v_h)^2 + \cancel{p_b} = \rho_a v_h^2 + \cancel{p_a}$$

$$v_h = \frac{\sqrt{\rho_b/\rho_a}}{1+\sqrt{\rho_b/\rho_a}} v_b$$

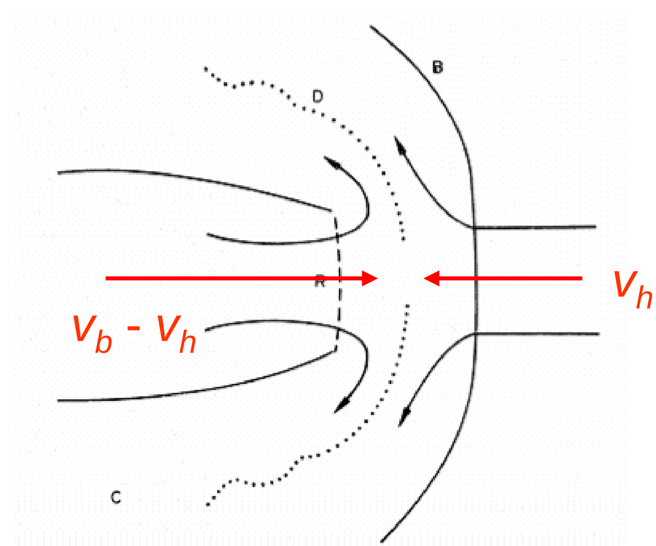

Large-scale morphology and long-term evolution.

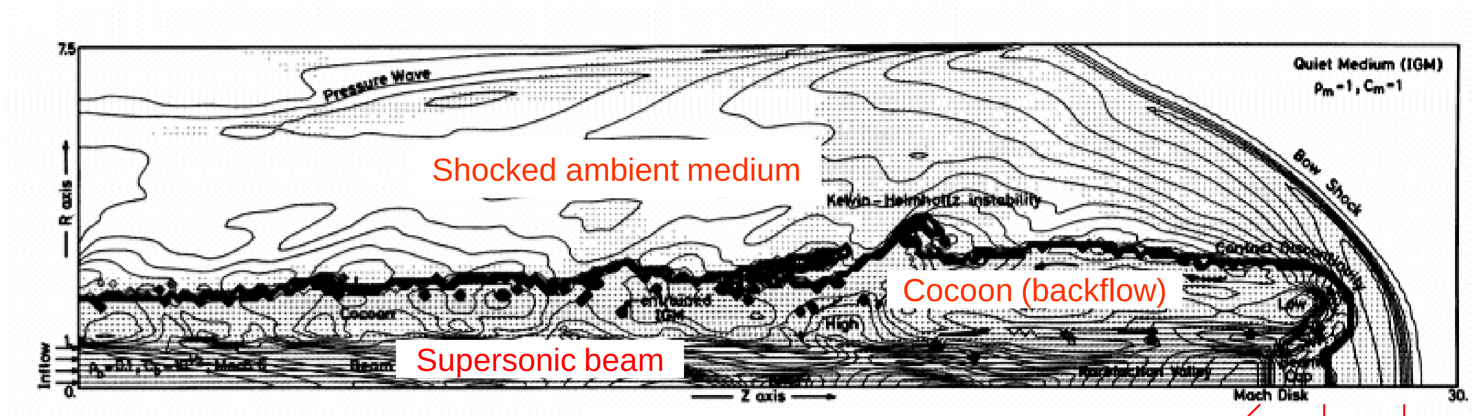

Head advance speed: 1D estimate from ram pressure equilibrium between jet and ambient in the rest frame of the jet working surface

relativistic jet

$$\rho_b h_b W_b'^2 v_b'^2 + p_b = \rho_a h_a W_a'^2 v_a'^2 + p_a \xrightarrow{v_{h,R} = -v_a'} \rho_b h_b W_b^2 (v_b - v_{h,R})^2 = \rho_a h_a v_{h,R}^2$$

$$v_{h,R} = \frac{\sqrt{\rho_b h_b W_b^2 / \rho_a h_a}}{1 + \sqrt{\rho_b h_b W_b^2 / \rho_a h_a}} v_b$$

cf. classical $$v_h = \frac{\sqrt{\rho_b / \rho_a}}{1 + \sqrt{\rho_b / \rho_a}} v_b$$

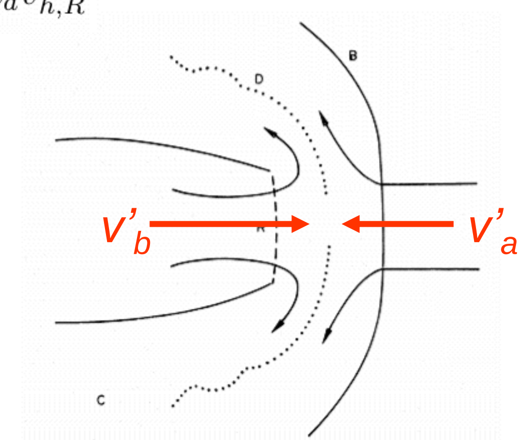

Large-scale morphology and long-term evolution.

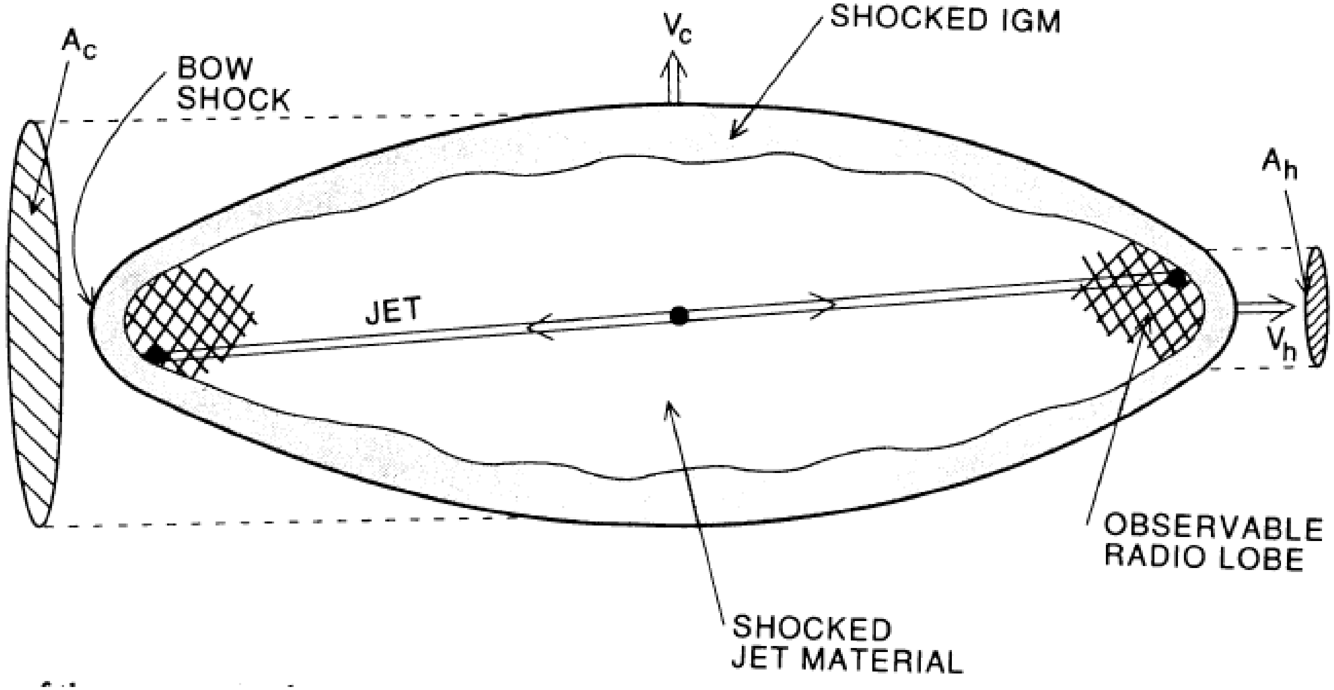

e.g., Begelman & Cioffi 1989, Kaiser & Alexander 1997, Scheck et al. 2002, Perucho & Martí 2007, Kino et al. 2007

$$P_s \propto \frac{L_s}{v_{bs} A_s} \qquad \pi R_s^2, \ R_s \text{ being the radius}$$

$$P_s = \rho_a \dot{R}_s^2$$

strong shock limit

Large-scale morphology and long-term evolution.

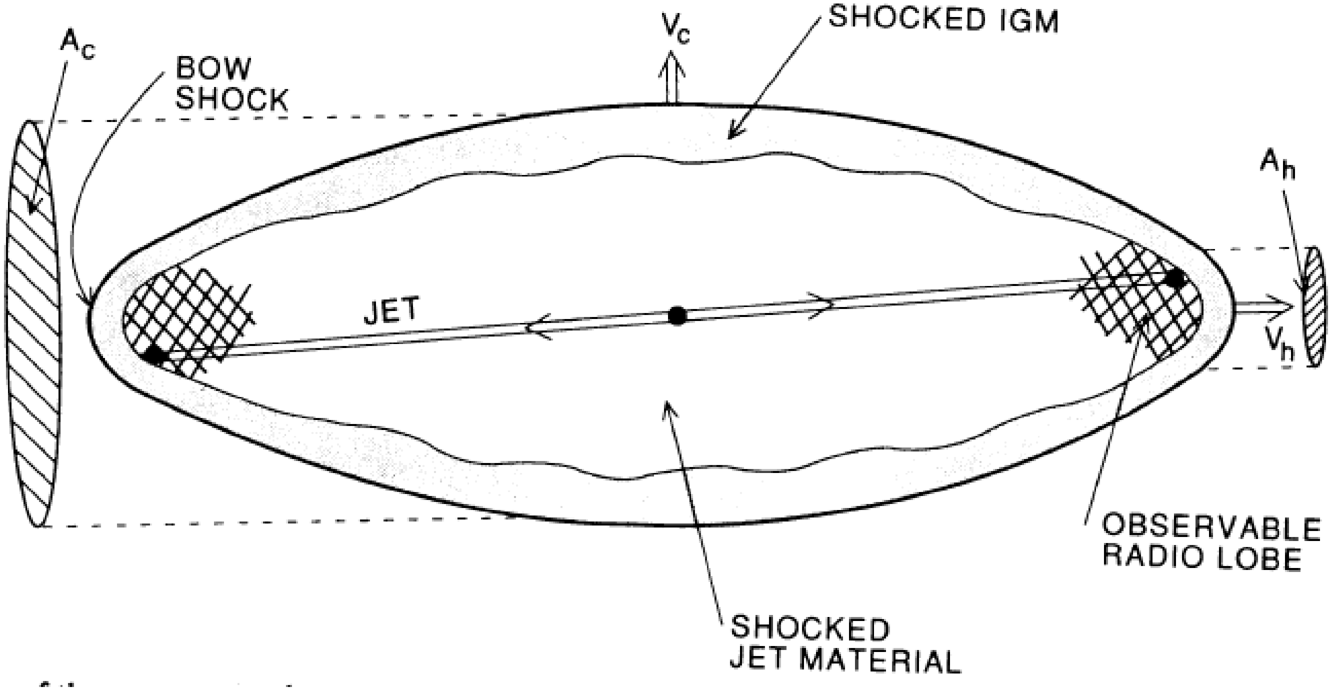

e.g., Begelman & Cioffi 1989, Kaiser & Alexander 1997, Scheck et al. 2002, Perucho & Martí 2007, Kino et al. 2007

$$P_s \propto \frac{L_s}{v_{bs} A_s} \qquad \pi R_s^2,\ R_s \text{ being the radius}$$

$$P_s = \rho_a \dot{R}_s^2$$

$$\longrightarrow \quad 1/R_s \propto \dot{R}_s$$

constant ambient density and bow-shock velocity

Large-scale morphology and long-term evolution.

constant velocity and ambient density

$$1/R_s \propto \dot{R}_s \longrightarrow R_s \propto t^{1/2}, \quad P_s \propto t^{-1}, \quad l_s/R_s \propto t^{1/2}$$

$$\left[P_s \propto \frac{L_s}{v_{bs} A_s} \right]$$

variable velocity

$$v_{bs} \propto t^{\alpha}$$

$$\dot{r}_s \propto t^{\beta}.$$

$$\longrightarrow P_s = \rho_a \dot{R}_s^2 \longrightarrow \frac{1}{t^{\alpha} t^{2(\beta+1)}} \propto t^{2\beta} \longrightarrow \beta = -1/2 - \alpha/4.$$

$$R_s \propto t^{1/2-\alpha/4}, \quad P_s \propto t^{-1-\alpha/2}, \quad l_s/R_s \propto t^{1/2+5\alpha/4}$$

$$\alpha \sim -1/3 \qquad R_s \propto t^{7/12}, \quad P_s \propto t^{-5/6}, \quad l_s/R_s \propto t^{1/12}$$

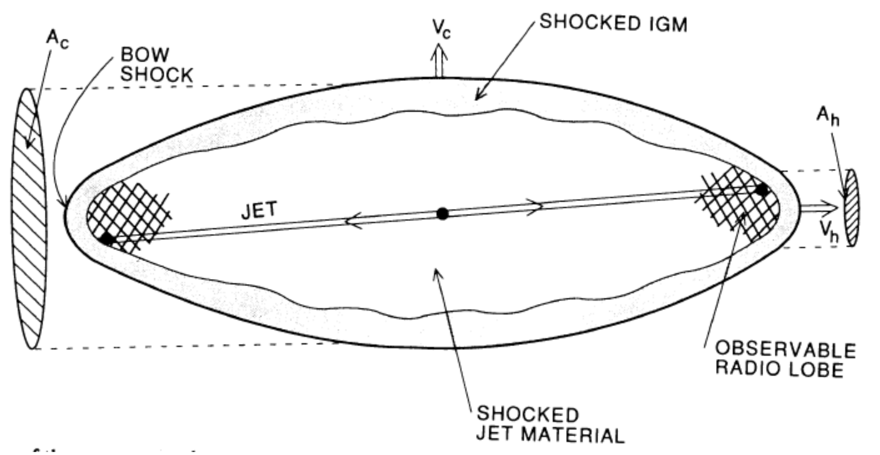

Large-scale morphology and long-term evolution.

variable velocity and density

$$v_c \propto t^{\alpha},\ \rho_a \propto r^{\beta} \quad R_s \propto t^{\frac{2-\alpha}{4+\beta}},\ P_s \propto t^{\frac{2(\alpha-2)-\alpha(4+\beta)}{4+\beta}}$$

$$\rho_a \propto R_s^{-1}$$

$$R_s \propto t^{0.7}, \quad P_s \propto t^{-1.3}, \quad l_s/R_s \propto t^{0.2}.$$

$$\alpha \sim -0.1$$

thermodynamical variables in the cocoon

$$P_c \sim P_s \propto \frac{L_s}{v_{bs} A_s} \qquad \rho_c = \frac{J_c}{v_{bs} A_c} \qquad T_c \propto \frac{L_s}{J_c}\frac{A_c}{A_s}$$

J_c : mass flux through the terminal shock (assumed constant)

$$\rho_c \propto t^{-1} \qquad \boxed{T_c \propto t^0}$$

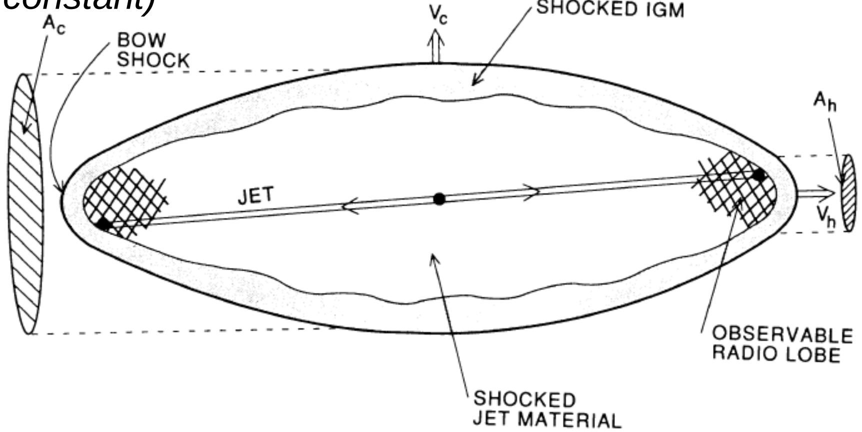

Large-scale morphology and long-term evolution.

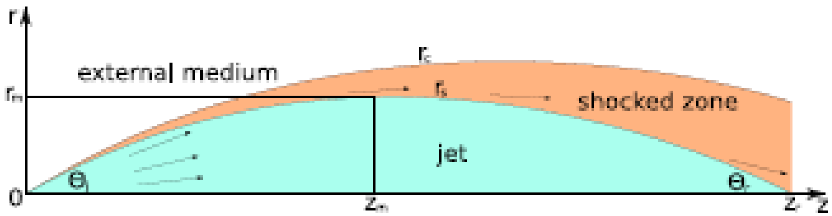

Figure 3.1: Structure of the reconfinement shock for static external medium.

$$z_1 = \left(\frac{2(2L_j J_j)^{1/2}}{\pi P_c (\gamma + 1)} \right)^{1/2}$$

Falle 1991

$$\frac{z_2}{z_1} = 3.58 \quad \text{for } \gamma = 5/3 \qquad \frac{z_2}{z_1} = 4.95 \quad \text{for } \gamma = 4/3$$

temporal evolution

$$z_{\rm s} \propto P_{\rm c}^{-1/2}$$

$$v_{\rm bs} \propto t^{\alpha}$$

$P_{\rm c} \propto t^{-1-\alpha/2}$ for homogeneous ambient $\longrightarrow$ $z_{\rm s} \propto t^{1/2+\alpha/4}$

$P_{\rm c} \propto t^{-2}$ for $\rho_{\rm a} \propto z^{-2}$ $\longrightarrow$ $z_{\rm s} \propto t$

Instabilities

KELVIN-HELMHOLTZ

$$\gamma_L^2\left(\rho+\frac{p}{c^2}\right)\left[\frac{\partial\vec{V}}{\partial t}+(\vec{V}\cdot\vec{\nabla})\vec{V}\right]+\vec{\nabla}p+\frac{\vec{V}}{c^2}\frac{\partial p}{\partial t}=0,$$

$$\gamma_L\left(\frac{\partial\rho}{\partial t}+\vec{V}\cdot\vec{\nabla}\rho\right)+\left(\rho+\frac{p}{c^2}\right)\left[\frac{\partial\gamma_L}{\partial t}+\vec{\nabla}(\gamma_L\vec{V})\right]=0.$$

$\rho=\rho_0(1+\varepsilon/c^2)$

ε - specific internal energy

$\rho_0\equiv mn$ - rest mass density, Γ - adiabatic index

$$p\rho_0^{-\Gamma}=\mathrm{const}$$

$$c_s^2=\frac{\Gamma p}{w}$$

$(w=\rho+\frac{p}{c^2}$, relativistic enthalpy)

$$\vec{V}'=\vec{V}+\vec{V}_1,\qquad p'=p+p_1,\qquad \rho'=\rho+\rho_1$$

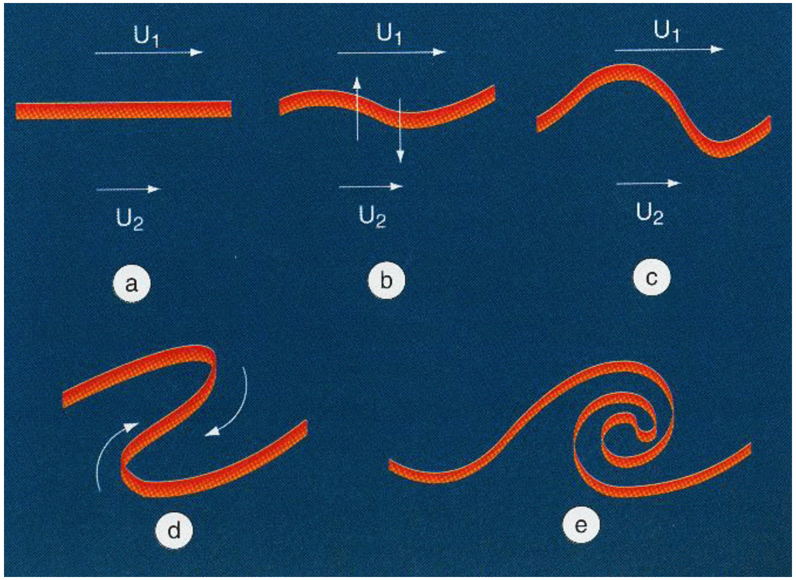

Instabilities

KELVIN-HELMHOLTZ

$$\vec{V}' = \vec{V} + \vec{V}_1, \qquad p' = p + p_1, \qquad \rho' = \rho + \rho_1$$

$$g = (p + p_1)/p = 1 + g_1$$

$$\Gamma \gamma_L^2 \left(\frac{\partial \vec{V}_1}{\partial t} + (\vec{V} \cdot \vec{\nabla}) \vec{V}_1 \right) + \vec{\nabla} g_1 + c_s^2 \vec{V} \frac{\partial g_1}{\partial t} = 0$$

$$\frac{1}{\Gamma - 1} \left(\frac{\partial g_1}{\partial t} + \vec{V} \cdot \vec{\nabla} g_1 \right) + \gamma_L^2 \Gamma \vec{V} \cdot \left(\frac{\partial \vec{V}_1}{\partial t} + \vec{\nabla} (\vec{V} \cdot \vec{V}_1) \right) + \frac{\Gamma}{c_s^2} \vec{\nabla} \vec{V}_1 = 0$$

linearized equations of RHD in planar coordinates

$$\frac{\partial^2 g_{1,b}}{\partial x^2} + \gamma_L^2 \left[\left(\frac{\partial}{\partial z} + M_b c_{s,b}^2 \frac{\partial}{\partial t} \right)^2 - \frac{c_{s,b}^2}{\Gamma_b - 1} \left(\frac{\partial}{\partial t} + M_b \frac{\partial}{\partial z} \right)^2 \right] g_{1,b} = 0 \longrightarrow$$ relativistic flow

$$\frac{\partial^2 g_{1,a}}{\partial x^2} + \left(\frac{\partial^2}{\partial z^2} - \frac{c_{s,b}^2}{\Gamma_a - 1} \frac{\partial^2}{\partial t^2} \right) g_{1,a} = 0 \longrightarrow$$ steady ambient

$$\delta = (\delta^+ F^+(x) + \delta^- F^-(x)) \, exp \, i(k_z z - wt) + b.c.$$

$$F^{\pm}(x) = exp(\pm i k_x x)$$

$p_a = p_b, \quad h_a = h_b$ at $r = R_b$ boundary conditions

Instabilities

KELVIN-HELMHOLTZ

DISPERSION RELATION

$$\frac{1}{\nu\Gamma_b}\frac{\omega}{\omega_{b0}}\frac{(\omega_{b0}^2-k_{b0}^2)^{1/2}}{\left(\frac{\omega^2}{\nu\Gamma_a}-k^2\right)^{1/2}} = \begin{cases} \coth i(\omega_{b0}^2-k_{b0}^2)^{1/2} & \text{for } s=1 \\ \mathrm{th}\, i(\omega_{b0}^2-k_{b0}^2)^{1/2} & \text{for } s=-1 \end{cases}$$

$s=\pm 1$	- symmetry index.
ω	- frequency in the rest frame.
k	- wavenumber in the rest frame
$\omega_{b0}=\gamma_L(\omega-M_b k)$	- frequency in the beam frame.
$k_{b0}=\gamma_L(k-\frac{c_{sb}^2}{c^2}M_b\omega)$	- wavenumber in the beam frame.
$\Gamma_a=\Gamma_b=4/3$	- adiabatic index.
$k_{b,x}=(w_{b0}^2-k_{b0}^2)^{1/2}$	- transversal wavenumber.

$$\delta=(\delta^+F^+(x)+\delta^-F^-(x))\,exp\,i(k_z z-wt)+b.c.$$

- Temporal approach: w complex (w_r+iw_i), k real. w_i is growth rate
- Spatial approach: k complex (k_r+ik_i), w real. k_i is growth length

Instabilities

KELVIN-HELMHOLTZ: solutions

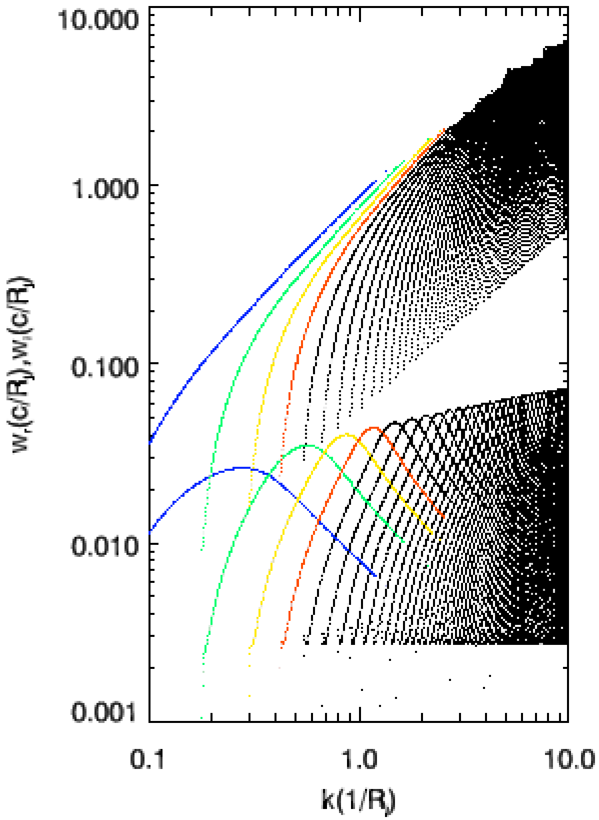

symmetric

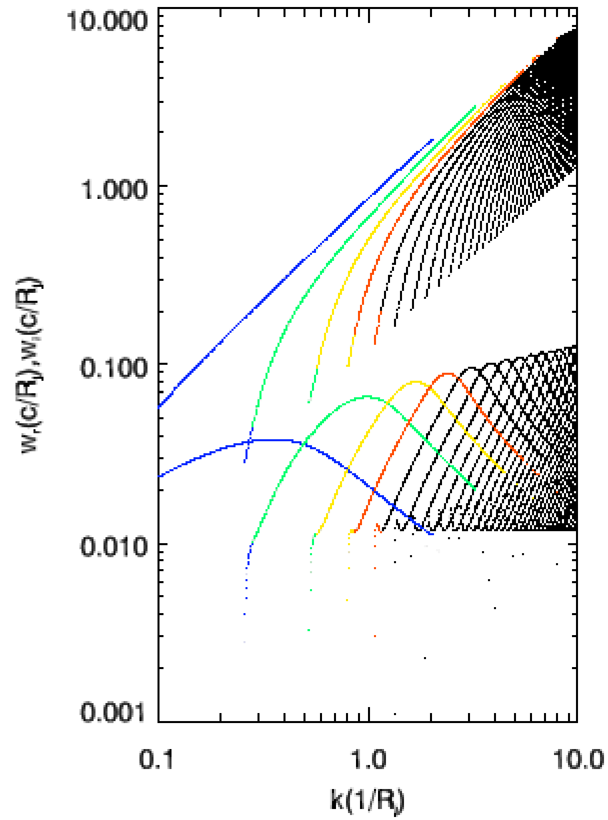

antisymmetric

hotter, slower or less dense jets show faster growth rates.

Instabilities

KELVIN-HELMHOLTZ: solutions

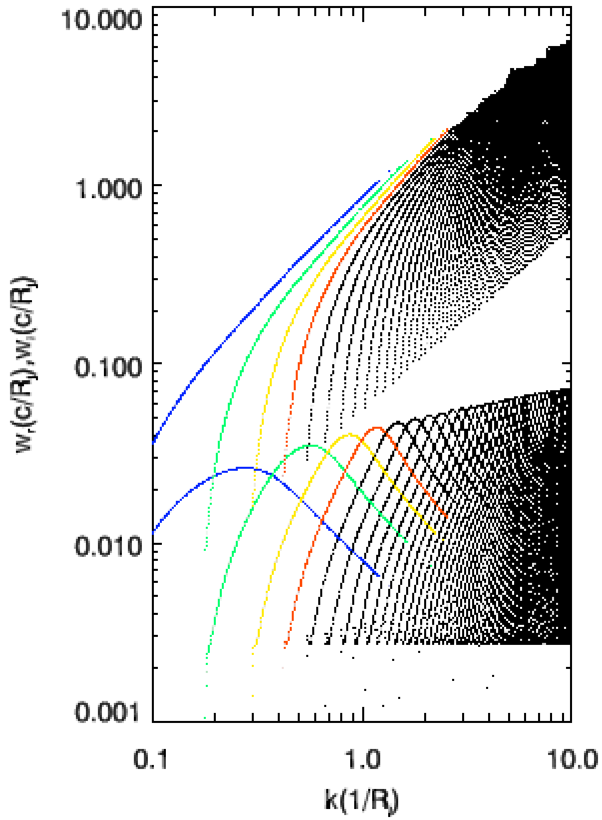

$$k_{j\perp} = (\omega'^2 - k_{\parallel}'^2)^{1/2}$$

with

$$\omega' = \gamma(\omega - v_j k_{\parallel})$$

$$k_{\parallel}' = \gamma(k_{\parallel} - \frac{v_j}{c^2}\omega)$$

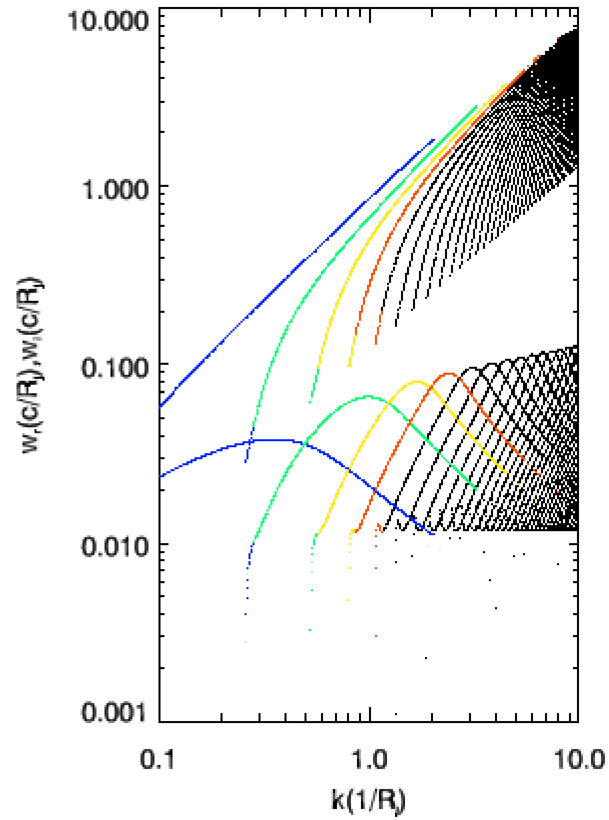

symmetric

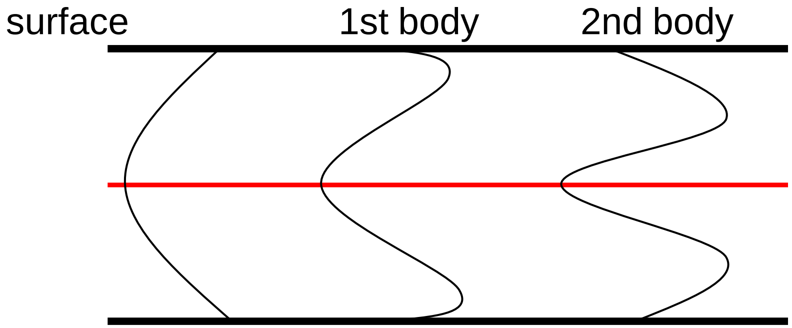

antisymmetric

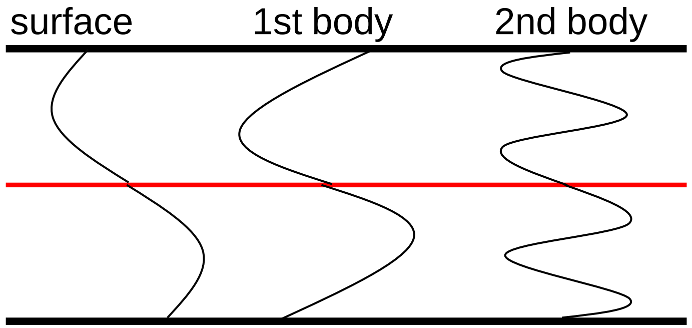

Instabilities

KELVIN-HELMHOLTZ: 3D cylindrical coordinates

$$\gamma^2 \left(\frac{\partial}{\partial t} + v_j \frac{\partial}{\partial z} \right)^2 p_{j1} - \frac{\partial^2 p_{j1}}{\partial r^2} - \frac{1}{r}\frac{\partial p_{j1}}{\partial r} - \gamma^2 \left(\frac{\partial}{\partial z} + \frac{v_j}{c^2}\frac{\partial}{\partial t} \right)^2 p_{j1} = 0,$$

$$\frac{\partial^2 p_{a1}}{\partial t^2} - \frac{\eta \Gamma_a}{\Gamma_j} \left(\frac{\partial^2 p_{a1}}{\partial r^2} + \frac{1}{r}\frac{\partial p_{a1}}{\partial r} + \frac{\partial^2 p_{a1}}{\partial z^2} \right) = 0.$$

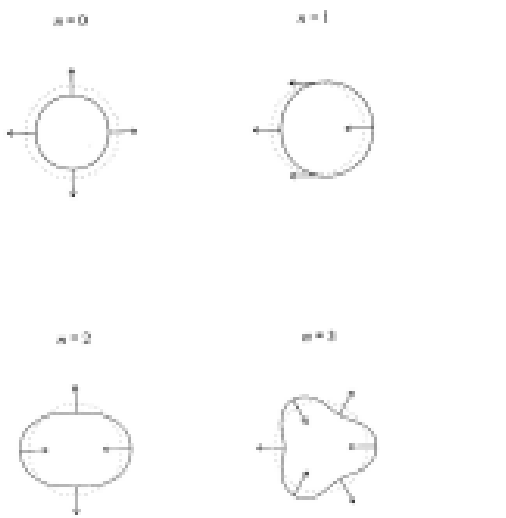

Fig. 6.2. A schematic diagram of the transverse beam deformations caused by Kelvin-Helmholtz modes with azimuthal mode numbers $n = 0$, 1, 2, and 3. The dotted lines indicate the location of the boundary of the unperturbed beam, and the full lines indicate the distortion of the boundary caused by the modes.

Cylindrical coordinates

Wave equation: Bessel form, e.g. Hardee 2000.

$$\frac{\beta_b}{\chi_b}\frac{J'_{\pm n}(\beta_b R_b)}{J_{\pm n}(\beta_b R_b)} = \frac{\beta_a}{\chi_a}\frac{H'_{\pm n}(\beta_a R_b)}{H_{\pm n}(\beta_a R_b)}$$

$$\beta_{b,a} = \gamma_{b,a}\left[\frac{(\omega - kV_{b,a})^2}{c^2_{s_{b,a}}} - \left(k - \frac{\omega V_{b,a}}{c^2}\right)^2\right]^{1/2}$$

$$\chi_{b,a} = \gamma^2_{b,a}\left(\rho_{0_{b,a}} + \frac{\Gamma_{b,a}}{\Gamma_{b,a} - 1}\frac{P}{c^2}\right)(\omega - kV_{b,a})^2$$

$$f_1(r, \phi, z) = f_1(r) \exp\left[i(kz \pm n\phi - \omega t)\right]$$

azimuthal wavenumber

Instabilities

KELVIN-HELMHOLTZ: magnetized flows

Hardee 2007

$$\boxed{r^2\frac{\partial^2}{\partial r^2}P_1^* + r\frac{\partial}{\partial r}P_1^* + \left[\beta^2 r^2 - n^2\right]P_1^* = 0}$$

$$a \equiv \left[\frac{\Gamma P}{\rho + \left(\frac{\Gamma}{\Gamma-1}\right)P/c^2}\right]^{1/2}$$

$$\beta^2 = \frac{YX}{\gamma_0^2 W_0}\left[1 + \frac{V_A^2}{\gamma_0^2}\frac{Y}{(ku-\omega)}\right]^{-1}$$

$$+kXC_z + \left[1 + \frac{V_A^2}{\gamma_0^2}\frac{Y}{(ku-\omega)}\right]^{-1}\left[2\gamma_0^2(ku-\omega)\frac{u}{c^2} - \frac{V_A^2}{\gamma_0^2}Y\frac{k}{(ku-\omega)}\right]XC_z \ .$$

$$v_A \equiv \left[\frac{V_A^2}{1 + V_A^2/c^2}\right]^{1/2}$$

$$\boxed{\frac{\beta_j}{\chi_j}\frac{J_n'(\beta_j R)}{J_n(\beta_j R)} = \frac{\beta_e}{\chi_e}\frac{H_n^{(1)'}(\beta_e R)}{H_n^{(1)}(\beta_e R)}}$$

$$\beta_j^2 \equiv \left[\frac{\gamma_j^2\left(\varpi_j^2 - \kappa_j^2 a_j^2\right)\left(\varpi_j^2 - \kappa_j^2 v_{Aj}^2\right)}{v_{msj}^2\varpi_j^2 - \kappa_j^2 v_{Aj}^2 a_j^2}\right]$$

$$\beta_e^2 \equiv \left[\frac{\gamma_e^2\left(\varpi_{ex}^2 - \kappa_e^2 a_e^2\right)\left(\varpi_e^2 - \kappa_e^2 v_{Ae}^2\right)}{v_{mse}^2\varpi_e^2 - \kappa_e^2 v_{Ae}^2 a_e^2}\right]$$

$$\chi_j \equiv \gamma_j^2\gamma_{Aj}^2 W_j\left(\varpi_j^2 - \kappa_j^2 v_{Aj}^2\right)$$

$$\chi_e \equiv \gamma_e^2\gamma_{Ae}^2 W_e\left(\varpi_e^2 - \kappa_e^2 v_{Ae}^2\right)$$

$$\varpi_{j,e}^2 \equiv (\omega - k u_{j,e})^2$$

$$\kappa_{j,e}^2 \equiv (k - \omega u_{j,e}/c^2)^2$$

$$\gamma_{j,e} \equiv (1 - u_{j,e}^2/c^2)^{-1/2}$$

$$\gamma_{Aj,e} \equiv (1 - v_{Aj,e}^2/c^2)^{-1/2}$$

$$W \equiv \rho + [\Gamma/(\Gamma-1)]P/c^2$$

$$f_1(r,\phi,z,t) = f_1(r)\exp[i(kz \pm n\phi - \omega t)]$$

Instabilities

KELVIN-HELMHOLTZ: sheared flows

$$P_1'' + \left(\frac{2\gamma_0^2 v_{0z}'(k_z - \omega v_{0z})}{\omega - v_{0z}k_z} - \frac{\rho_{e,0}'}{\rho_{e,0} + P_0} \right) P_1' + \gamma_0^2 \left(\frac{(\omega - v_{0z}k_z)^2}{c_{s,0}^2} - (k_z - \omega v_{0z})^2 \right) P_1 = 0$$

planar coordinates

$$\frac{\partial^2 p}{\partial r^2} + F_1(r)\frac{\partial p}{\partial r} + F_2(r)p = 0.$$

cylindrical coordinates

$$F_1(r) = \frac{1}{r} - 2\frac{dv_{z,0}}{dr}\frac{\gamma_0^2 v_{z,0}(\omega - k_z v_{z,0}) + k_z}{\omega - k_z v_{z,0}} - \frac{d\rho_0'/dr}{\rho_0' h_0}$$

$$F_2(r) = \frac{(\omega - k_z v_{z,0})^2 \gamma_0^2}{c_{sj,0}} - \frac{n}{r^2} + \left(\gamma_0^2 v_{z,0}(\omega - k_z v_{z,0}) + k_z\right)(\omega v_{z,0} - k_z).$$

No dispersion relation.

Instabilities

KELVIN-HELMHOLTZ: sheared flows

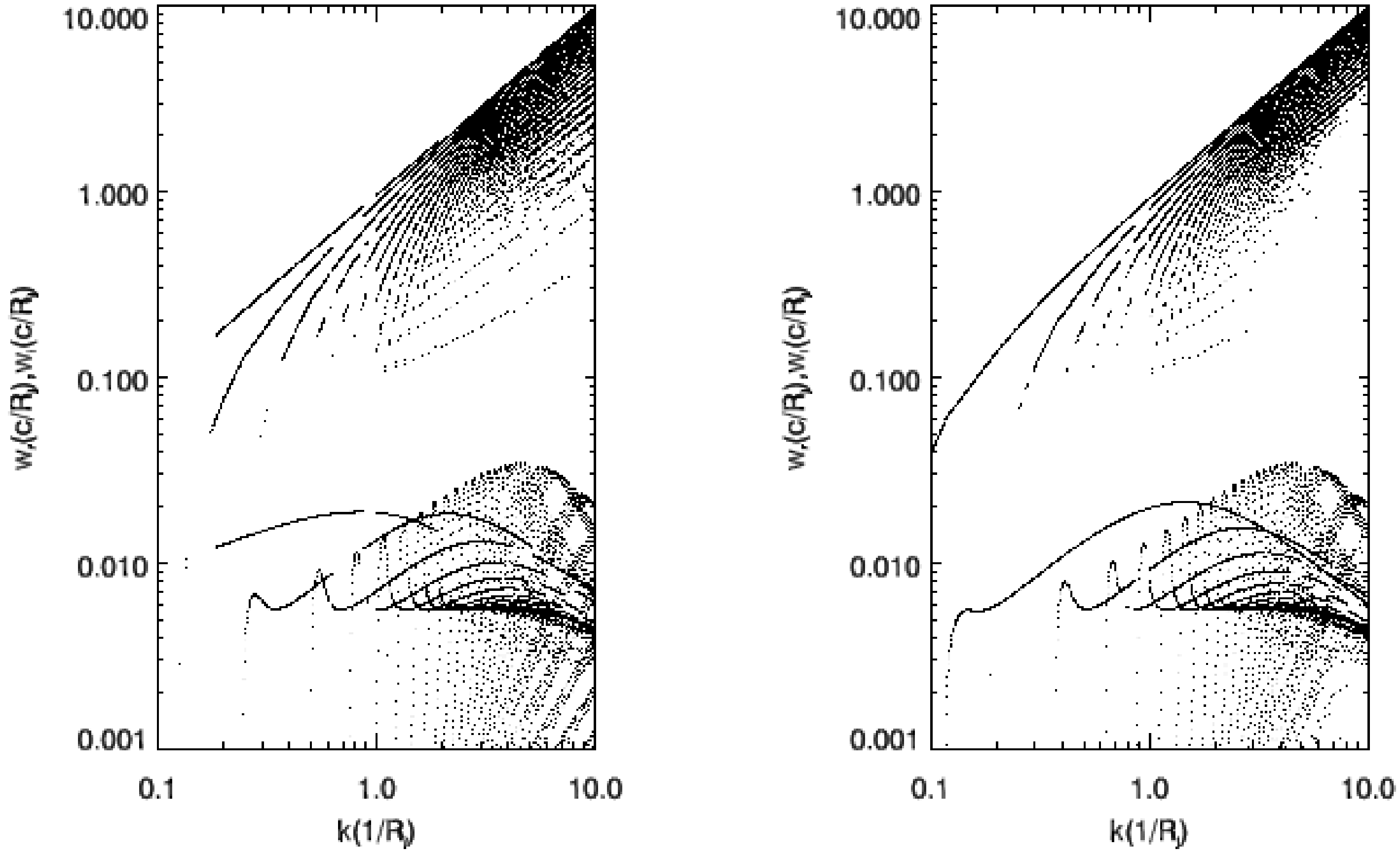

thin shear layer

resonant modes: faster growing for larger Lorentz factors.

Instabilities

KELVIN-HELMHOLTZ: sheared flows

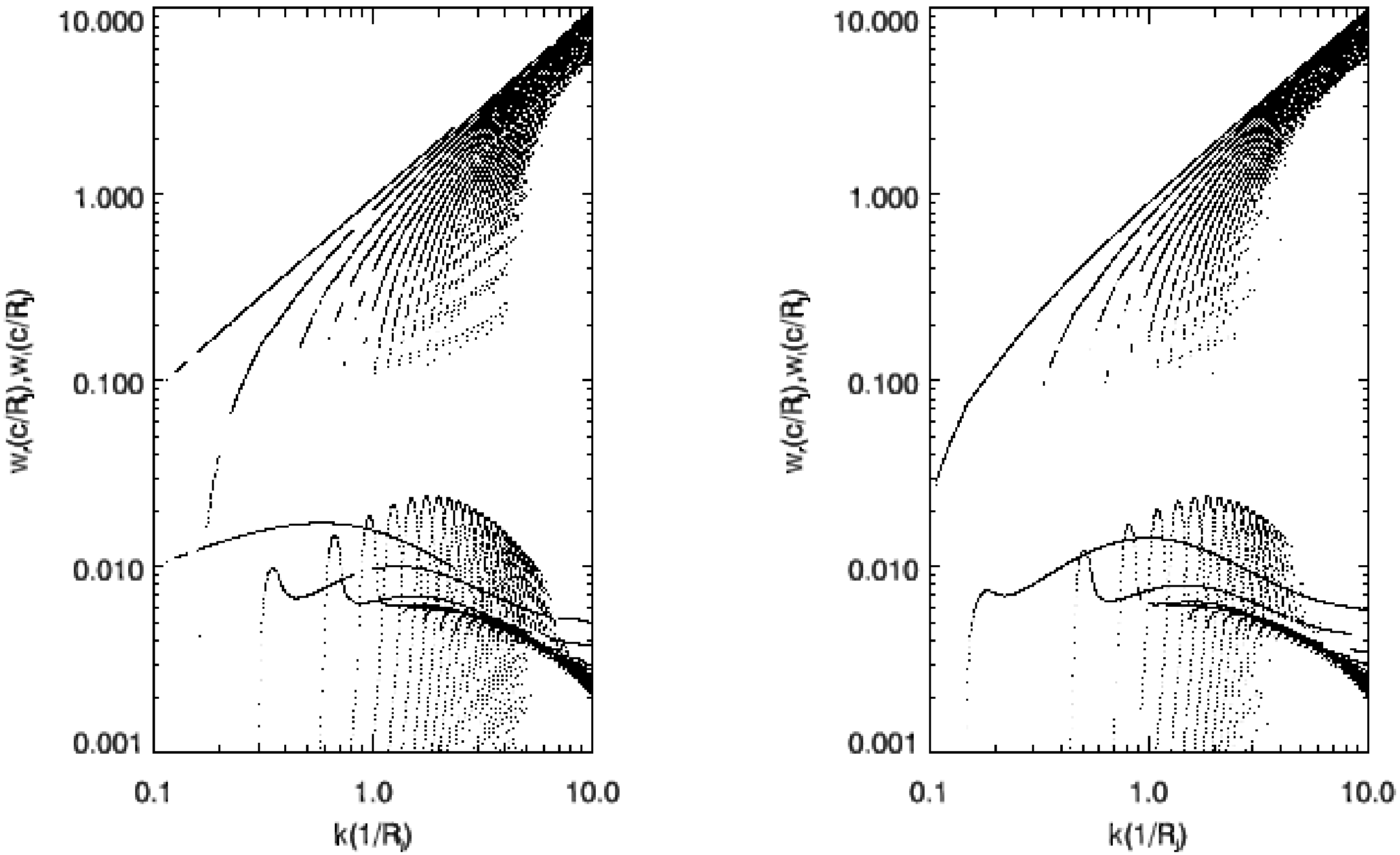

thicker shear layer

resonant modes: slower growing for thicker shear layers.

Instabilities

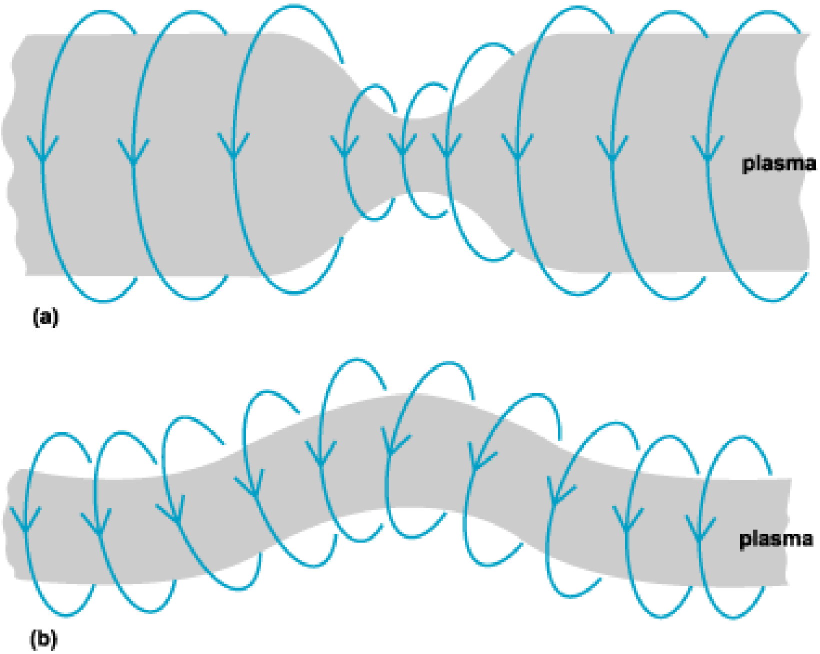

sausage instability

kink instability

an axial magnetic field would prevent their growth.

Only numerical works for relativistic flows.

Classical flows: e.g. Appl & Camenzind 1992, Appl 1996, Istomin & Pariev 1994, 1996, Begelman 1998, Lyubarskii 1992, 1999, Bonanno & Urpin 2010

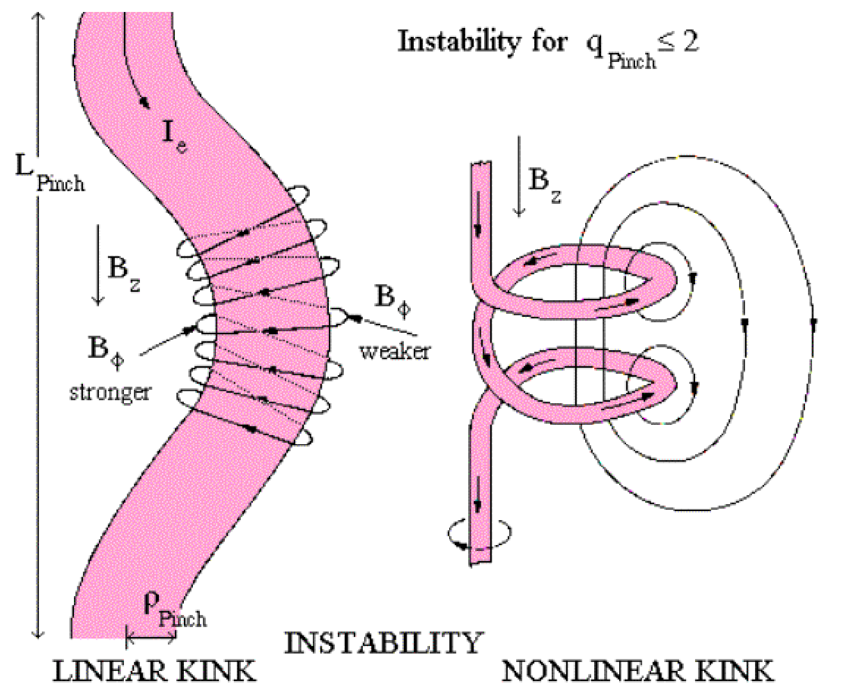

Outline of the second part
numerical simulations of relativistic jets

- Introduction.
- Numerical codes and first simulations.
- Parsec-scale jets.
- Long-term evolution.
- Instabilities.
- The largest scales: energy deposition in the ambient.

Relativistic hydrodynamics: SRHD equations

$$\frac{\partial D}{\partial t} + \nabla \cdot (D\mathbf{v}) = 0 \quad \text{(mass conservation)}$$

$$\frac{\partial \mathbf{S}}{\partial t} + \nabla \cdot (\mathbf{S} \otimes \mathbf{v} + p\mathbf{I}) = 0 \quad \text{(momentum conservation)}$$

$$\frac{\partial \tau}{\partial t} + \nabla \cdot (\mathbf{S} - D\mathbf{v}) = 0 \quad \text{(energy conservation)}$$

STATE VECTOR

$$\mathbf{U} = (D, S^1, S^2, S^3, \tau)$$

FLUX VECTORS

$$\mathbf{F}^i = (Dv^i, S^1 v^i + \delta^{1i}, S^2 v^i + \delta^{2i}, S^3 v^i + \delta^{3i}, S^i - Dv^i)$$

DEFINITIONS

$D = \rho W$: relativistic rest-mass density.

$\mathbf{S} = \rho h W^2 \mathbf{v}$: relativistic momentum density.

$\tau = \rho h W^2 c^2 - p - \rho W c^2$: relativistic energy density.

$\mathbf{v}$: fluid flow velocity.

$W = 1/\sqrt{1 - \mathbf{v}^2/c^2}$: flow Lorentz factor.

FLUID REST FRAME QUANTITIES

ρ: proper rest-mass density.

$h = 1 + \varepsilon/c^2 + p/\rho c^2$: specific enthalpy.

ε: specific internal energy.

p: pressure.

RELATIVISTIC EFFECTS

$$h \geq 1 \ (\varepsilon \geq c^2)$$

$$W \geq 1 \ (v \rightarrow c)$$

Relativistic Magnetohydrodynamics

RMHD: Describes the dynamics of relativistic, electrically conducting fluids in the presence of magnetic fields.

Ideal RMHD: Absence of viscosity effects and heat conduction in the limit of infinite conductivity.

The relativistic description is easier in terms of the MAGNETIC FIELD FOUR-VECTOR IN THE LOCAL FLUID REST FRAME, $b^\mu = (b^0, \mathbf{b})$.

EQUATIONS

$$\frac{\partial D}{\partial t} + \nabla \cdot (D\mathbf{v}) = 0 \quad (\text{mass conservation})$$

$$\frac{\partial \mathbf{S}^*}{\partial t} + \nabla \cdot ((\mathbf{S}^* + b^0\mathbf{b}) \otimes \mathbf{v} + p^*\mathbf{I} - \mathbf{b} \otimes \mathbf{b}) = 0$$

$$(\text{momentum conservation})$$

$$\frac{\partial \tau^*}{\partial t} + \nabla \cdot (\mathbf{S}^* - D\mathbf{v}) = 0 \quad (\text{energy conservation})$$

$$\frac{\partial \mathbf{B}}{\partial t} - \nabla \times (\mathbf{v} \times \mathbf{B}) = 0 \quad (\text{induction equation})$$

$$\nabla \cdot \mathbf{B} = 0 \quad (\text{magnetic flux conservation})$$

$$b^0 = W(\boldsymbol{v} \cdot \boldsymbol{B}),$$

$$b^i = \frac{B^i}{W} + v^i b^0.$$

$$\sigma \equiv \frac{|b|^2}{\rho} \left(= \frac{2p_{\rm mag}}{\rho} \right).$$

DEFINITIONS

$\mathbf{S}^* = \rho h^* W^2 \mathbf{v} - b^0\mathbf{b}$: relativistic momentum density.

$\tau^* = \rho h^* W^2 c^2 - p^* - (b^0)^2 - \rho W c^2$: relativistic energy density.

$\mathbf{B} = W(\mathbf{b} - b^0\mathbf{v}/c)$: *laboratory* magnetic field

FLUID REST FRAME QUANTITIES

$p^* = p(1+\beta)$; β: magnetization, magnetic to internal (gas) energy density ratio.

$h^* = h + \sigma$; σ: magnetic to rest mass energy density ratio.

RELATIVISTIC/MAGNETIC EFFECTS

$\beta \geq 1$

$\beta, \sigma \geq 1$: force-free magnetic field; Poynting flux dominated flow

relativistic hydrodynamics

$$\frac{\partial \mathbf{u}}{\partial t} + \frac{\partial \mathbf{F}^i(\mathbf{u})}{\partial x^i} = 0 \qquad \mathbf{u} = (D, S^1, S^2, S^3, \tau)^T$$

$$\mathbf{F}^i(\mathbf{u}) = (D\, v^i\,,\ S^1\, v^i + p\delta^{1\,i}\,,\ S^2\, v^i + p\delta^{2\,i}\,,\ S^3\, v^i + p\delta^{3\,i}\,,\ S^i - D\, v^i)^T$$

$$D = \rho\, W \quad , \qquad v^i = u^i / u^0$$

$$S^i = \rho\, h\, W^2\, v^i\,, \quad i = 1, 2, 3 \quad , \qquad W = u^0 = \frac{1}{\sqrt{1 - v^i v_i}}$$

$$\tau = \rho\, h\, W^2 - p - D \quad ,$$

$$\frac{d\mathbf{U}_{\mathbf{i,j,k}}}{dt} = -\frac{1}{\Delta x}\left(\tilde{\mathbf{F}}^x_{i+\frac{1}{2},j,k} - \tilde{\mathbf{F}}^x_{i-\frac{1}{2},j,k}\right) - \frac{1}{\Delta y}\left(\tilde{\mathbf{F}}^y_{i,j+\frac{1}{2},k} - \tilde{\mathbf{F}}^y_{i,j-\frac{1}{2},k}\right) - \frac{1}{\Delta z}\left(\tilde{\mathbf{F}}^z_{i,j,k+\frac{1}{2}} - \tilde{\mathbf{F}}^z_{i,j,k-\frac{1}{2}}\right) + \mathbf{S}_{i,j,k} \equiv \mathbf{L}(\mathbf{U}),$$

Time integration using Runge-Kutta method.

relativistic hydrodynamics

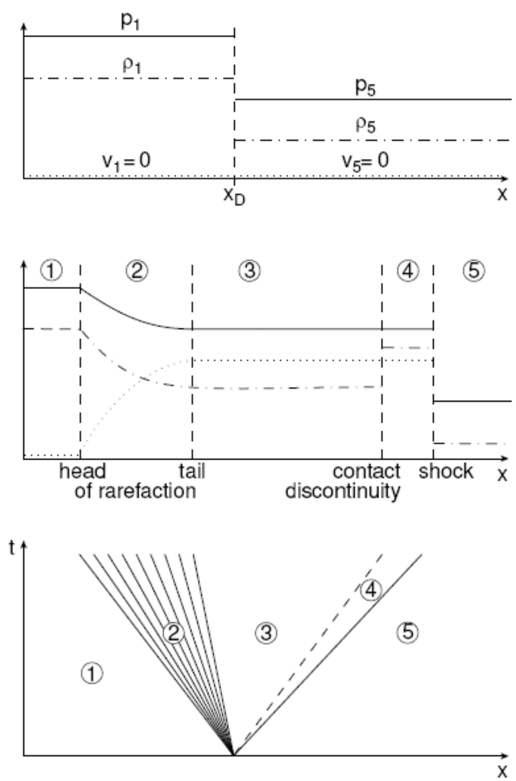

Figure 1: *Schematic solution of a Riemann problem in special relativistic hydrodynamics. The initial state at $t = 0$ (top figure) consists of two constant states 1 and 5 with $p_1 > p_5$, $\rho_1 > \rho_5$, and $v_1 = v_2 = 0$ separated by a diaphragm at x_D. The evolution of the flow pattern once the diaphragm is removed (middle figure) is illustrated in a spacetime diagram (bottom figure) with a shock wave (solid line) and a contact discontinuity (dashed line) moving to the right. The bundle of solid lines represents a rarefaction wave propagating to the left.*

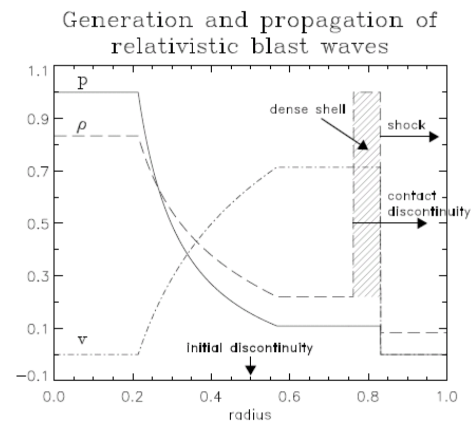

Figure 7: *Generation and propagation of a relativistic blast wave (schematic). The large pressure jump at a discontinuity initially located at $r = 0.5$ gives rise to a blast wave and a dense shell of material propagating at relativistic speeds. For appropriate initial conditions both the speed of the leading shock front and the velocity of the shell approach the speed of light, producing very narrow structures.*

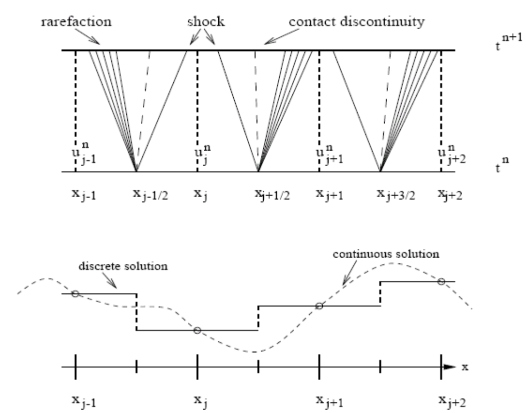

Figure 2: Godunov's scheme: local solutions of Riemann problems. At every interface, $x_{j-\frac{1}{2}}$, $x_{j+\frac{1}{2}}$ and $x_{j+\frac{3}{2}}$, a local Riemann problem is set up as a result of the discretization process (bottom panel), when approximating the numerical solution by piecewise constant data. At time t^n these discontinuities decay into three elementary waves which propagate the solution forward to the next time level t^{n+1} (top panel). The time step of the numerical scheme must satisfy the Courant-Friedrichs-Lewy condition, being small enough to prevent the waves from advancing more than $\Delta x/2$ in Δt.

relativistic hydrodynamics

See Martí & Müller, Numerical Hydrodynamics in Special Relativity,Living Reviews in Relativity, http://www.livingreviews.org/Articles/lrr-2003-7

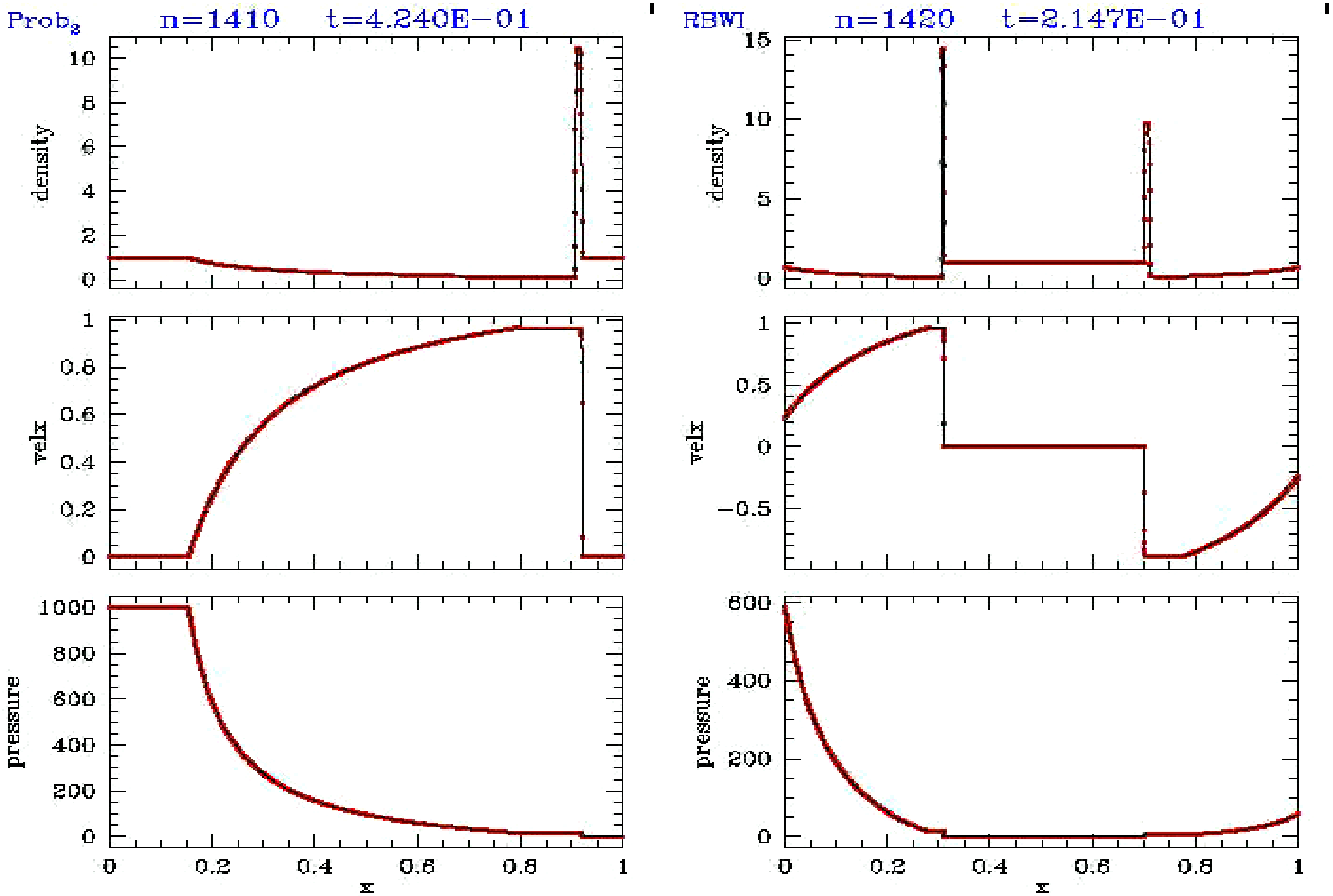

HRSC METHODS DESCRIBE ACCURATELY HIGHLY RELATIVISTIC FLOWS WITH STRONG SHOKS AND THIN STRUCTURES

relativistic magnetohydrodynamics

Fast, slow shocks & rarefactions; Alfvén waves; shock tubes.

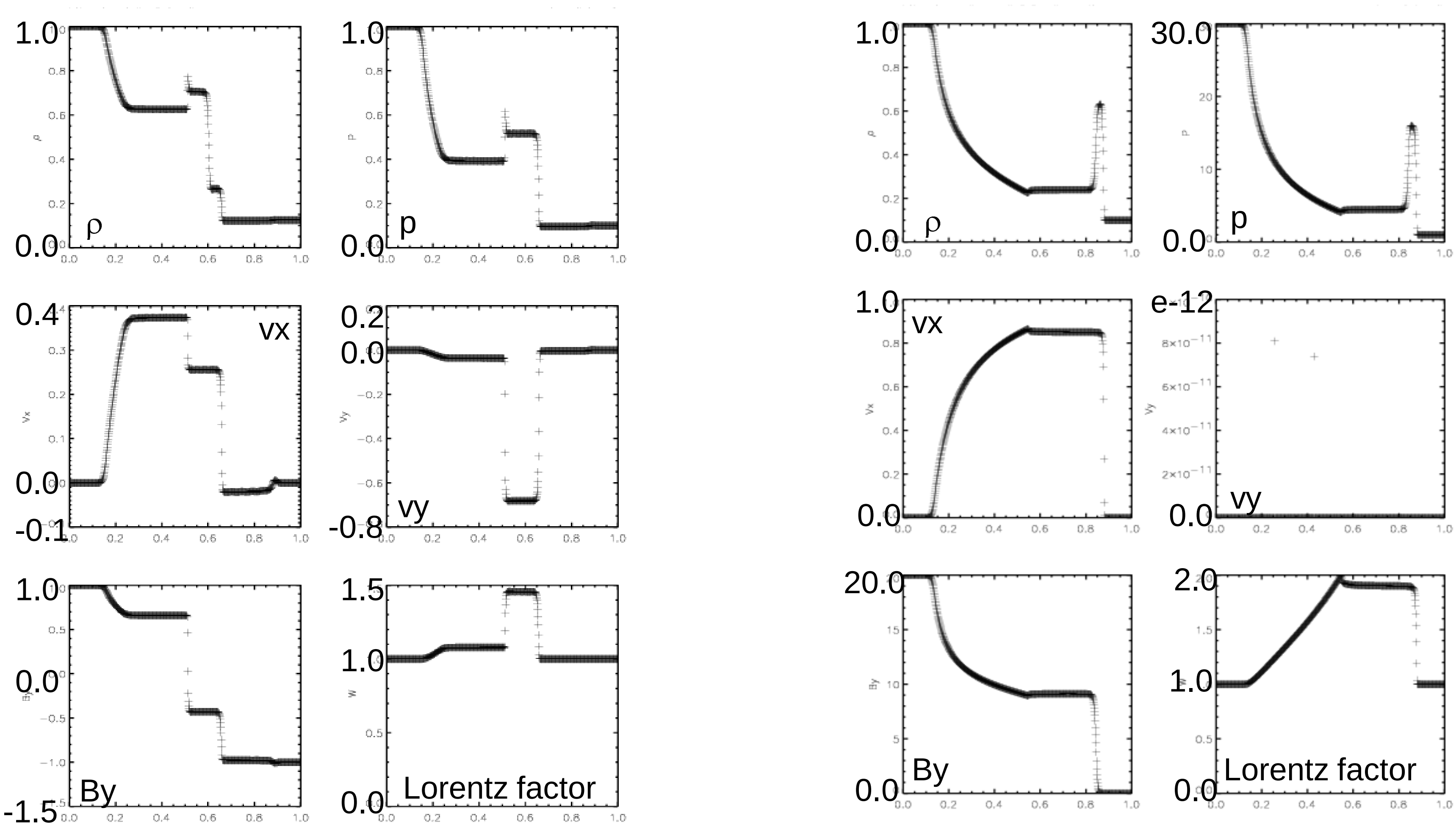

Antón et al. 2005 (also Komissarov 1999, van Putten 1993, Balsara 2001, Del Zanna et al. 2002, De Villiers & Hawley 2003, …)

first jet simulations (classical jets)

Hydrodynamical non-relativistic simulations (Rayburn 1977; Norman et al. 1982) verified the basic jet model for classical radio sources (Blandford & Rees 1974; Scheuer 1974) and allowed to identify the structural components of jets.

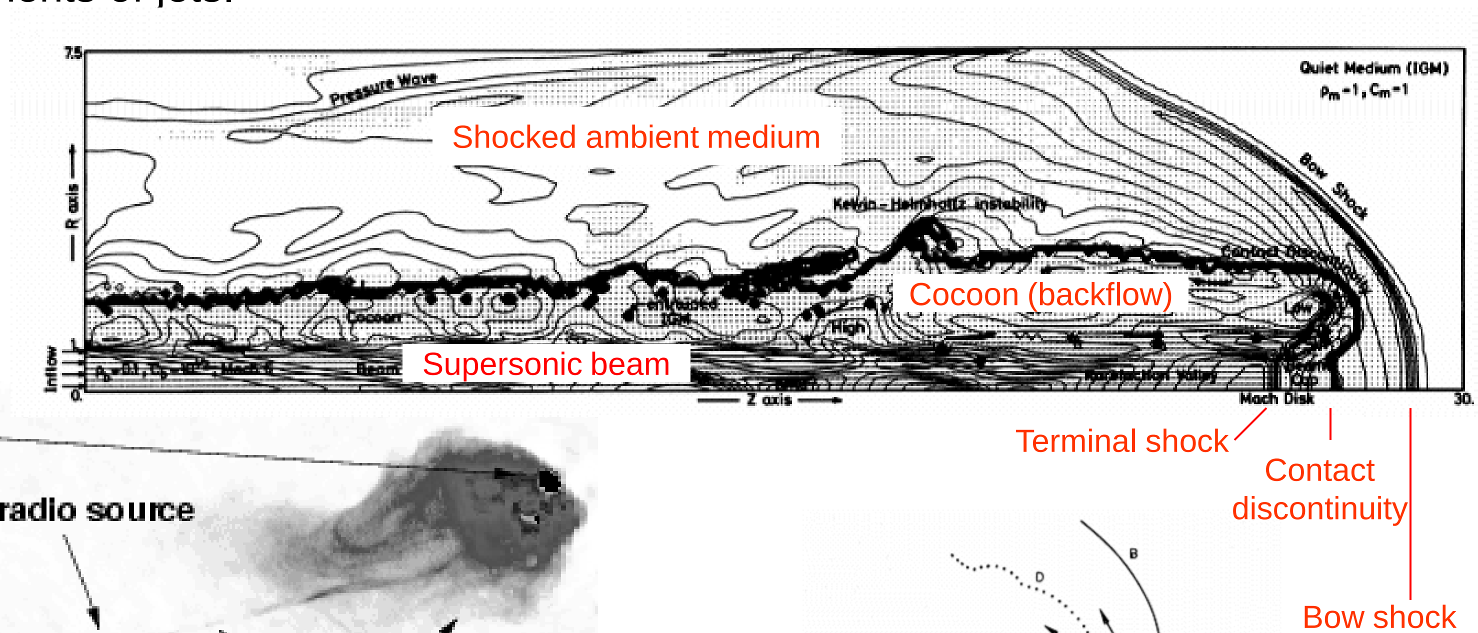

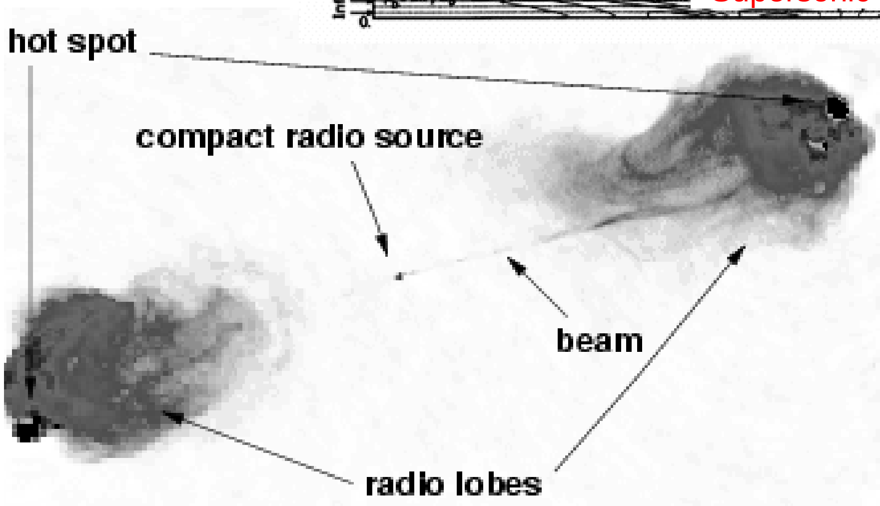

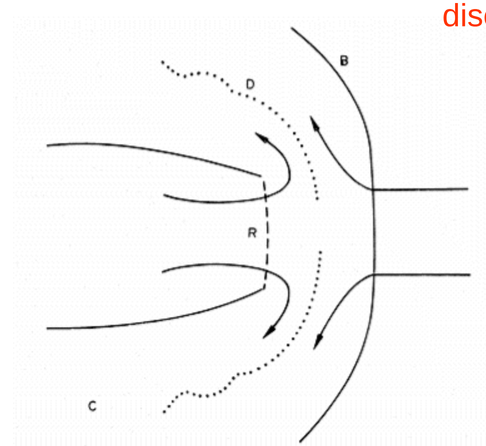

Morphology and dynamics governed by the interaction with the external medium.

relativistic jet simulations

First relativistic simulations (2D): van Putten 1993, Martí et al. 1994, 1995, 1997; Duncan & Hughes 1994

Relativistic, hot jet models

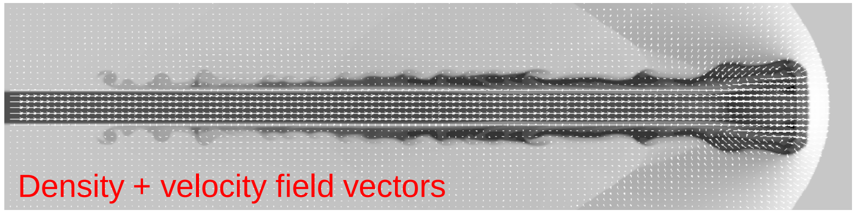

“featureless” jet + thin cocoons without backflow + stable terminal shock: naked quasar jets (e.g., 3C273)

Relativistic, cold jet models

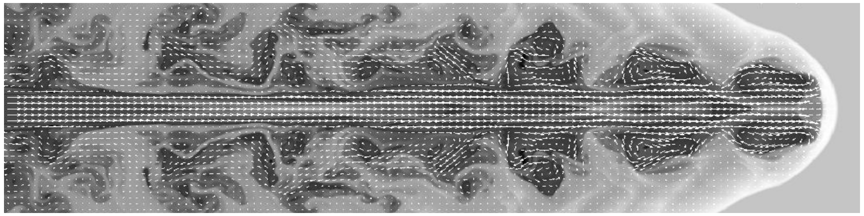

“knotty” jet + extended cocoon + dynamical working surface: FRII radio galaxies and lobe dominated quasars (e.g., Cyg A)

3D simulations (Nishikawa et al. 1997, 1998; Aloy et al. 1999; Hughes et al. 2002, Perucho et al. 2006, …)

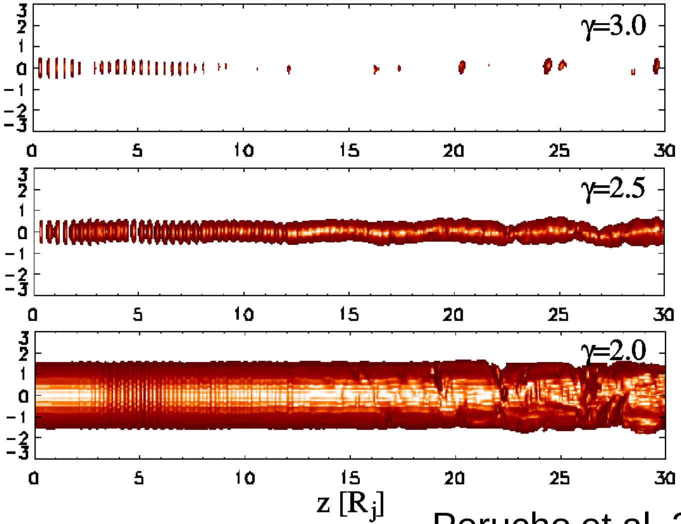

20-30 Mcells

Perucho et al. 2006

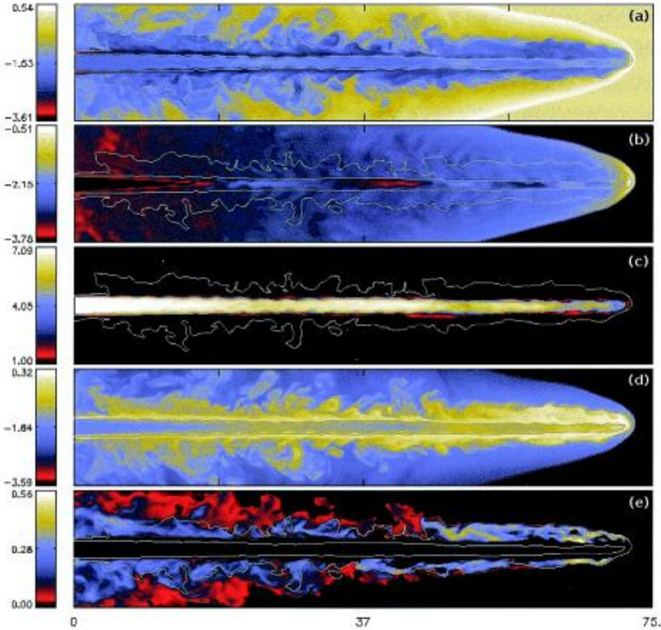

8.6 Mcells

Aloy et al. 1999

RMHD simulations

(Nishikawa et al. 1997, 1998; Komissarov 1999; Leismann et al. 2005, Keppens et al. 2008)

Relativistic jet propagation along aligned and oblique magnetic fields (Nishikawa et al. 1997, 1998)

Relativistic jets carrying toroidal magnetic fields (Komissarov 1999):

- Beams are pinched
- Large nose cones (already discovered in classical MHD simulations) develop in the case of jets with Poynting flux
- Low Poynting flux jets may develop magnetically confining cocoons (large scale jet confinement by dynamically important magnetic fields)

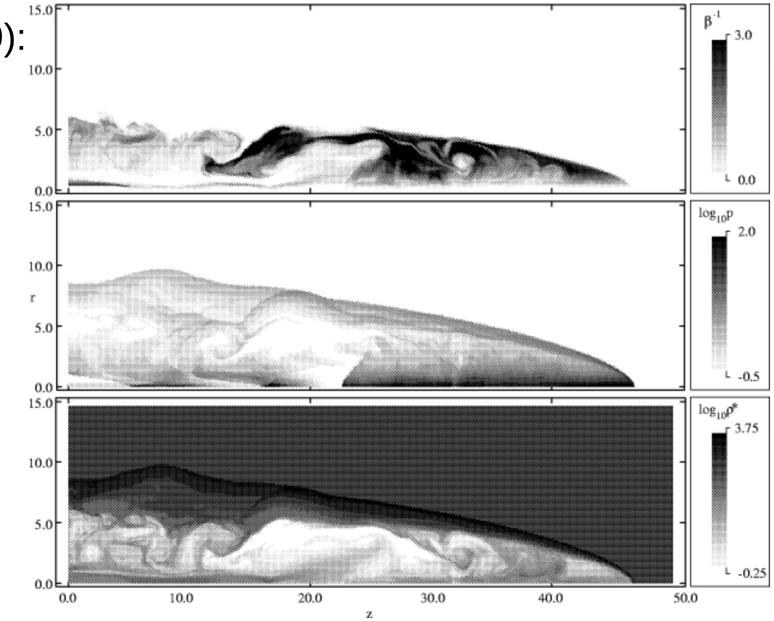

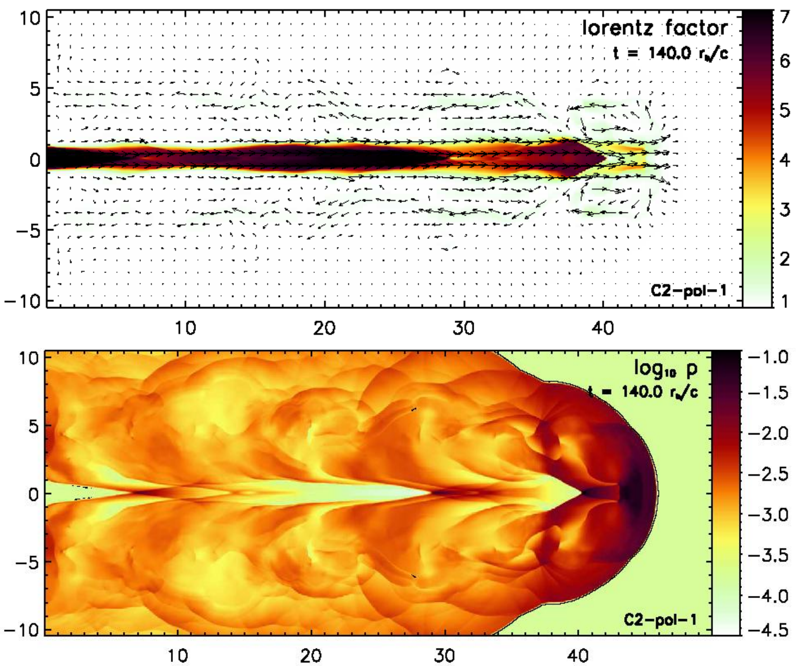

Models with poloidal magnetic fields (Leismann et al. 2005):

- The magnetic tension along the jet affects the structure and dynamics of the flow.
- Comparison with models with toroidal magnetic fields:
  - -The magnetic field is almost evacuated from the cocoon. Cocoons are smoother.
  - - Oblique shocks in the beam are weaker.

parsec-scale jets

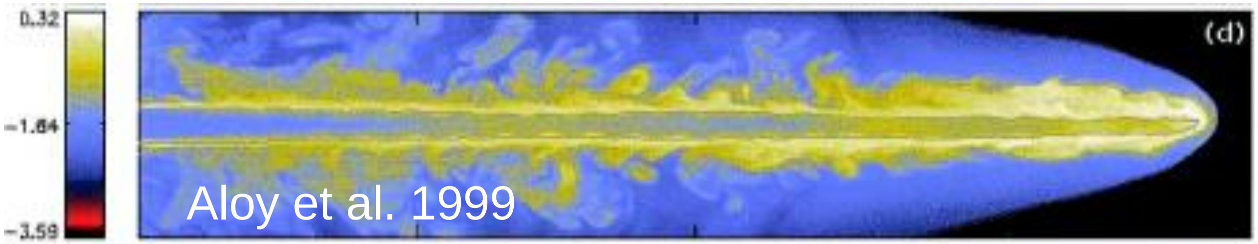

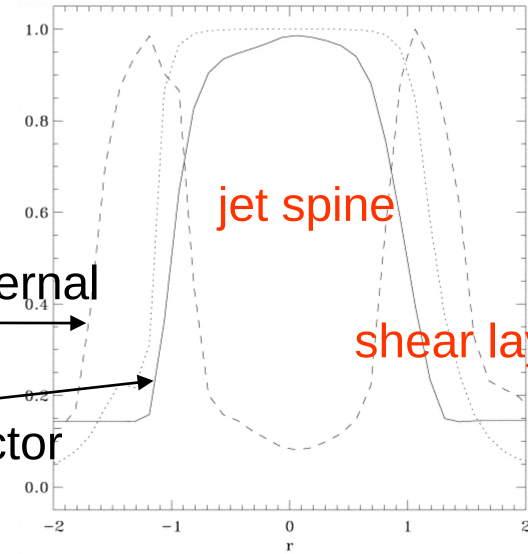

specific internal energy

Lorentz factor

shear layers in relativistic jets

Intensity across the jet

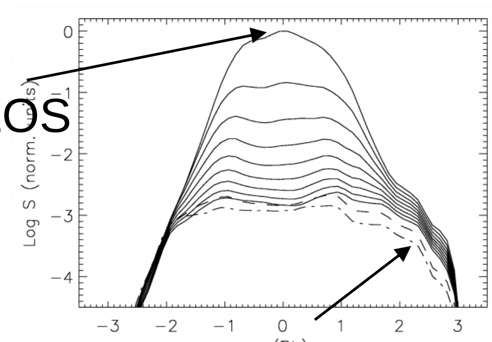

10º to the LOS

90º to the LOS

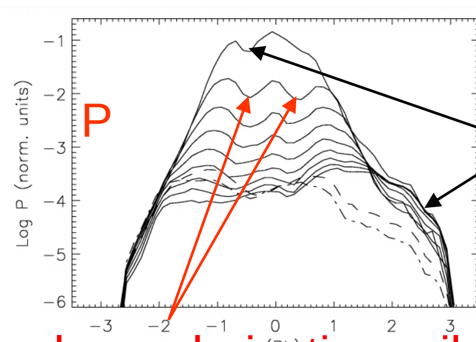

low polarization rails

top/down asymmetry

Aloy et al. 2000

parsec-scale jets

In order to compare with observations, simulations of parsec scale jets must account for relativistic effects (light aberration, Doppler shift, light travel time delays) in the emission

Basic hydro/emission coupling (only synchrotron emission considered so far; Gómez et al. 1995, 1997; Mioduszewski et al. 1997; Komissarov and Falle 1997):

- Dynamics governed by the thermal (hydrodynamic) population
- Particle and energy densities of the radiating (non-thermal) and hydrodynamic populations proportional (valid for adiabatic processes)
- (Dynamically negligible) ad-hoc magnetic field with the energy density proportional to fluid energy density
- Integration of the radiative transfer eqs. in the observer's frame for the Stokes parameters along the LoS
  - Time delays: emission (ε_ν) and absorption coefficients (κ_ν) computed at retarded times
  - Doppler boosting (aberration + Doppler shift):

$$\varepsilon^{ob}_{\nu^{ob}} = \delta^2 \varepsilon_\nu, \, \kappa^{ob}_{\nu^{ob}} = \delta^{-1} \kappa_\nu, \, \delta = \nu^{ob} / \nu = \delta(\Gamma, \cos\theta)$$

Improvements:

- Include magnetic fields consistently (passive magnetic fields: Hughes 2006; RMHD models: Roca-Sogorb, MP et al.)

- Compute relativistic electron transport during the jet evolution to acount for adiabatic and radiative losses and particle acceleration of the non-thermal population (non-relativistic MHD sims.: Jones et al. 1999; R(M)HD sims: Mimica et al. 2009)

- Include inverse Compton to account for the spectra at high energies

- Include emission back reaction on the flow (important at high frequencies)

parsec-scale jets

RHD jet simulations and emission:

- Komissarov & Falle 1996, 1997
- Gomez et al 1996, 1997, Agudo et al. 2001, Aloy et al. 2003

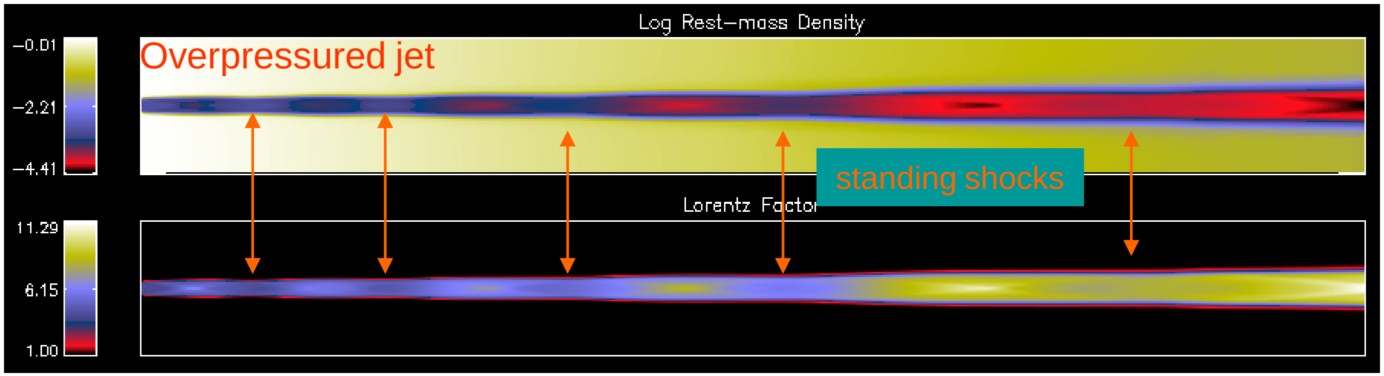

Gómez et al. 1997

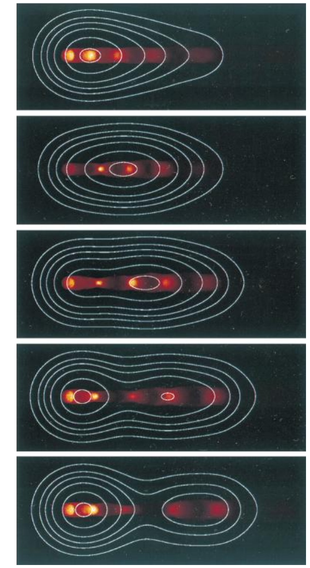

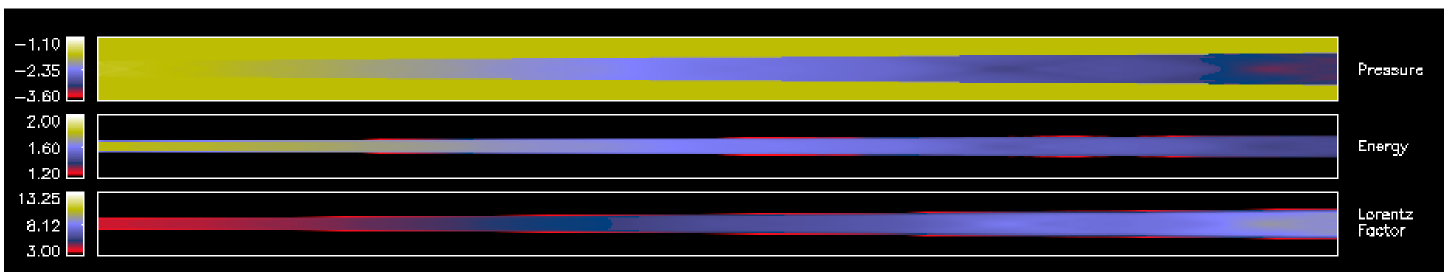

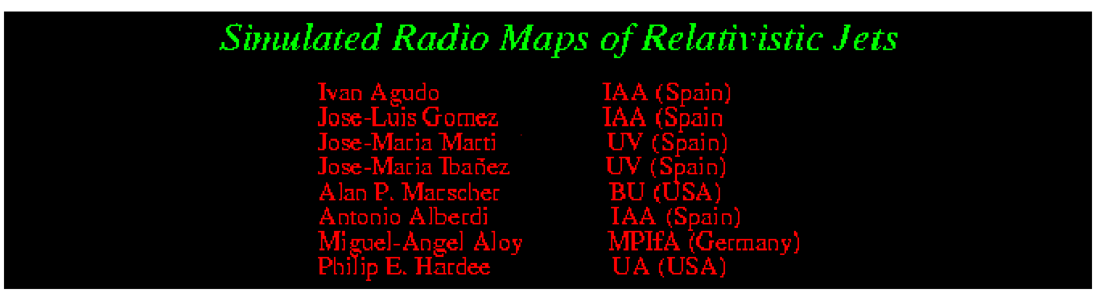

Agudo et al. 2001

parsec-scale jets

Precession and component injection in 3D and comparison with observations

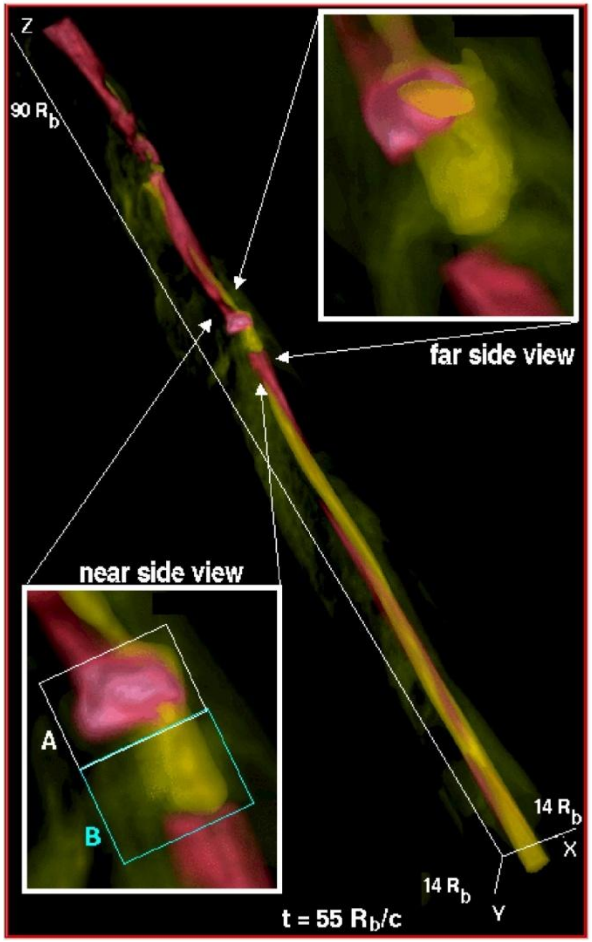

Three-dimensional ray-casting view of the simulated jet in the LAB frame. The image is produced by ray-tracing the Lorentz factor and the pressure, assigning an opacity to each volume element proportional to the magnitude of each variable.

Time sequence of the simulated radio maps (total intensity in arbitrary units using a square root brightness scale) as seen in the O-frame. The epoch is shown at the right of each snapshot. The maps are computed for a viewing angle of 15º and an optically thin frequency of 22 GHz.

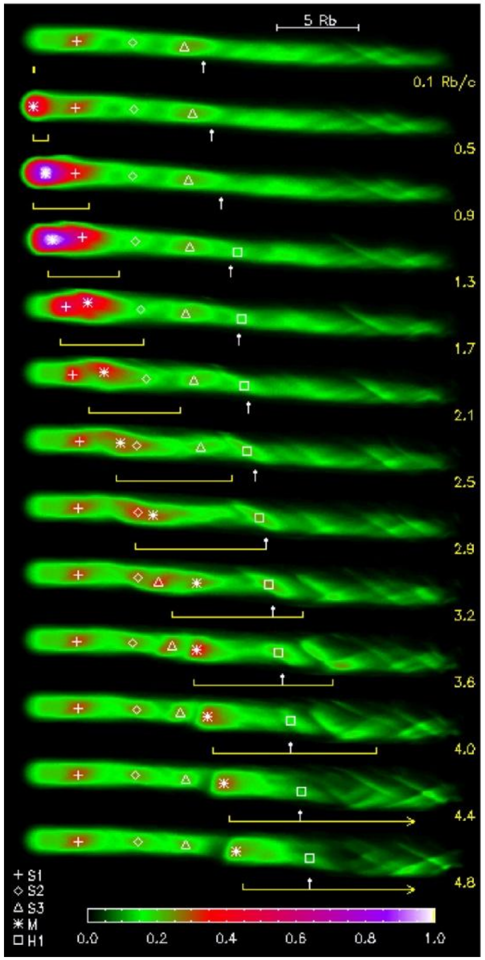

Aloy et al. 2003: 3D hydro + **emission (synchrotron) sims**. of relativistic precessing jets (including light aberration, Doppler shift and light travel time delays)

parsec-scale jets

Roca-Sogorb, MP, et al.

Goals:

- Interpret the phenomenology of polarization radio maps (role of shear layers, shocks, magnetic field configurations,…)
- probe the dynamical importance of magnetic fields

RMHD model:

- Beam flow velocity: 0.99c
- (hydrodynamic) beam Mach number: 1.75
- Overpressured jet: beam-to-ambient hydrodynamic pressure = 2
- Equipartition helical magnetic field (pitch angle: 20º)

Results confirm emission asymmetry variations as a function of the observer's angle to the LoS, θ'

(Aloy et al. 2000)

θ'

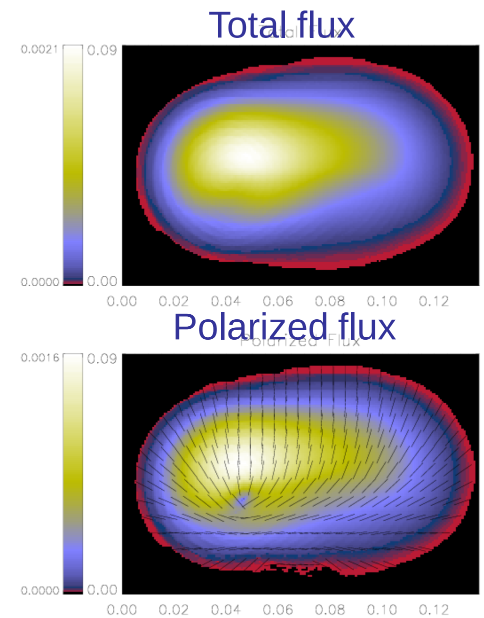

1.4º

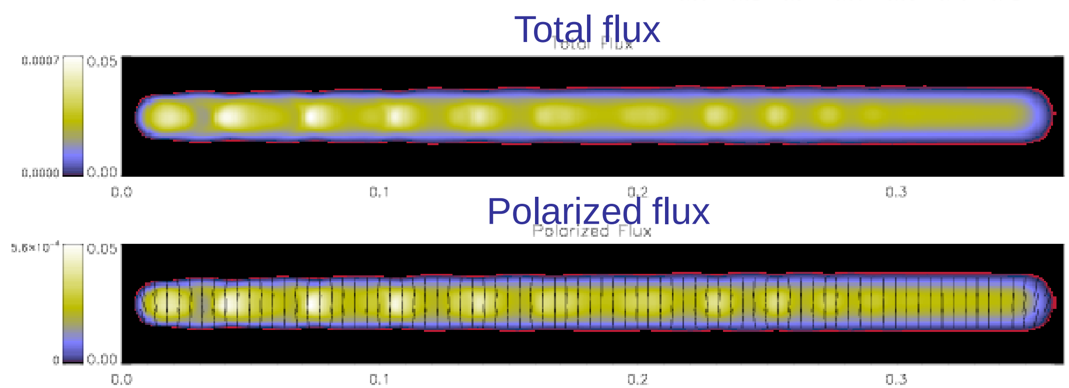

8.1º

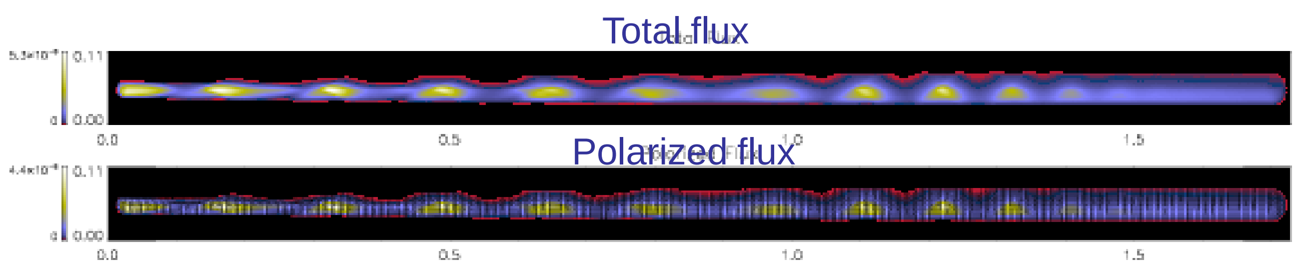

43.8º

parsec-scale jets

RMHD jet simulations and emission:
- Roca-Sogorb, MP et al.

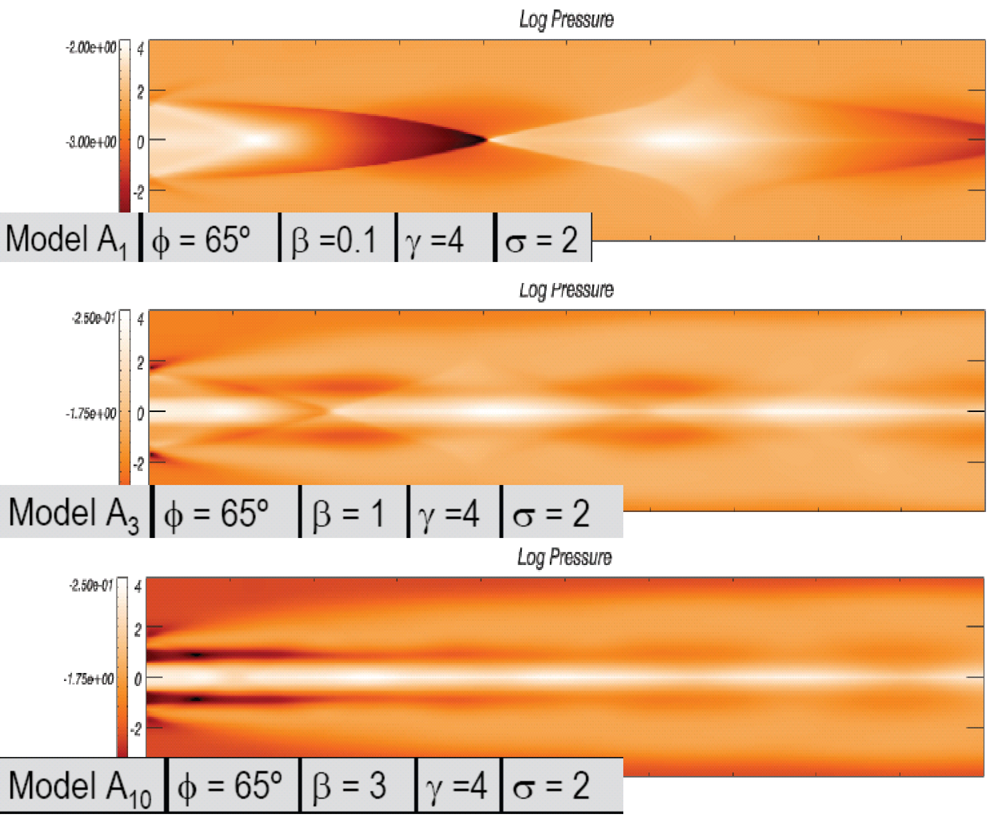

α=14º

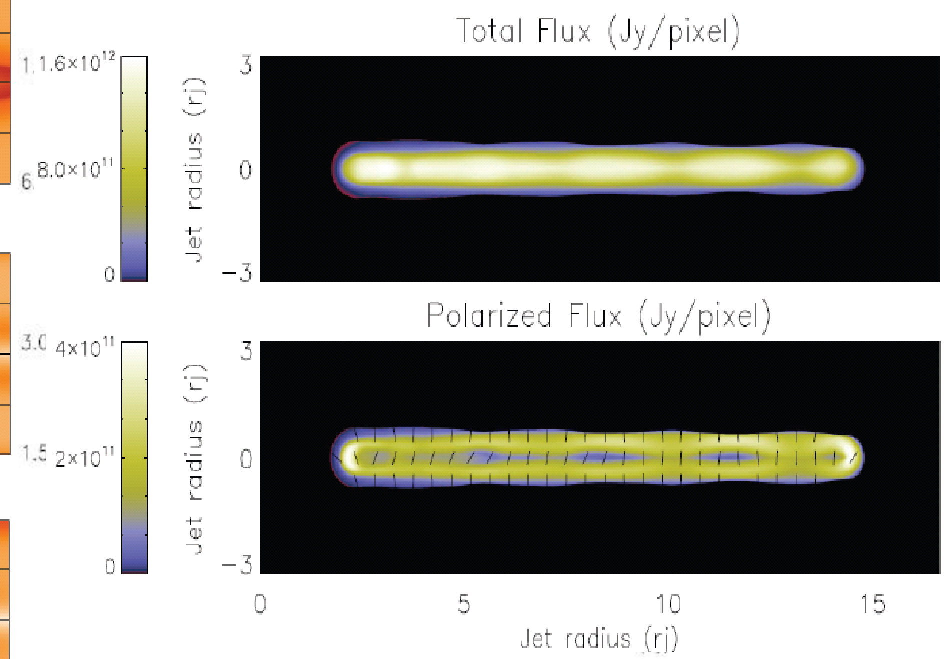

✓ For values of β>1, is the magnetic field, instead of the thermal pressure, the one that controls the jet dynamics. Jets more magnetized present more and weaker shocks in the grid length.

✓ We suggest that jets presenting stationary components may have a relative weak magnetization, with β close or below equipartition.

parsec-scale jets

Mimica et al. 2008

Spectral evolution along with the RHD simulation:

- expensive, implies evolving the ultrarelativistic particles along with the RHD eqs.

Emission: SPEV (Spectral Evolution) – LOSE (Local Synchrotron Emissivity)

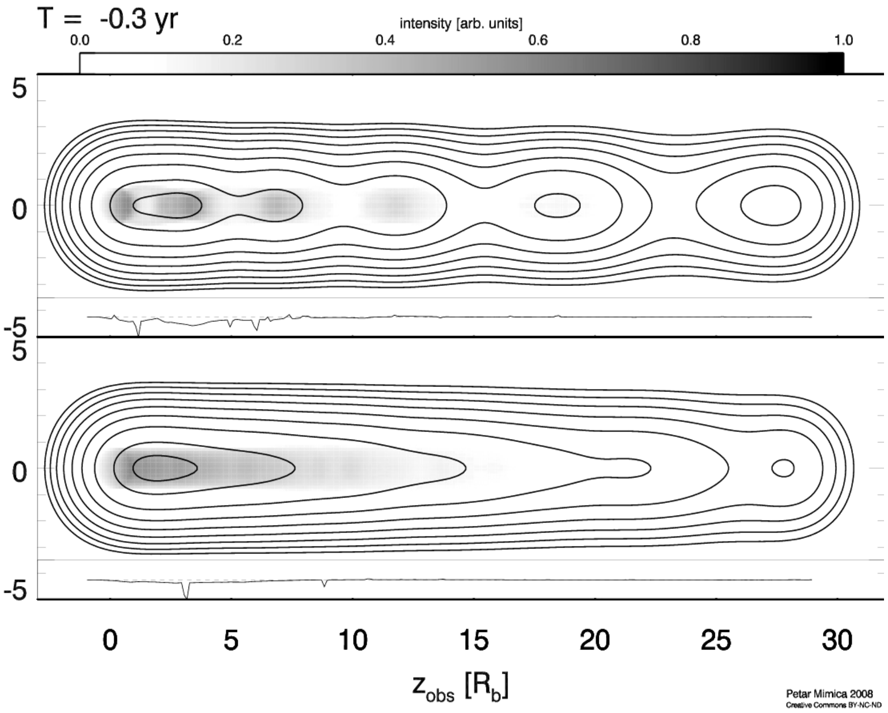

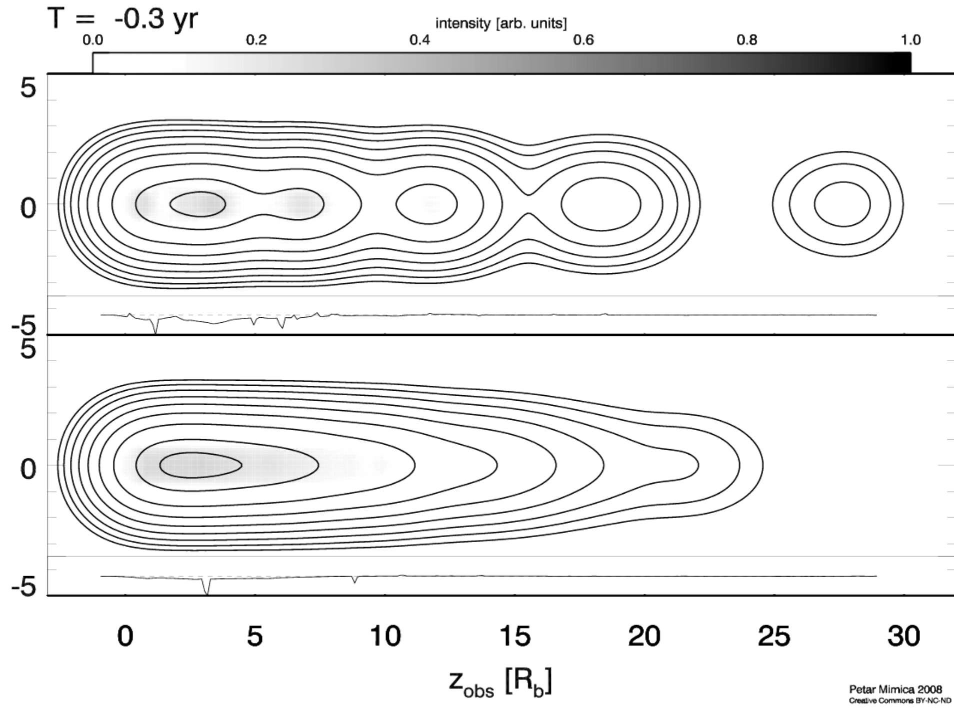

long-term evolution

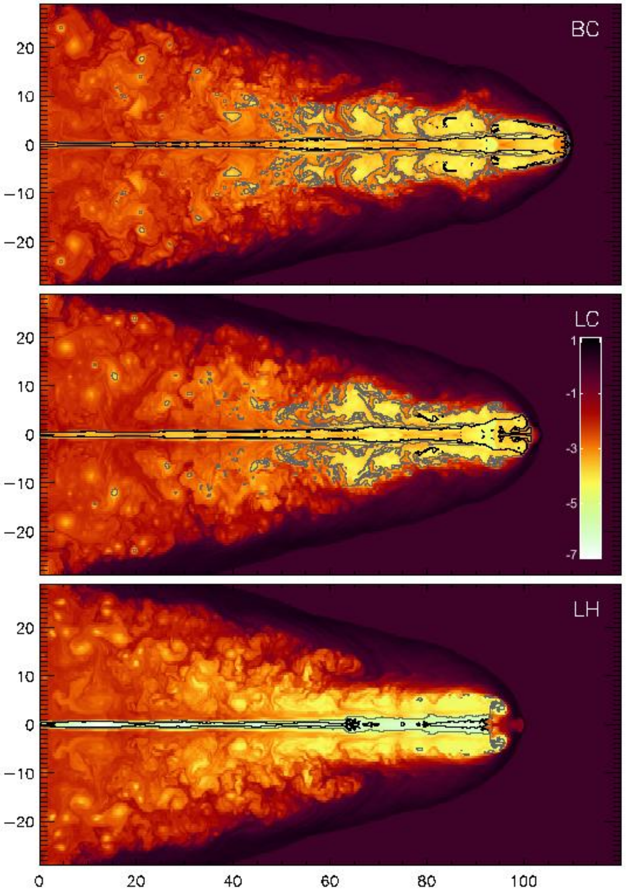

Long term evolution and jet composition (Scheck et al. 2002):

- Evolution followed up to 6 10^6 y (10% of a realistic lifetime).
- Realistic EoS (mixture of e-, e+, p)
- Long term evolution consistent with that inferred for powerful radio sources
- Relativistic speeds up to kpc scales
- Neither important morphological nor evolutionary differences related with the plasma composition

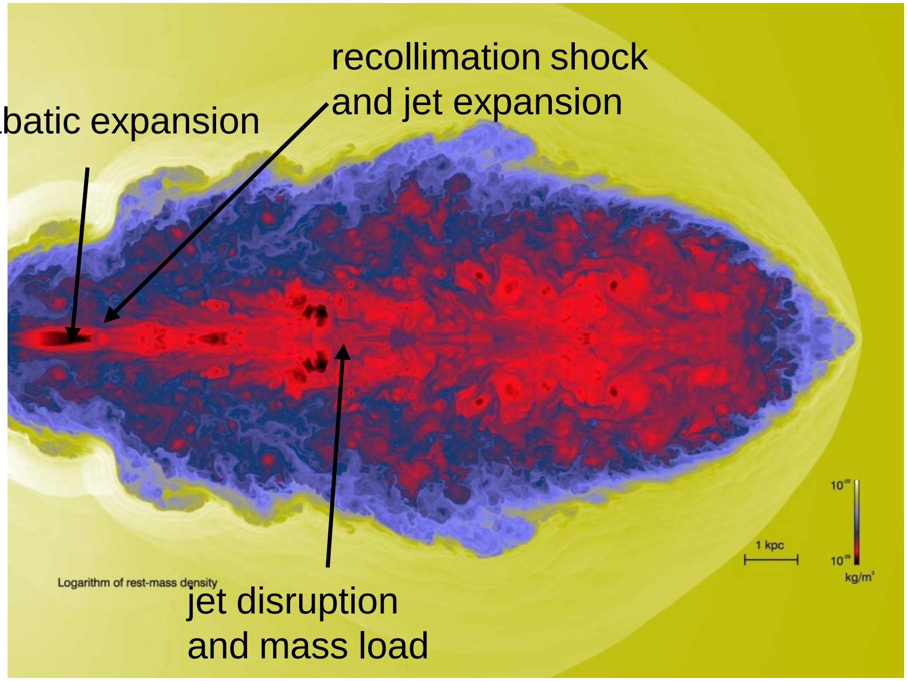

Simulations of FRI jets (Perucho & Martí 2007):

•confirm the FRI paradigm qualitatively,
•interaction with the ambient (temperatures, expected X-ray emission...),
•information on the evolution.

long-term evolution

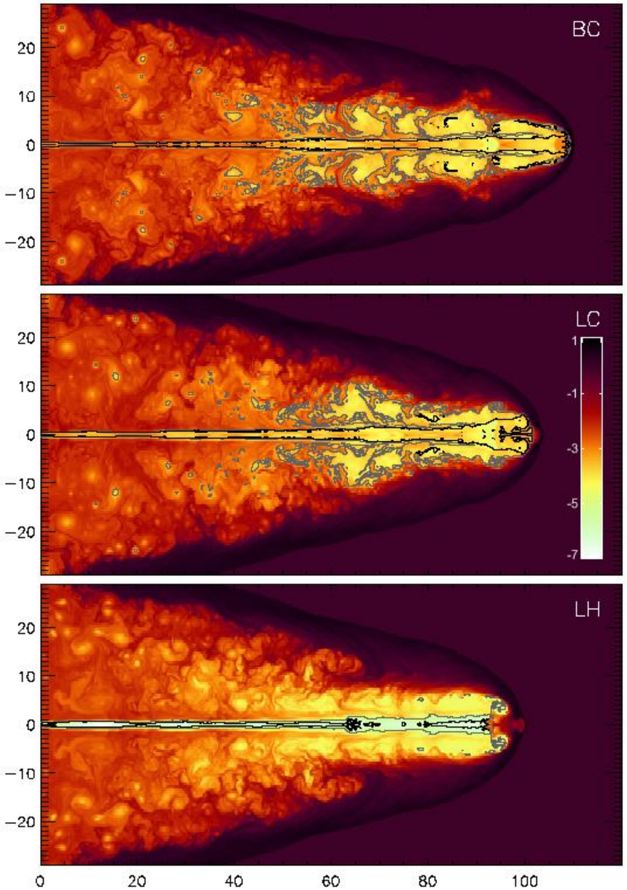

Long term evolution and jet composition (Scheck et al. 2002):

- Evolution followed up to 6 10^6 y (10% of a realistic lifetime).
- Realistic EoS (mixture of e-, e+, p)
- Long term evolution consistent with that inferred for powerful radio sources
- Relativistic speeds up to kpc scales
- Neither important morphological nor evolutionary differences related with the plasma composition

Simulations of FRI jets (Perucho & Martí 2007):

•confirm the FRI paradigm qualitatively,
•interaction with the ambient (temperatures, expected X-ray emission...),
•information on the evolution.

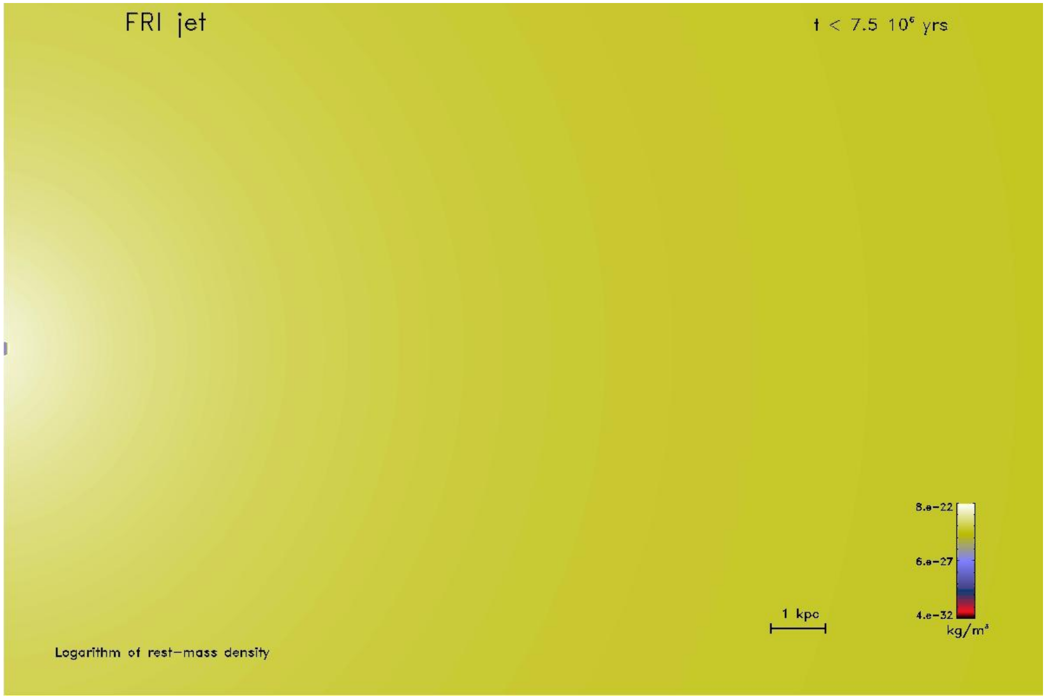

long-term evolution

Perucho & Martí 2007

Last snapshot (T = 7 10^6 yrs ~ 10 % lifetime of 3C31)

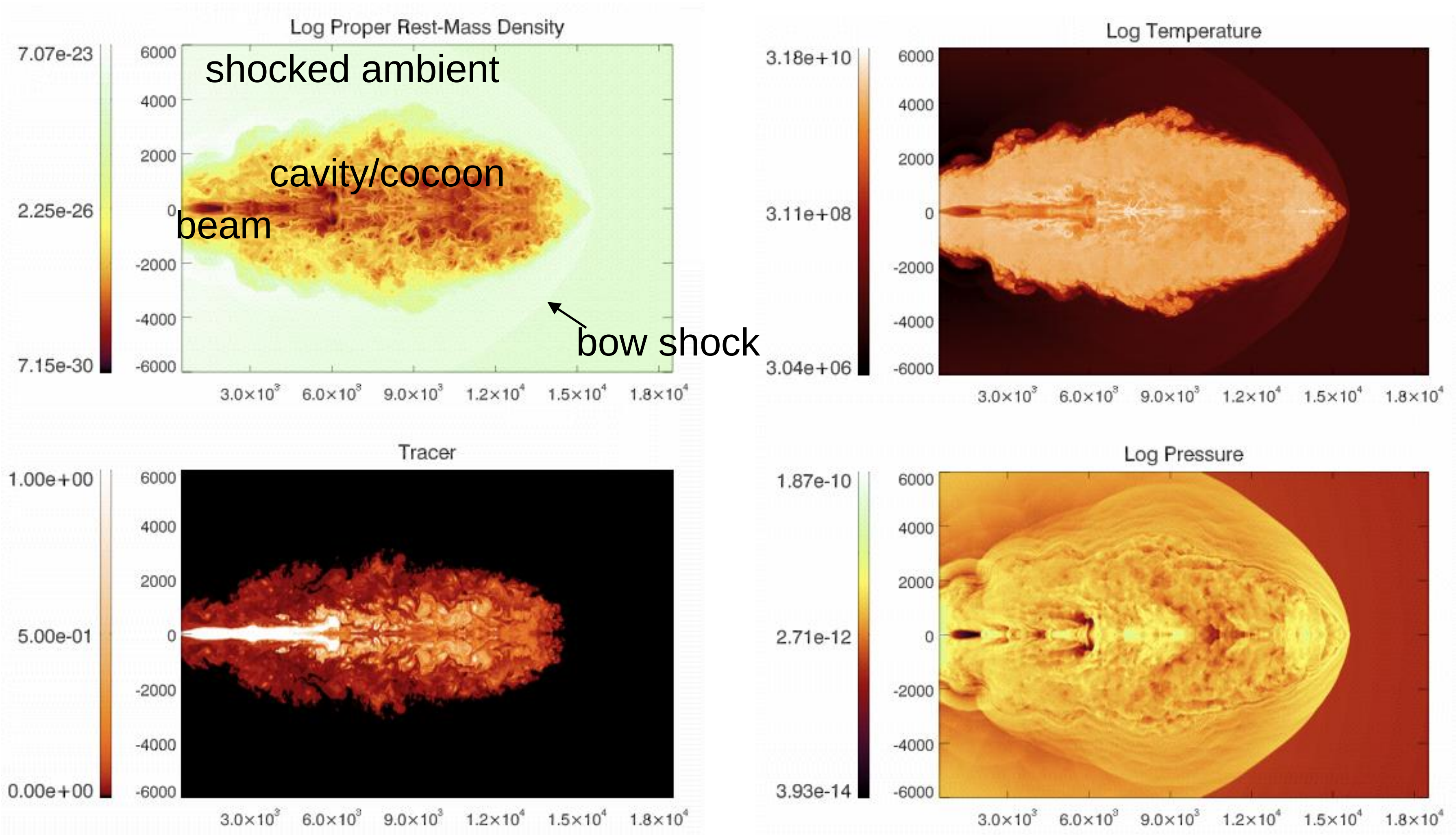

Bow shock Mach number ~ 2.5, consistent with recent X-ray observations by Kraft et al. 2003 (Cen A) and Croston et al. 2007 (NGC3081)

long-term evolution

Perucho & Martí 2007

Extended B&C model: (Perucho & Martí)

$v_{bs} \propto t^{\alpha}$

$\rho_a \propto R_s^{\beta}$

α ~ –0.1, β ~ –1

$R_s \propto t^{0.7}$

$P_s \propto t^{-1.3}$

$l_s / R_s \propto t^{0.2}$

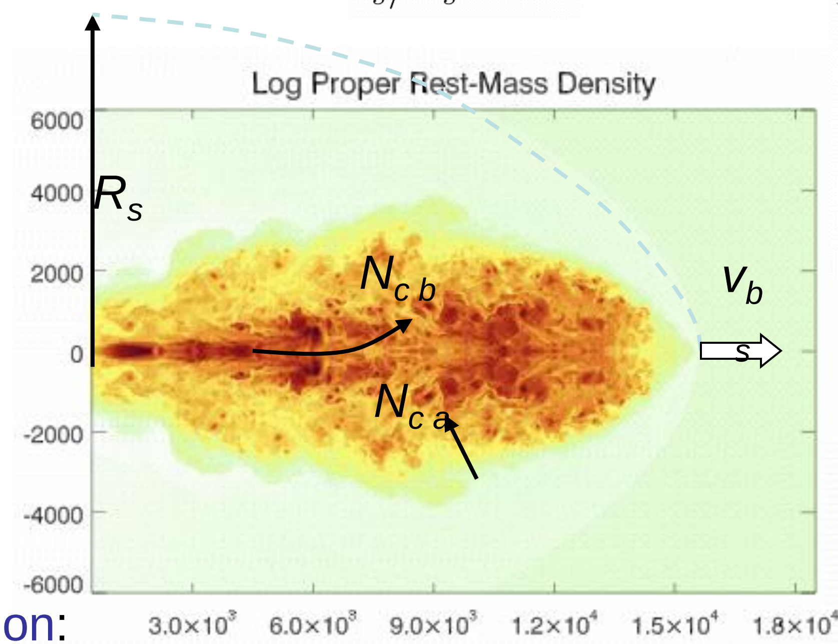

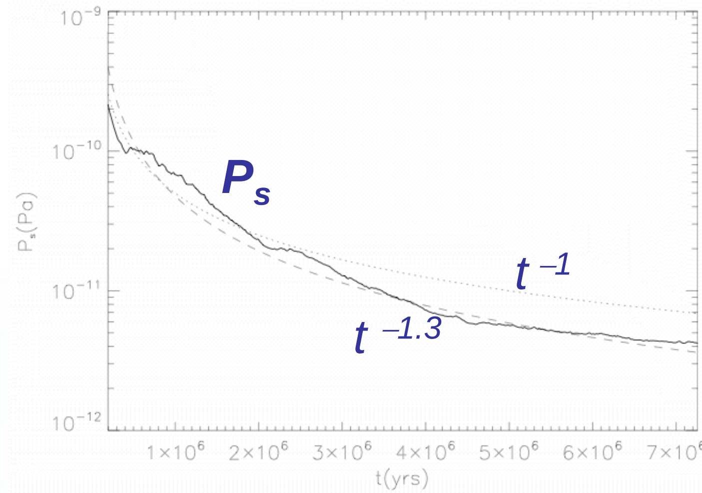

Cocoon evolution:

$$P_c \sim P_s \propto \frac{L_j}{v_{bs} A_s}$$

$$\rho_c \propto \frac{J_j}{v_{bs} A_c}$$

$$T_c \propto \frac{L_j}{J_j} \frac{A_c}{A_s}$$ ~ constant

for negligible pollution with ambient particles ($N_{c\,b}$ ~ 20 - 200 $N_{c\,a}$), and assuming selfsimilar transversal expansion

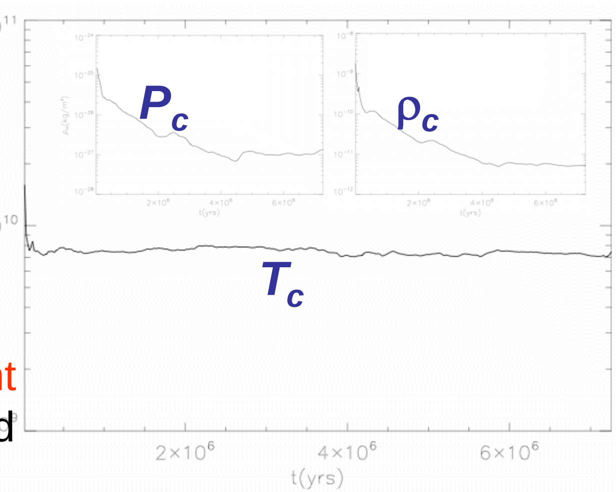

long-term evolution

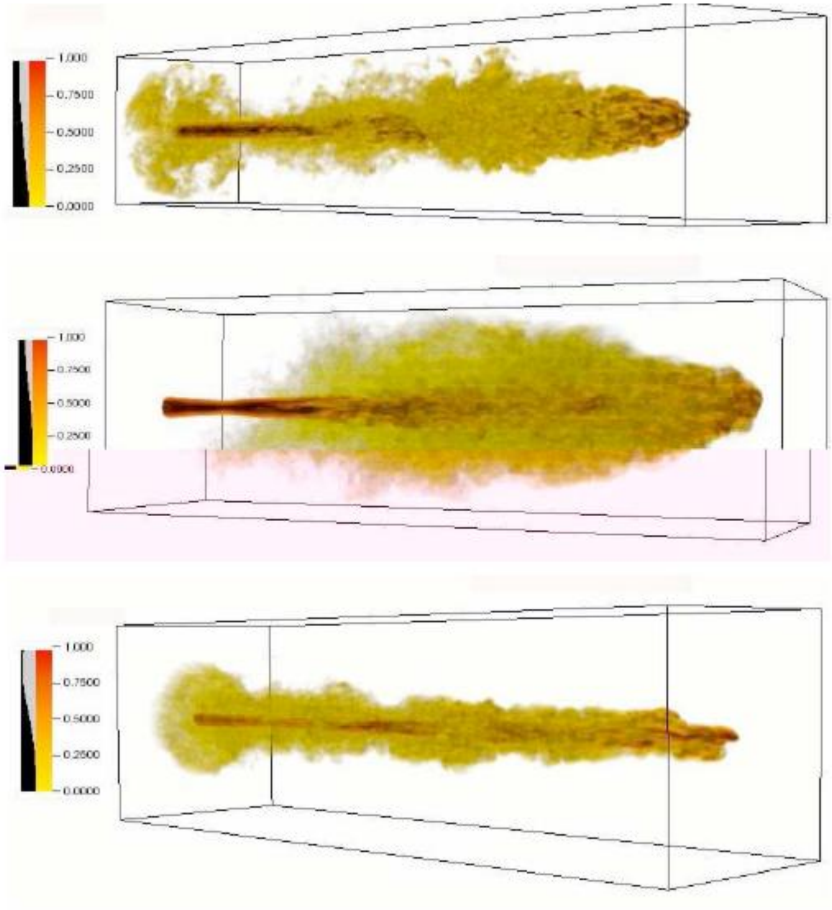

FRI jet disruption by instabilities:
Rossi et al. 2008

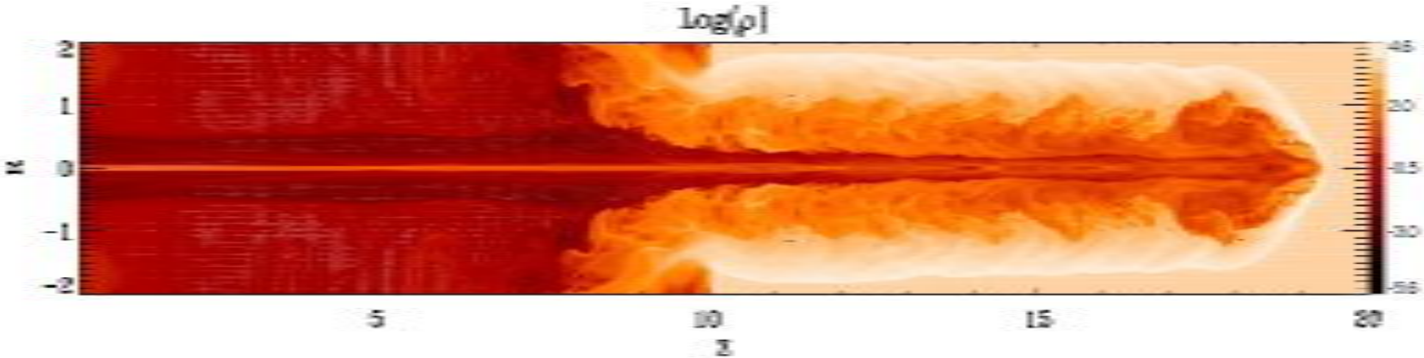

Inhomogeneous ambient medium:
Meliani & Keppens 2008

Instabilities

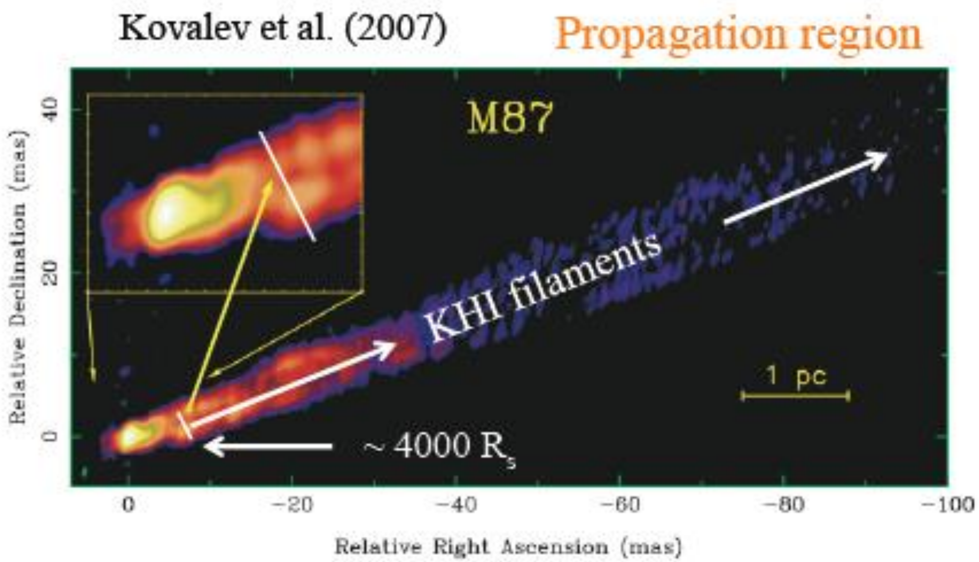

Propagation region: (KHI)

> (7 mas/sin 15^0) ~ 4000 R_s

Collimation region: (CDI/KHI)

~ 200 R_s to ~ 4000 R_s

Launching region: (CDI)

< (0.4 mas/sin 15^0) ~ 200 R_s

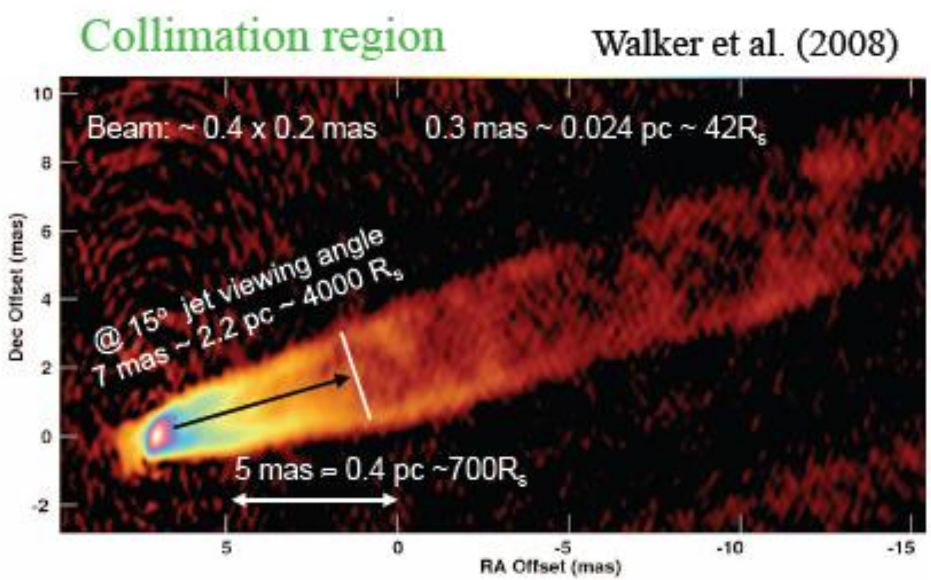

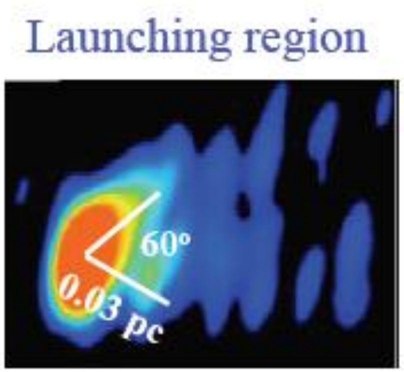

Junor, Biretta & Livio (1999)
Ly, Walker & Wrobel (2004)

Copy and paste from Phil Hardee's talk at IAU 275 meeting (with permission) .

The sub-parsec scales: CD instability

Mizuno et al. (2009, 2010, see poster)

Sub-Alfvénic regime

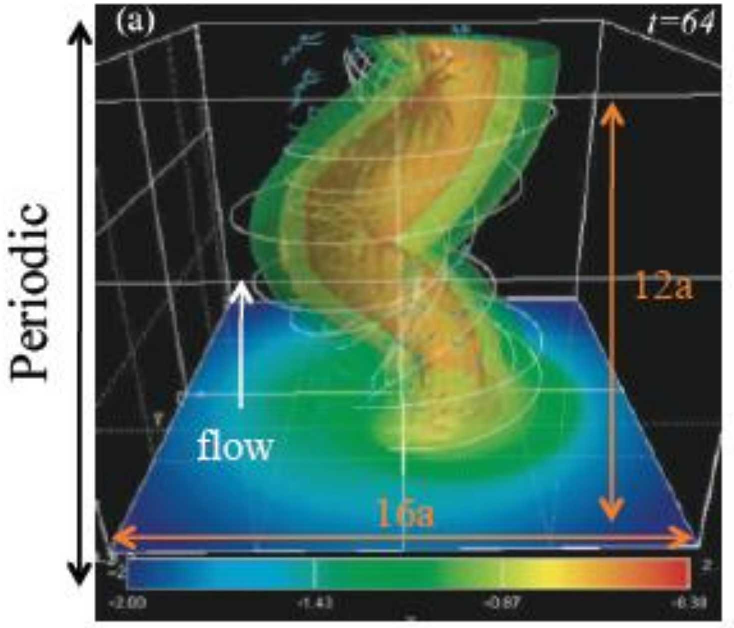

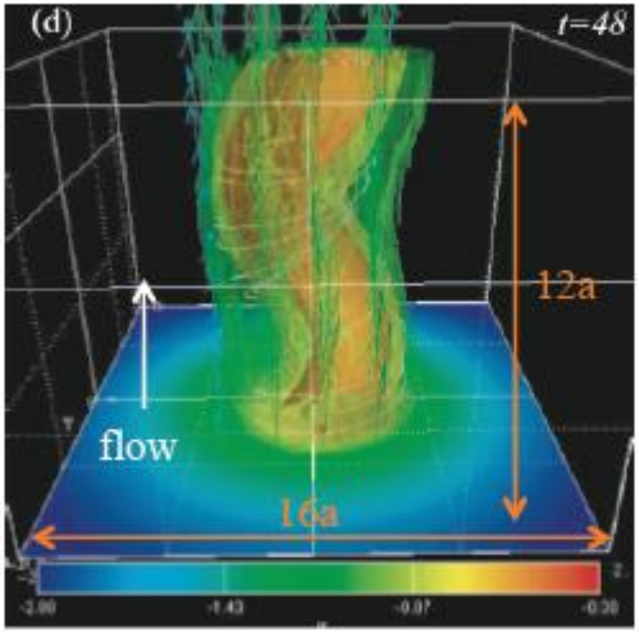

R_j = a/2: Jet flows through kink

R_j = 4a: Kink propagates with the flow

The position of the velocity shear with respect to the characteristic radius of the magnetic field has an important effect on the propagation of the CD instabilities .

CD INSTABILITY

There is an efficient conversion of energy from the Poyinting flux to particles.

The sub-parsec scales: CD/KH

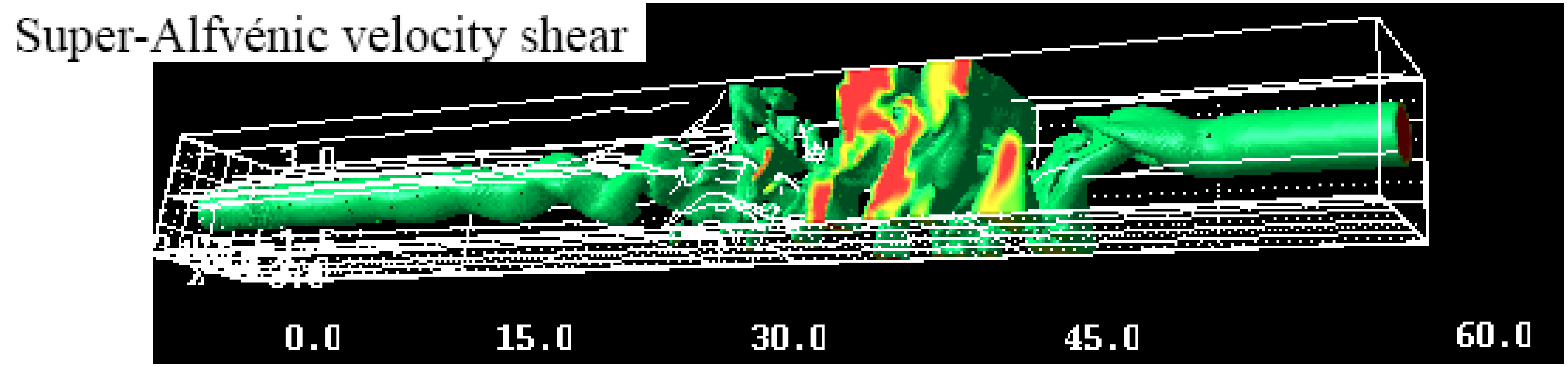

3D isovolume of density with B-field lines show the jet is disrupted by the growing KH instability

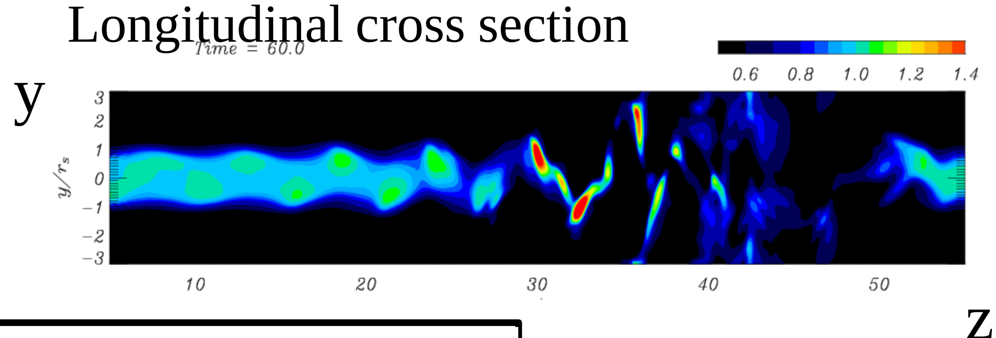

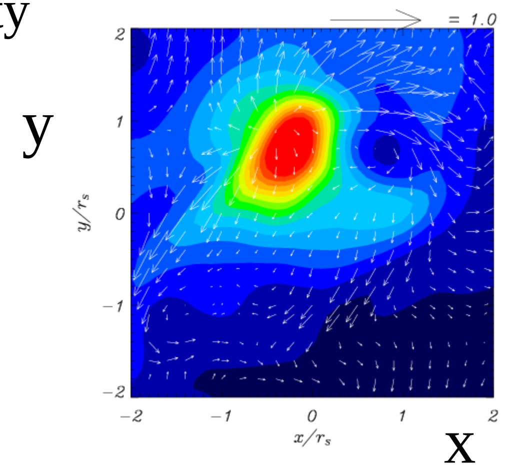

Transverse cross section

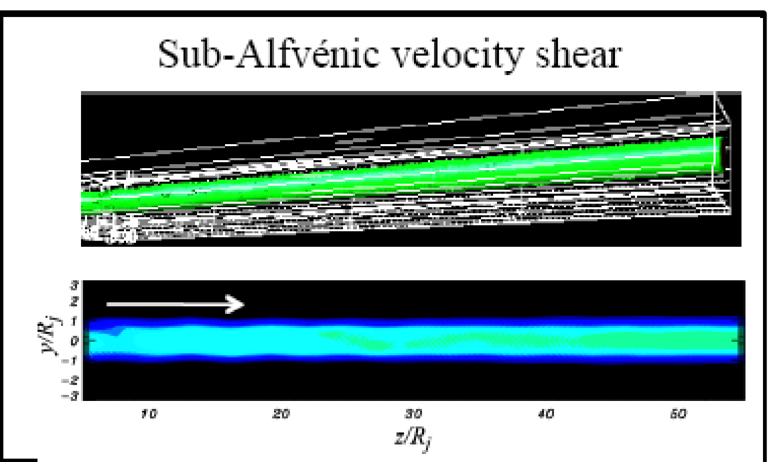

Mizuno et al. 2007

Non-relativistic: Hardee & Rosen 1999, 2002: Helical B field stabilizes the jet (magnetic tension).

The parsec scales and beyond: KH instability

Perucho et al. (2004a, 2004b)

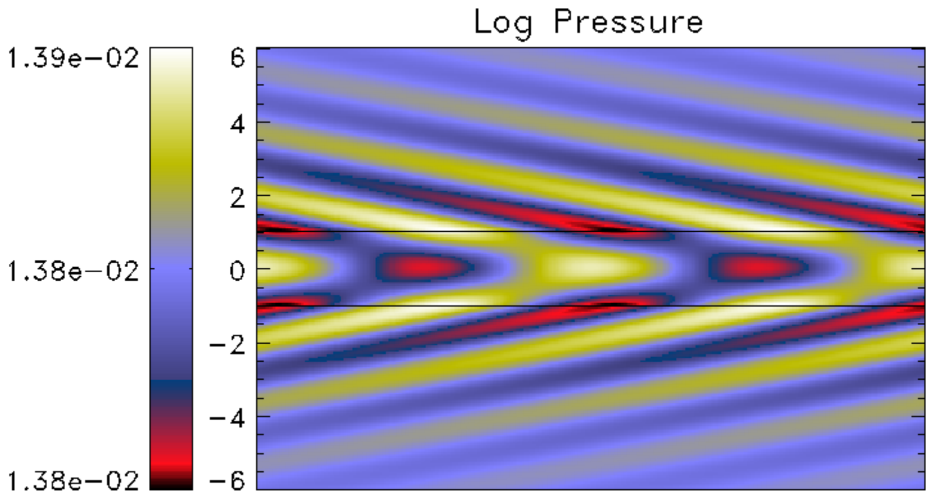

Initial model

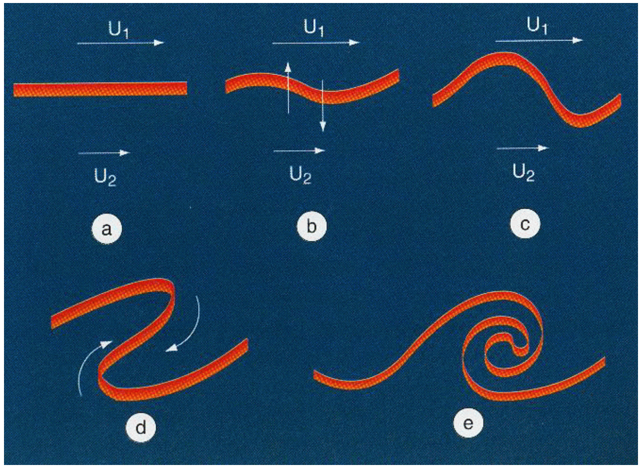

- Parameters:
  - Lorentz factor.
  - Rest-mass density contrast.
  - Specific internal energy.
  - Pressure equilibrium.

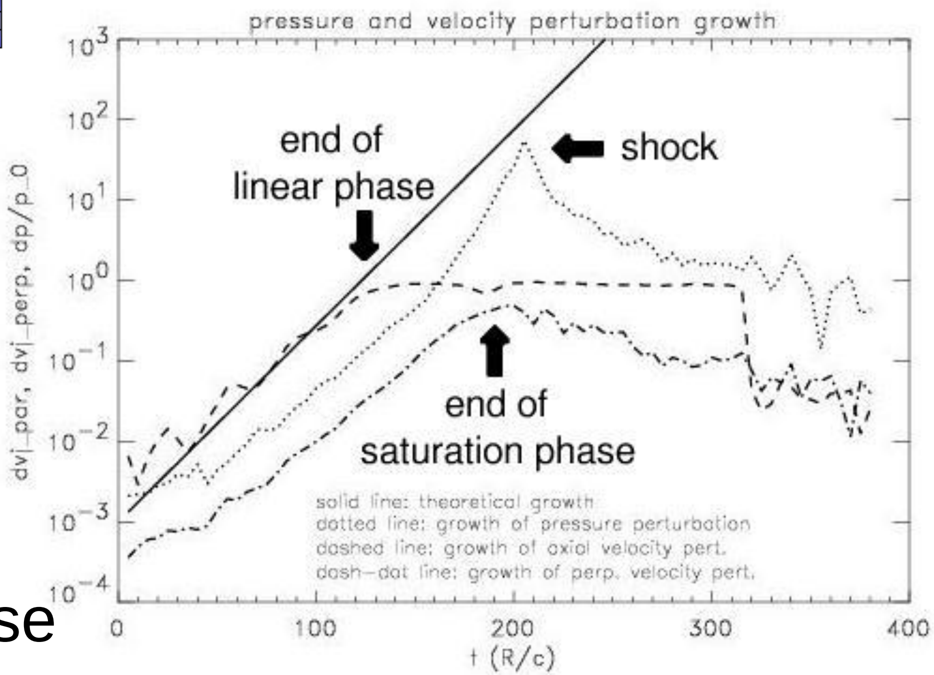

Linear phase

The parsec scales and beyond: KH instability

Axial velocity pert.

Pressure pert.

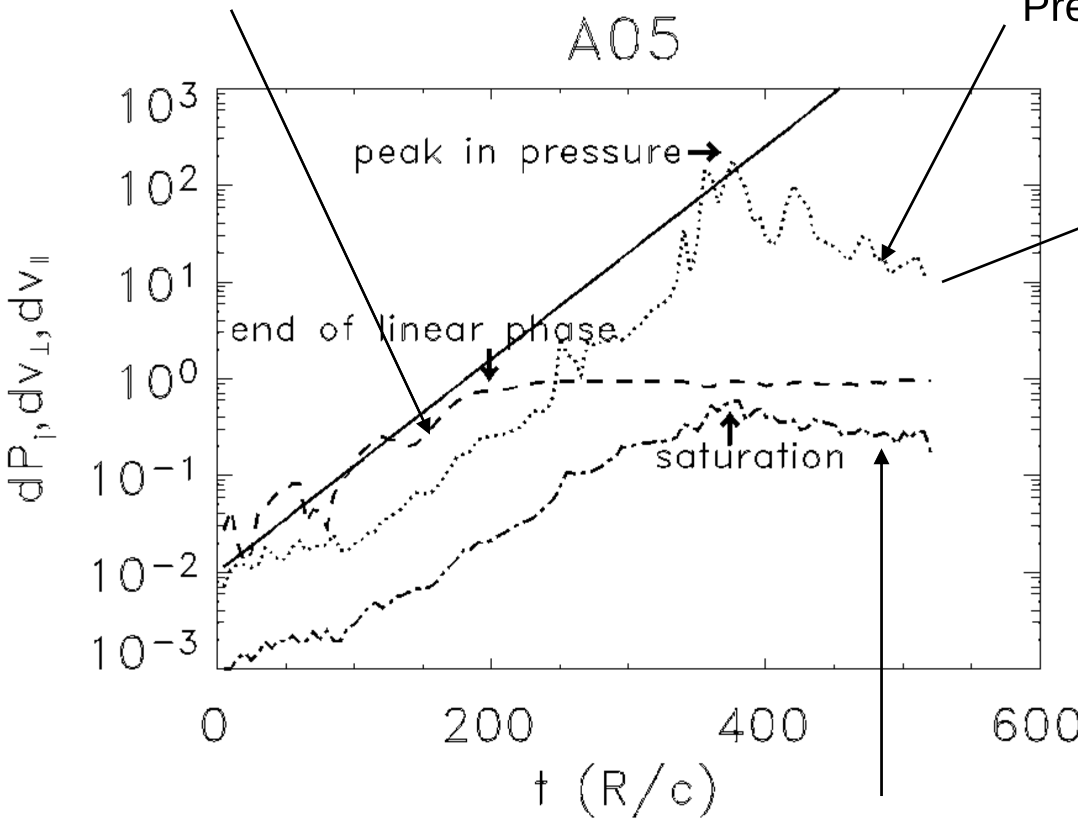

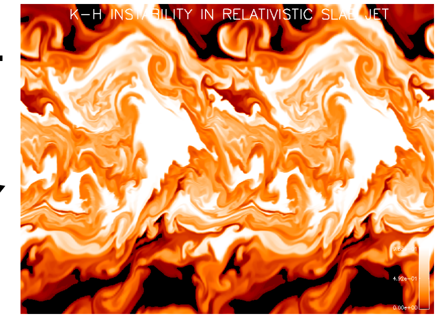

Perp. velocity pert.

SATURATION

$$V_\parallel^{(e)\pm} < \frac{c}{2\gamma^2}$$

$$V_\perp^{(e)\pm} < \frac{c}{2\gamma}$$

$$V_\parallel^{(j)} = \gamma^2 V_\parallel^{(e)},$$

$$V_\perp^{(j)} = \gamma V_\perp^{(e)},$$

-KH instabilities saturate when the amplitude of the perturbation of axial velocity (in the jet reference frame) reaches the speed of light (Hanasz 1995, 1997).

The parsec scales and beyond: KH instability

Discovery of resonant modes and their effect via numerical simulations (Perucho et al. 2005, 2007)

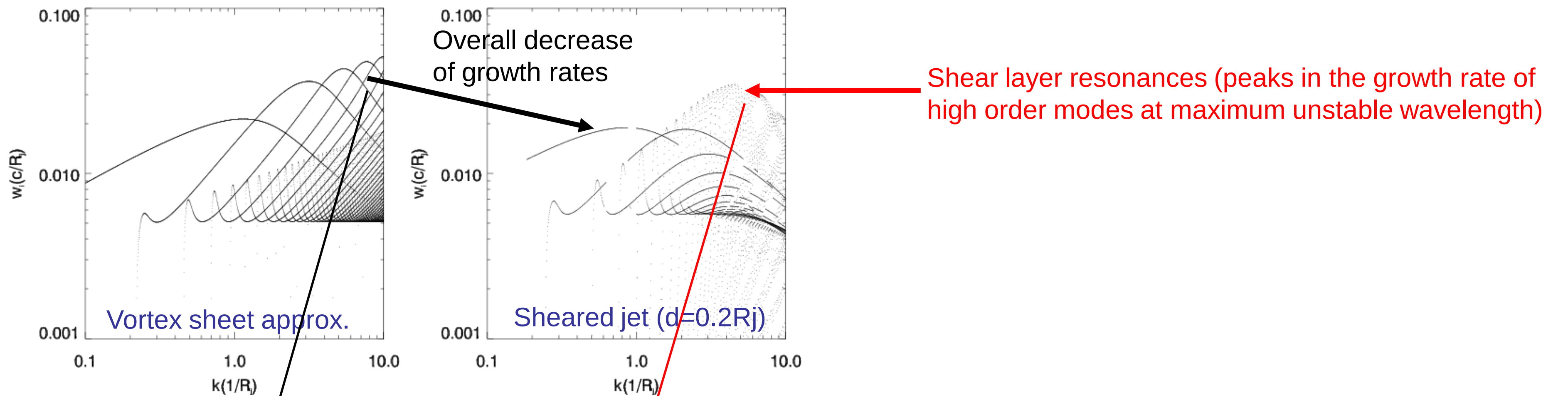

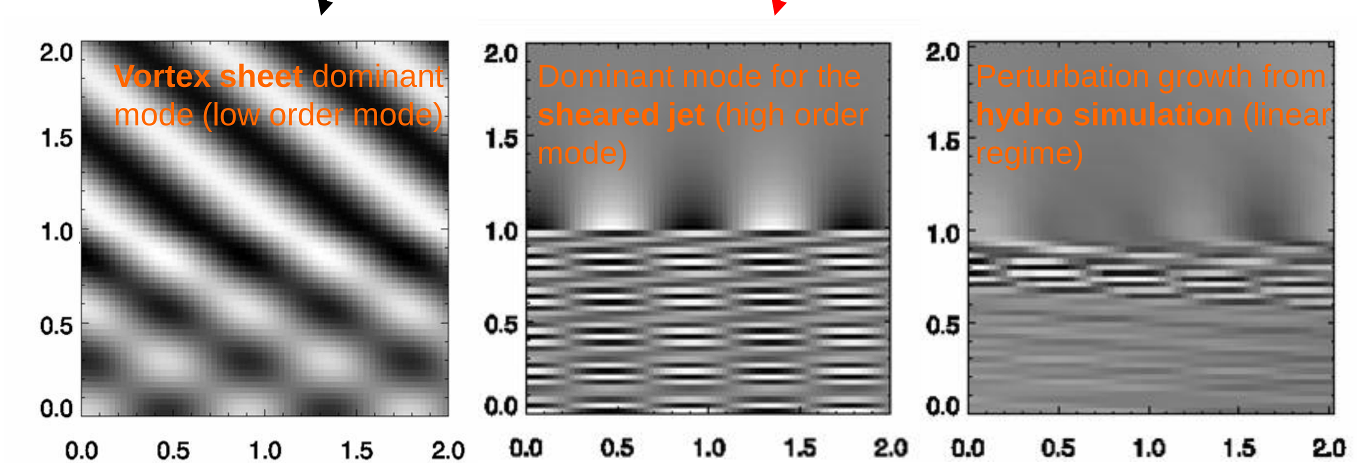

theoretical representation | theoretical representation | numerical simulation

Numerical simulations confirm the dominance of resonant modes in the perturbation growth

The parsec scales and beyond:
KH instability

Perucho et al. 2005, 2007

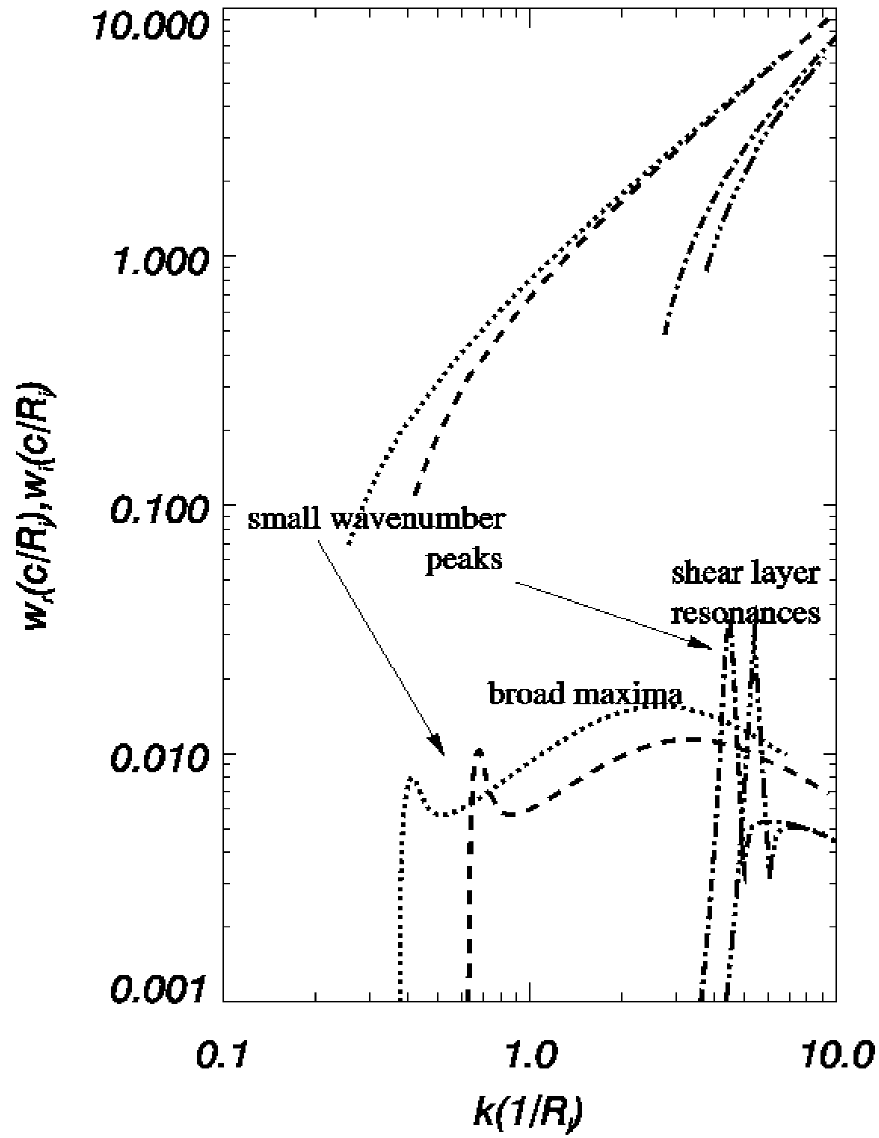

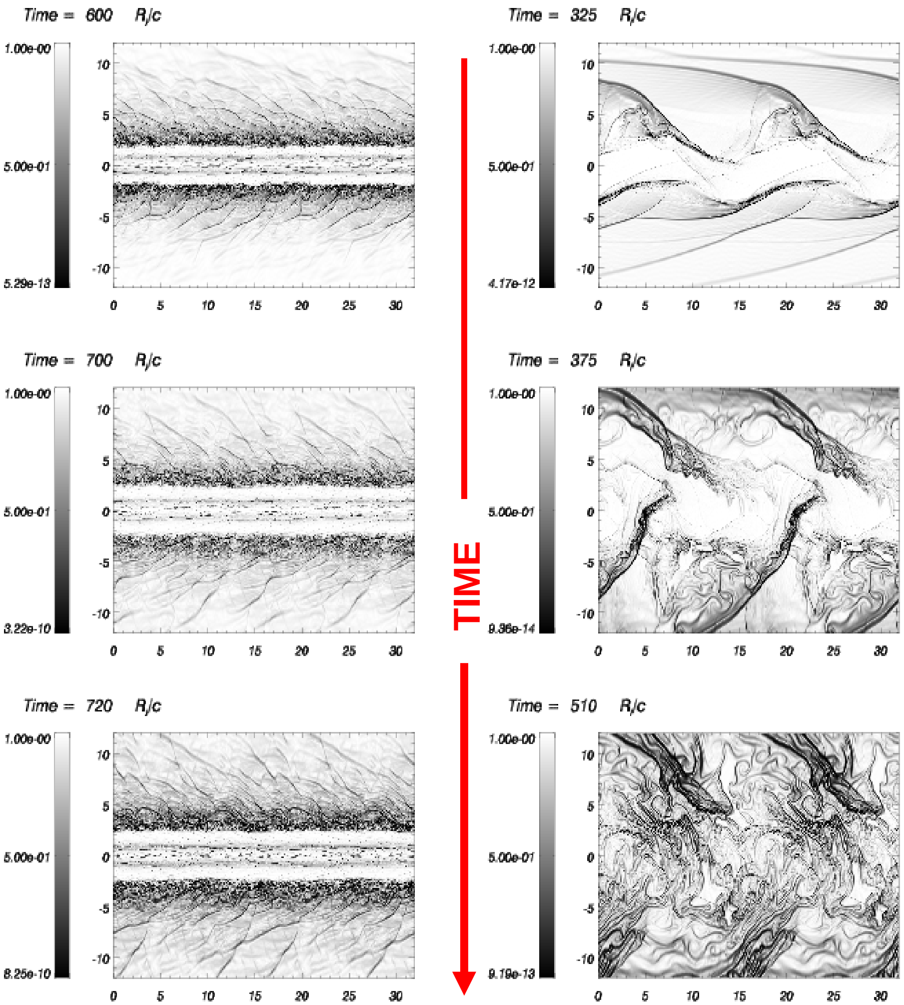

Sheared jet (d=0.2 Rj)
Lorentz factor 20

Sheared jet (d=0.2 Rj)
Lorentz factor 5

See also short λ saturation (Hardee 2011)

The parsec scales and beyond: KH instability

- UST1: efficiently mixed and slowed down.
- UST2: progressive mixing and slowing.
- ST: resonant modes avoid disruption and generate a hot shear layer that protects the fast core.

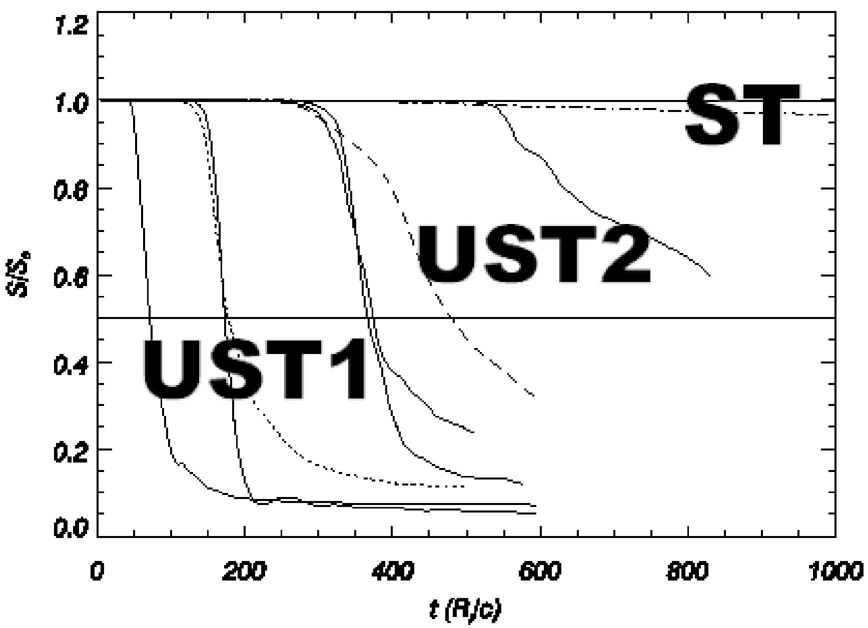

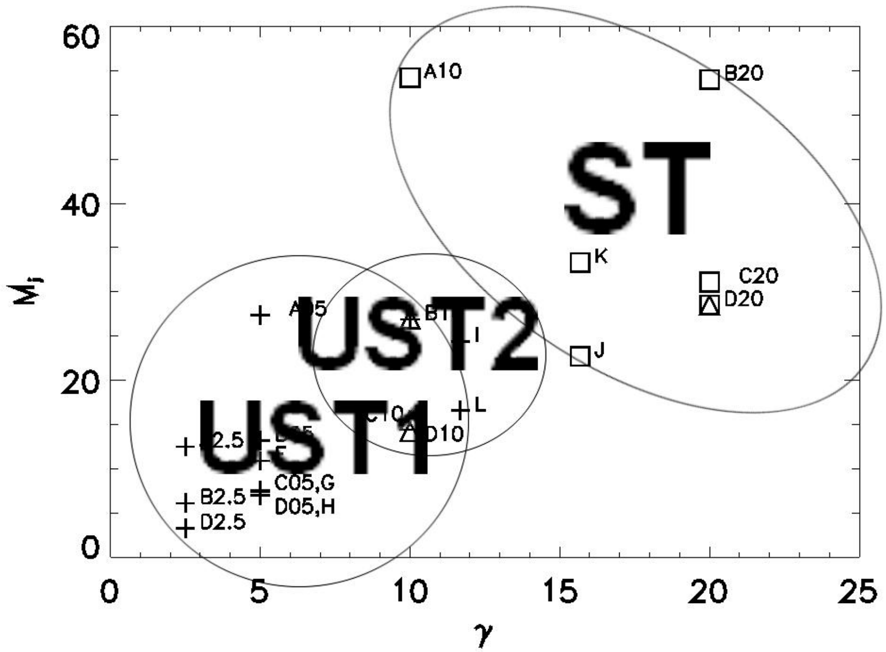

The parsec scales and beyond: KH instability

- Shear layer (mean profiles of variables).
  - Upper panels: thermodynamical variables.
  - Lower panels: dynamical variables.

Perucho et al. 2005

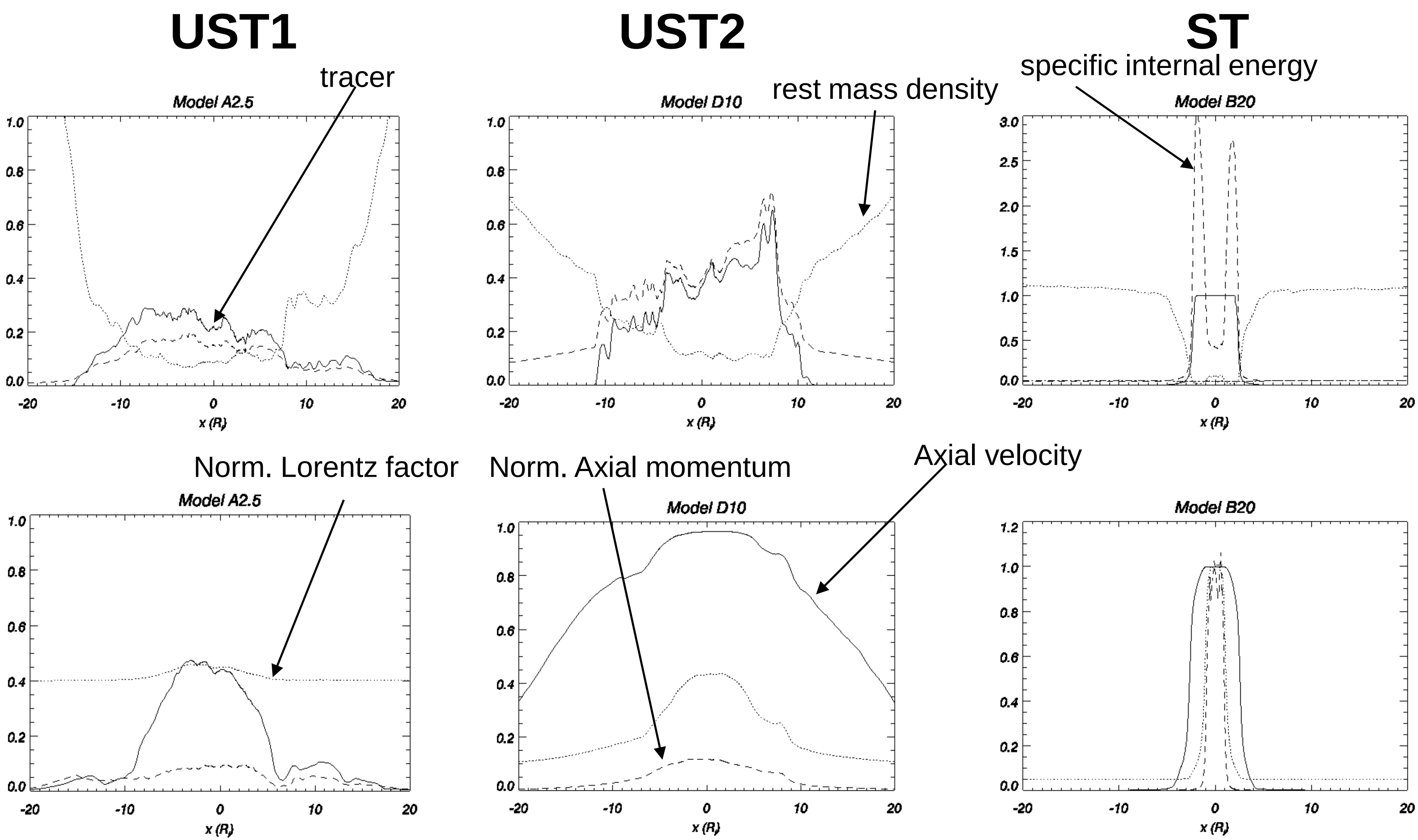

The parsec scales and beyond: KH instability

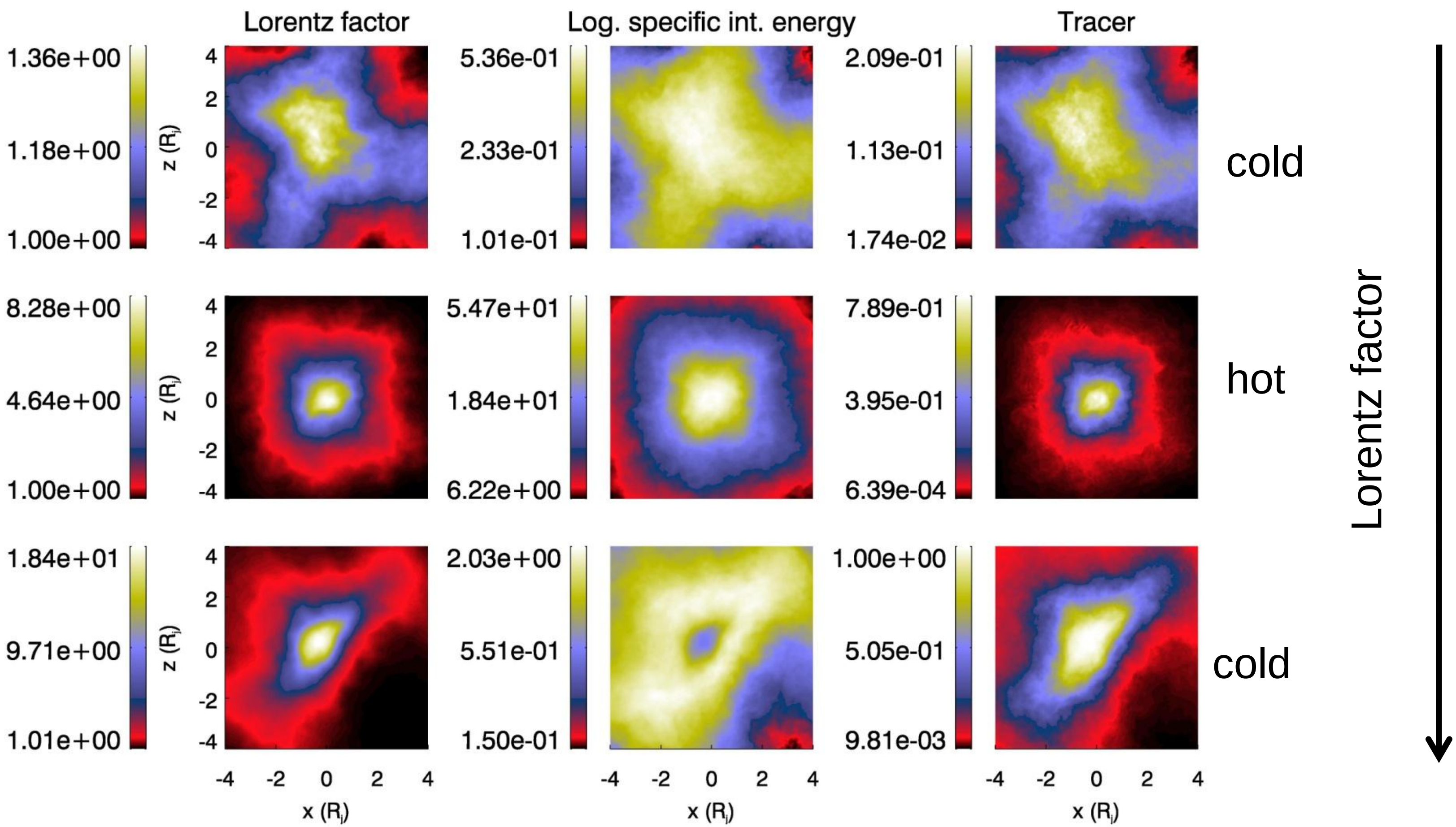

3D RHD simlations of jet stability using RATPENAT.

- $512^3 = 1.342\ 10^8$ cells
- 128 processors
- 21-28 days

Perucho et al. 2010

The parsec scales and beyond: KH instability

Axial momentum in the jet material versus time

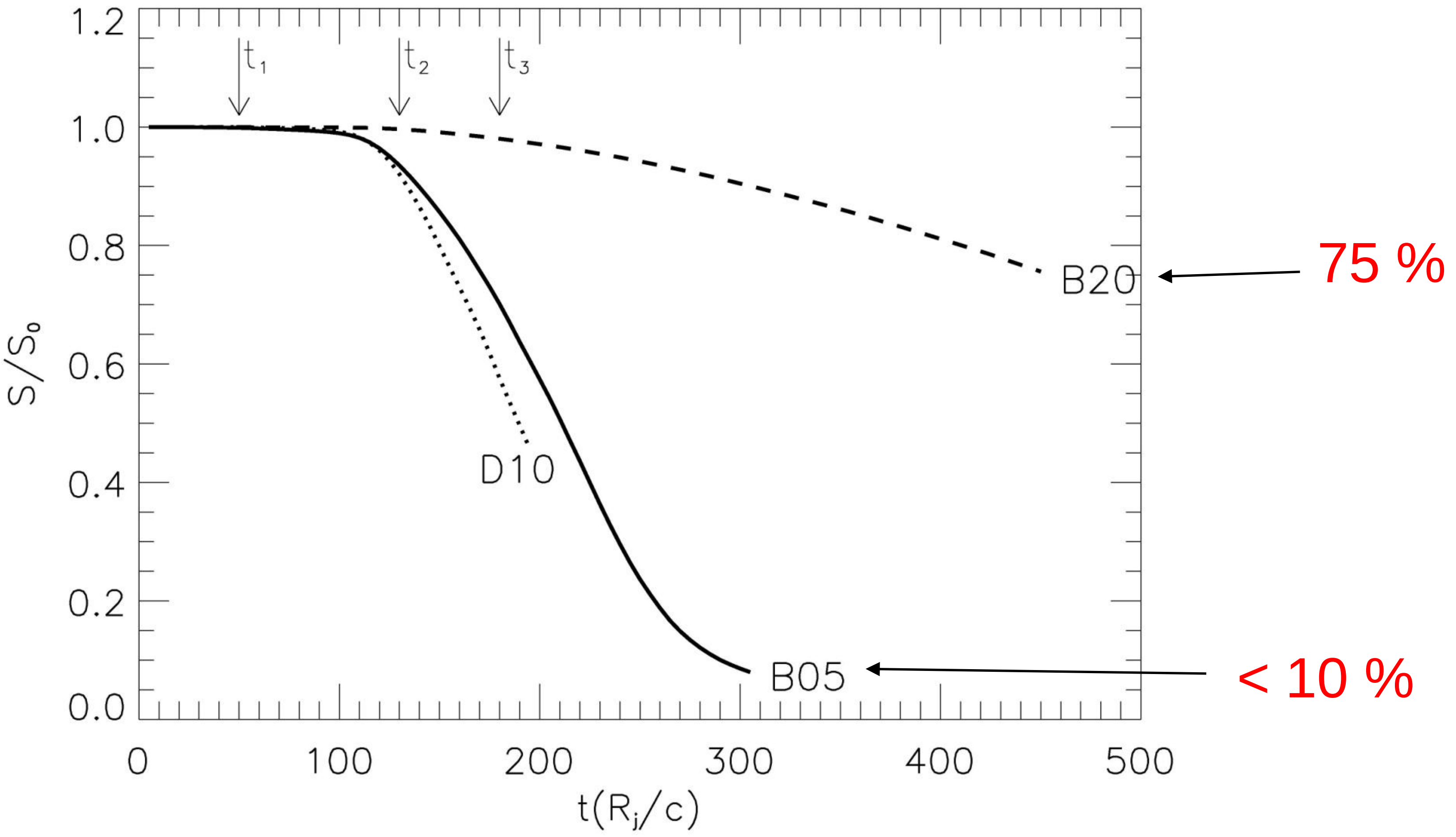

3D RHD simlations of jet stability using RATPENAT.

- $512^3 = 1.342\ 10^8$ cells
- 128 processors
- 21-28 days

Perucho et al. 2010

The parsec scales and beyond: KH instability

Agudo et al. 2001

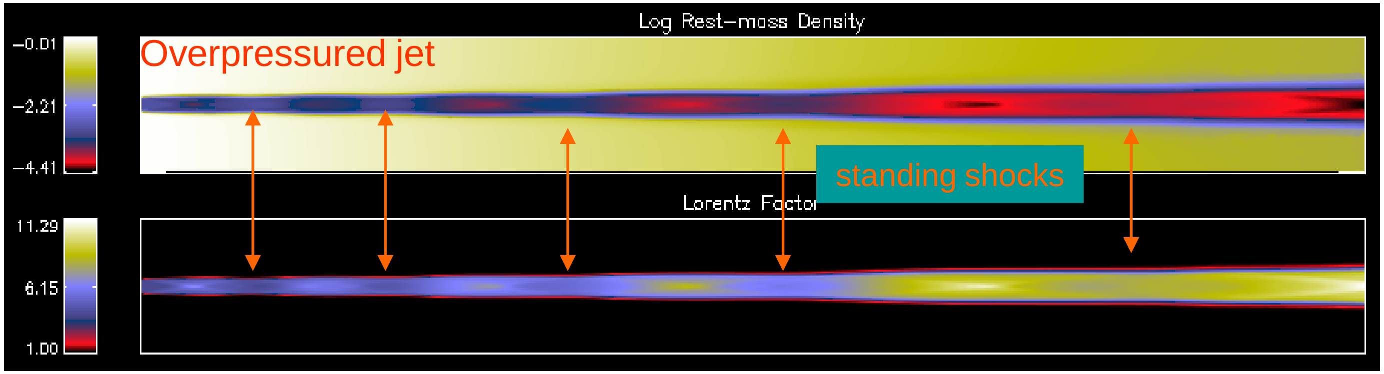

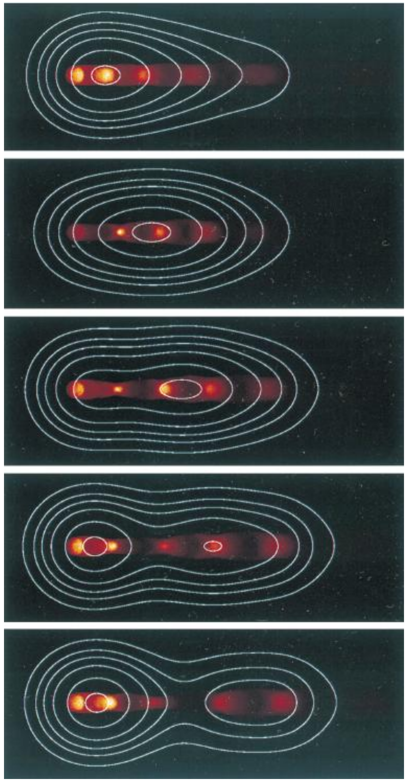

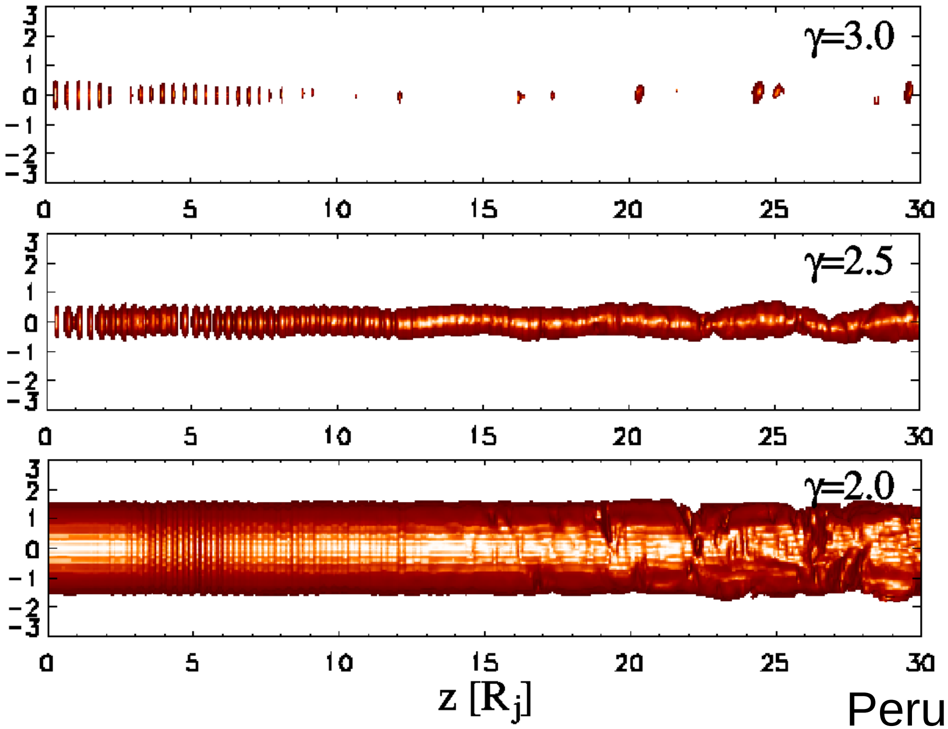

KH pinching instabilities triggered by an injected perturbation.

Different structures may appear at different frequencies in jets with transversal structure.

Perucho et al. 2006

The parsec scales and beyond: KH instability

3C120 Gómez et al. 2000

3C111 Kadler et al. 2008

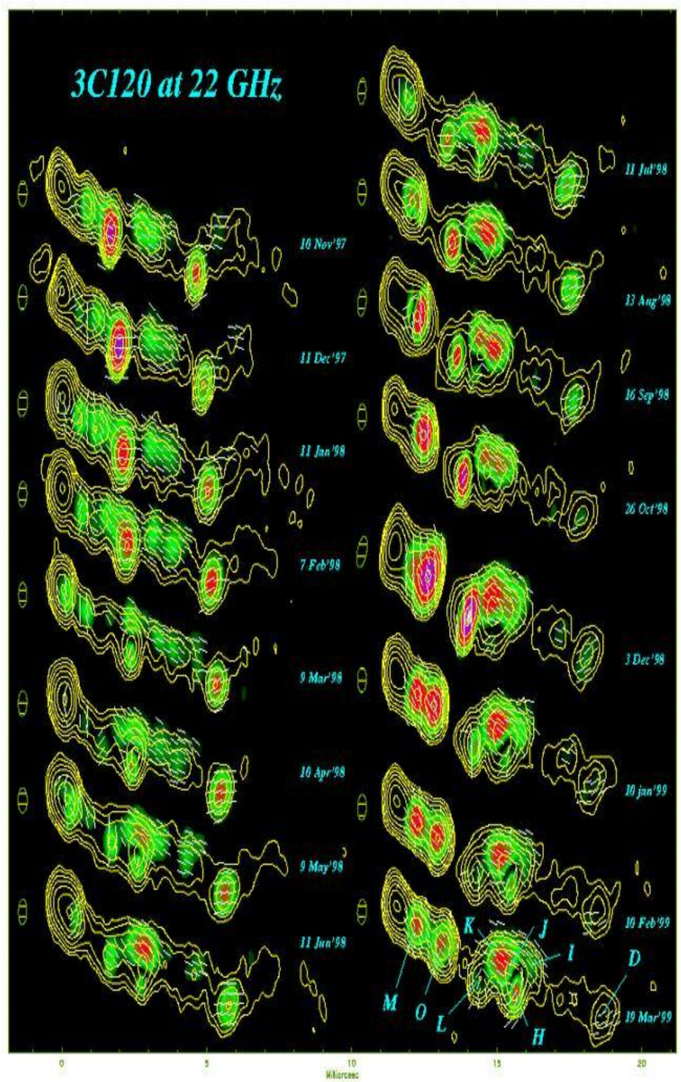

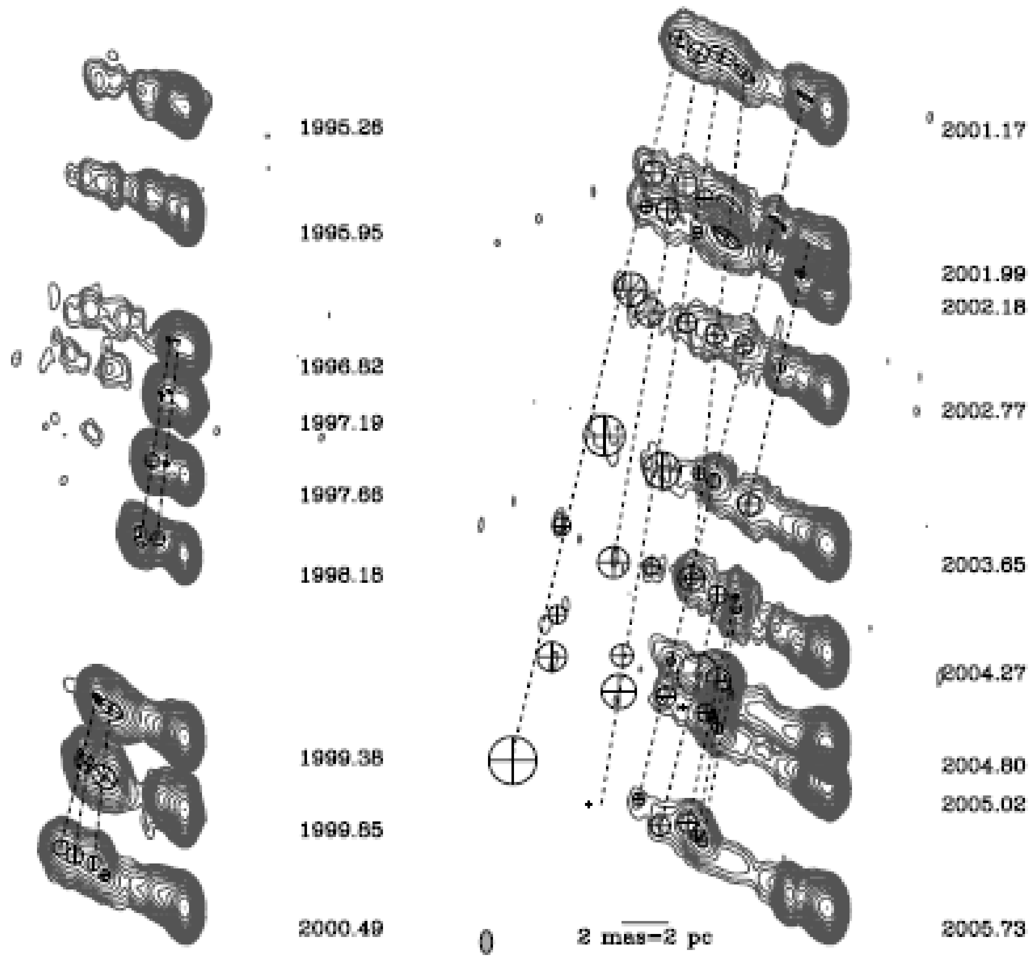

The parsec scales and beyond: KH instability

Agudo et al. 2001

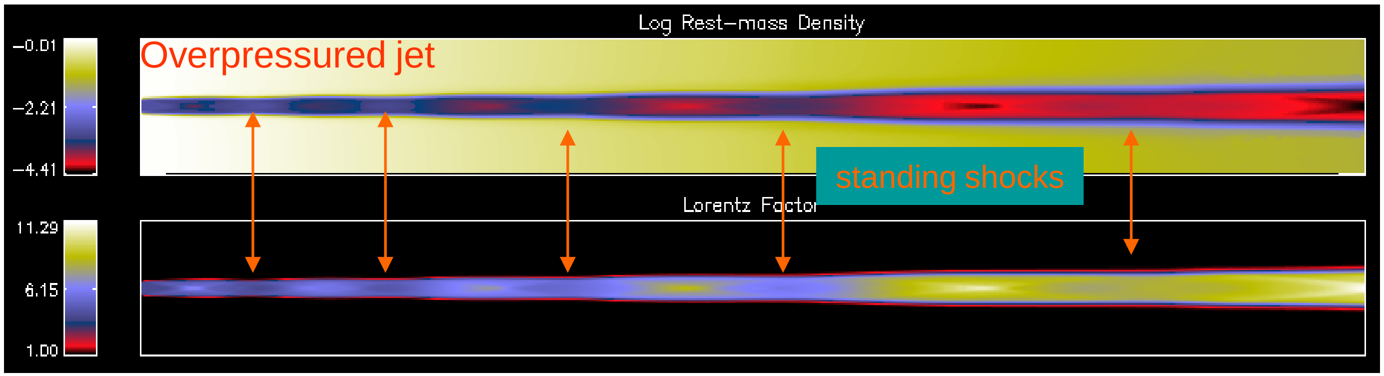

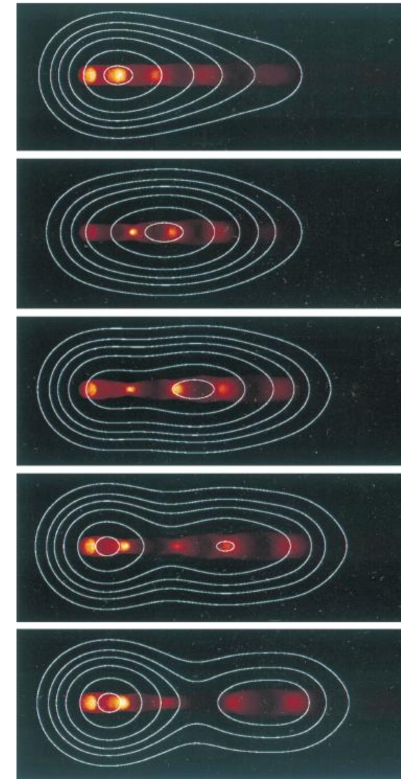

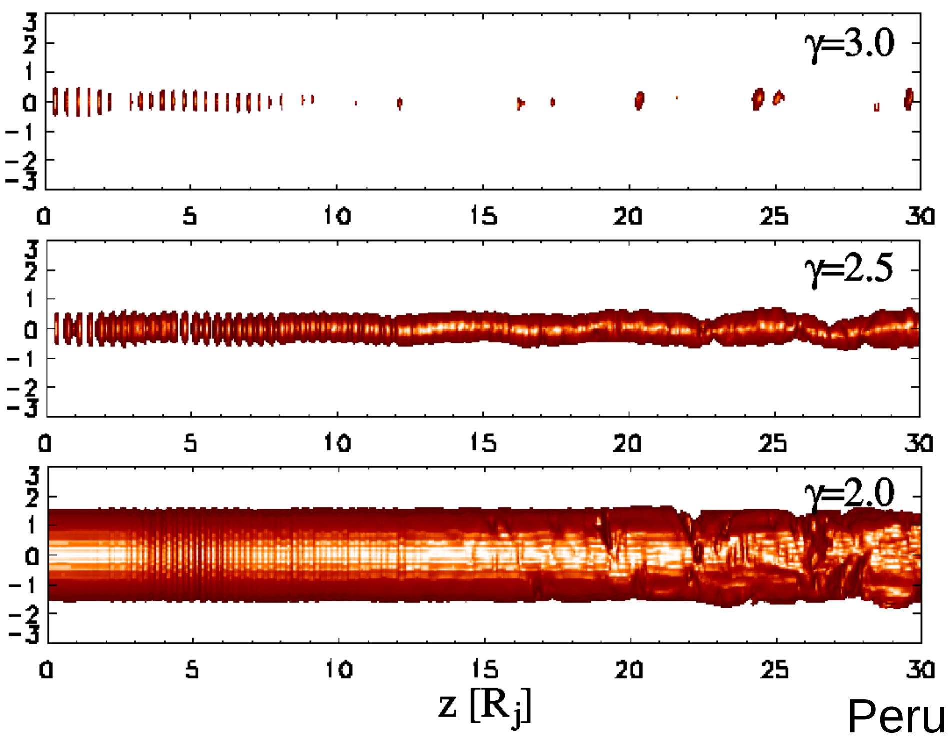

KH pinching instabilities triggered by an injected perturbation.

Different structures may appear at different frequencies in jets with transversal structure.

Perucho et al. 2006

The parsec scales and beyond: KH instability

3C 120: Goméz et al. (2001)

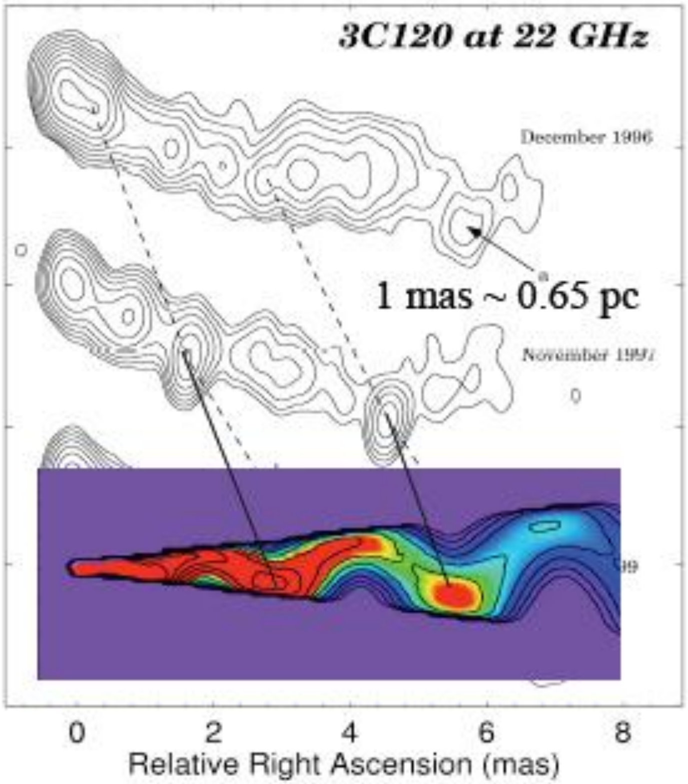

3C 120 Model: (Hardee et al. 2005)

0836+710: Perucho et al. 2008, Perucho et al., in prep.

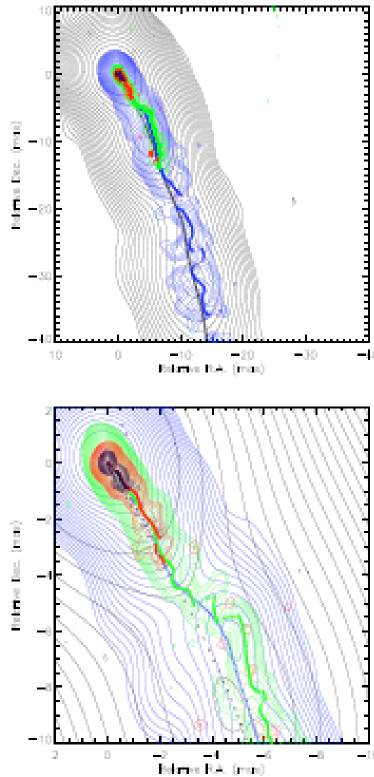

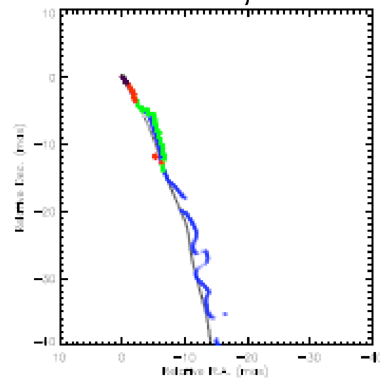

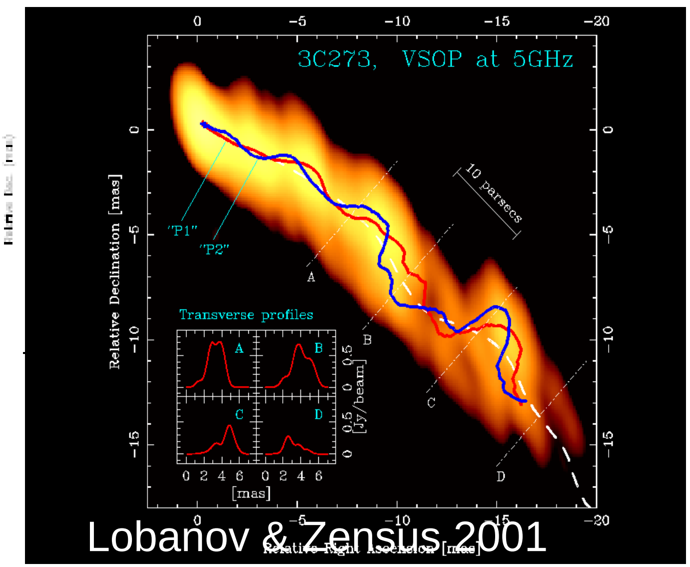

Lobanov & Zensus 2001

M87: Lobanov et al. (2003)

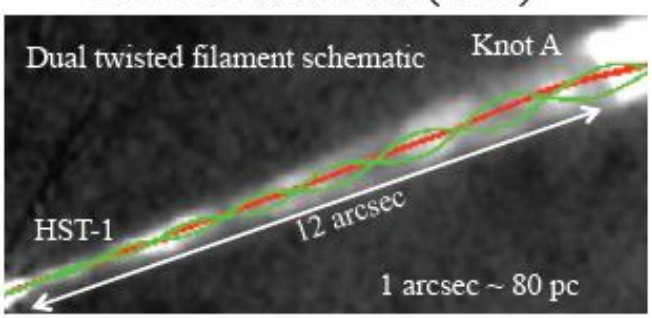

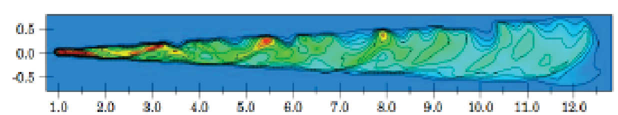

M87 Model: (Hardee & Eilek 2010)

Non-linear effects

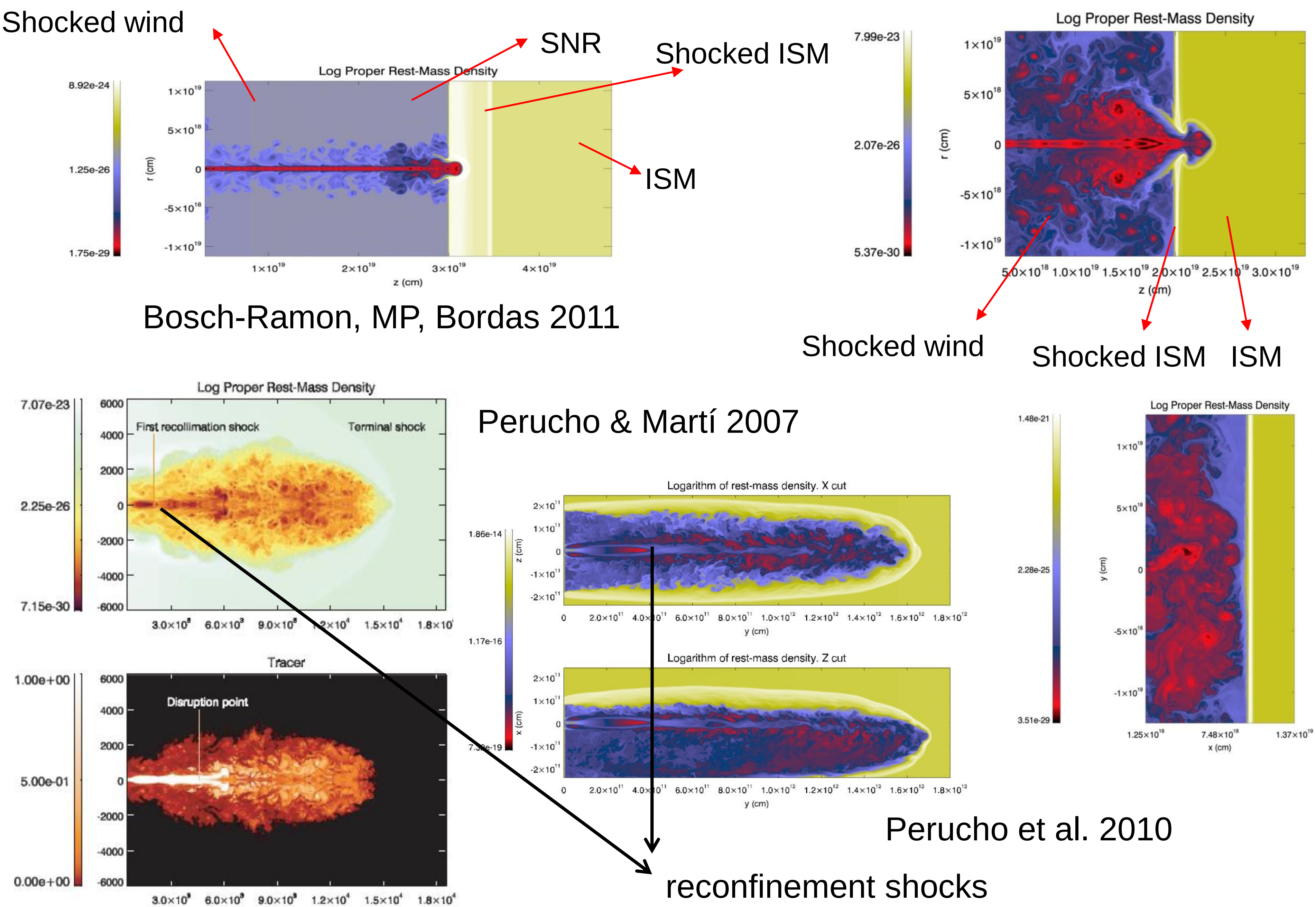

Bosch-Ramon, MP, Bordas 2011

Perucho & Martí 2007

Perucho et al. 2010

Non-linear effects

Wind-jet interaction in massive X-ray binaries

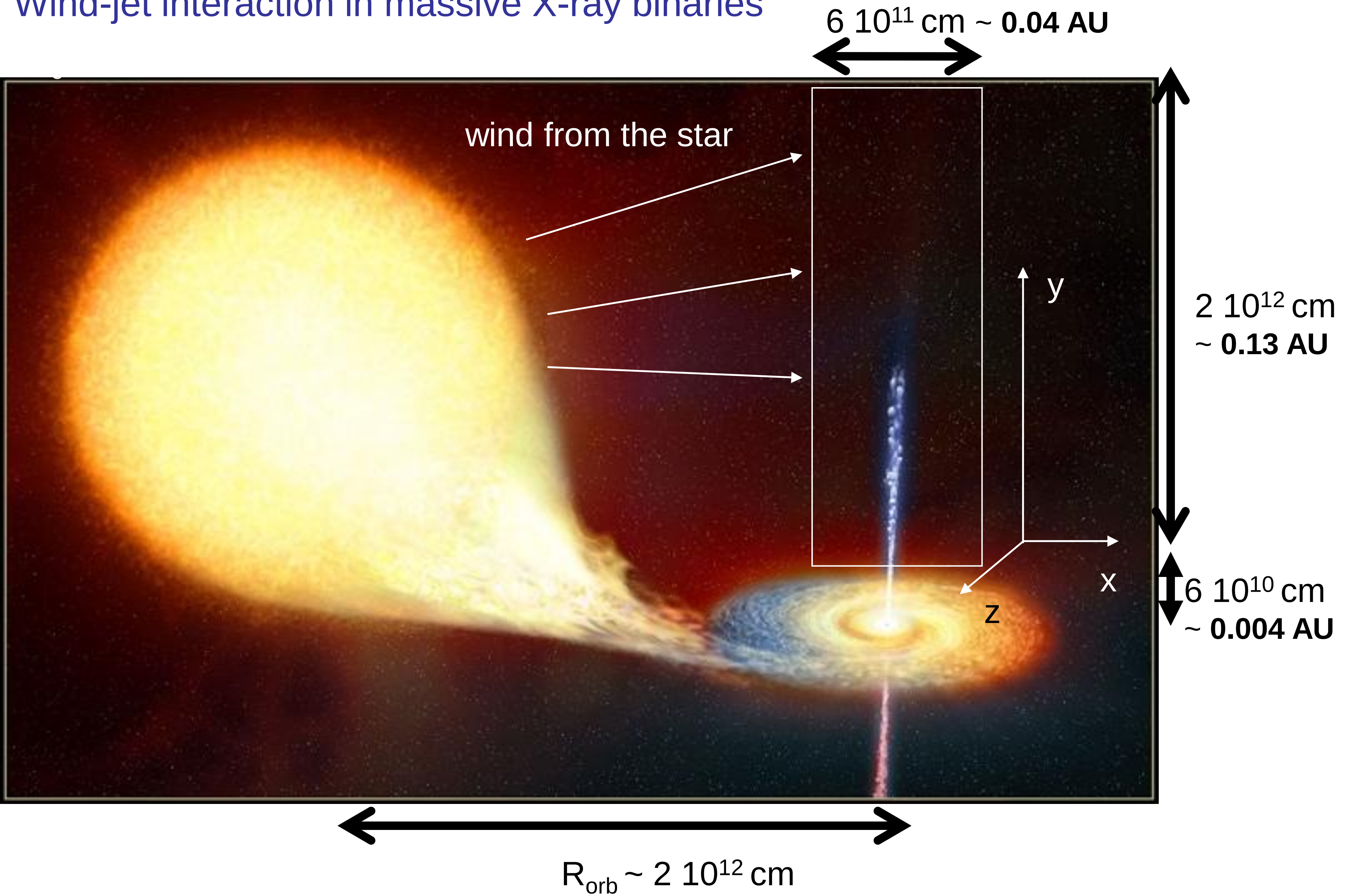

Non-linear effects

Wind-jet interaction in massive X-ray binaries: 3D simulations

Perucho, Bosch-Ramon & Khangulyan 2010

t = 977 s

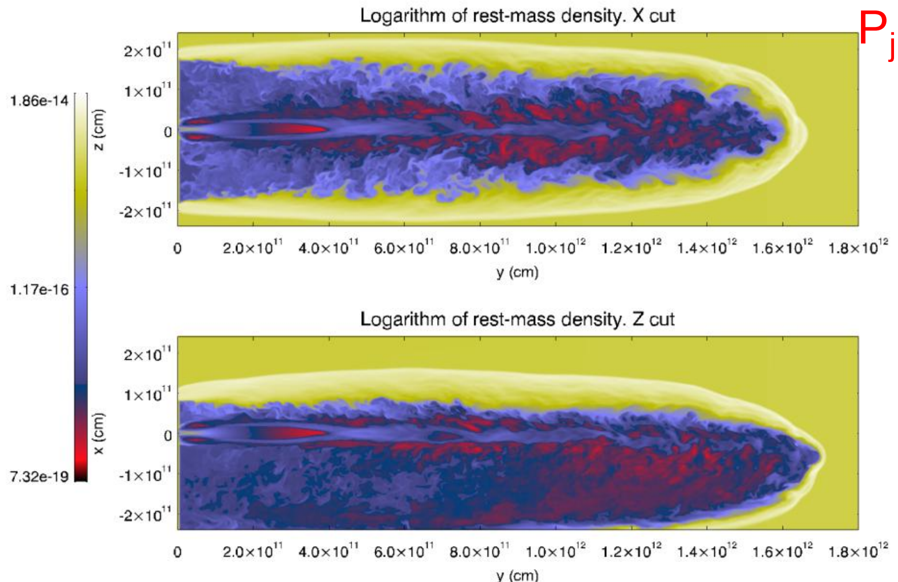

$P_j = 3\ 10^{36}$erg/s

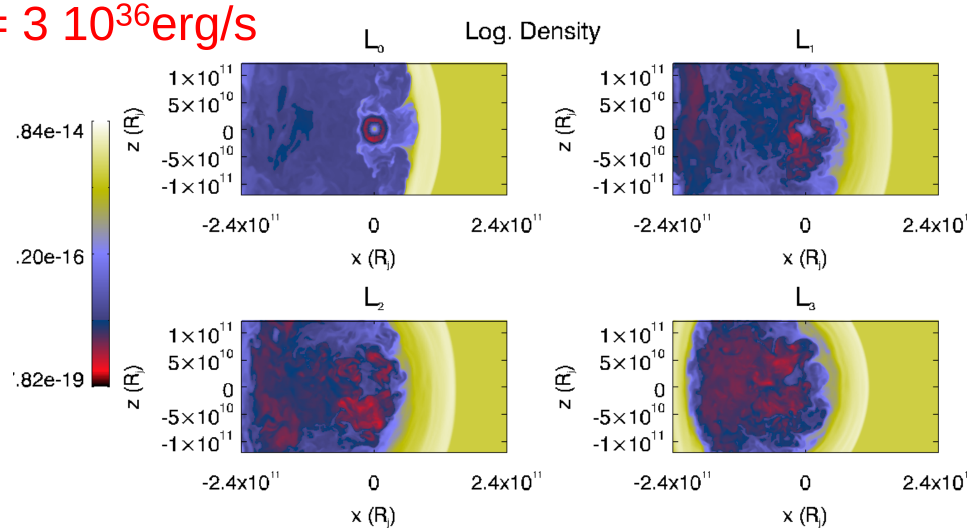

t = 192 s

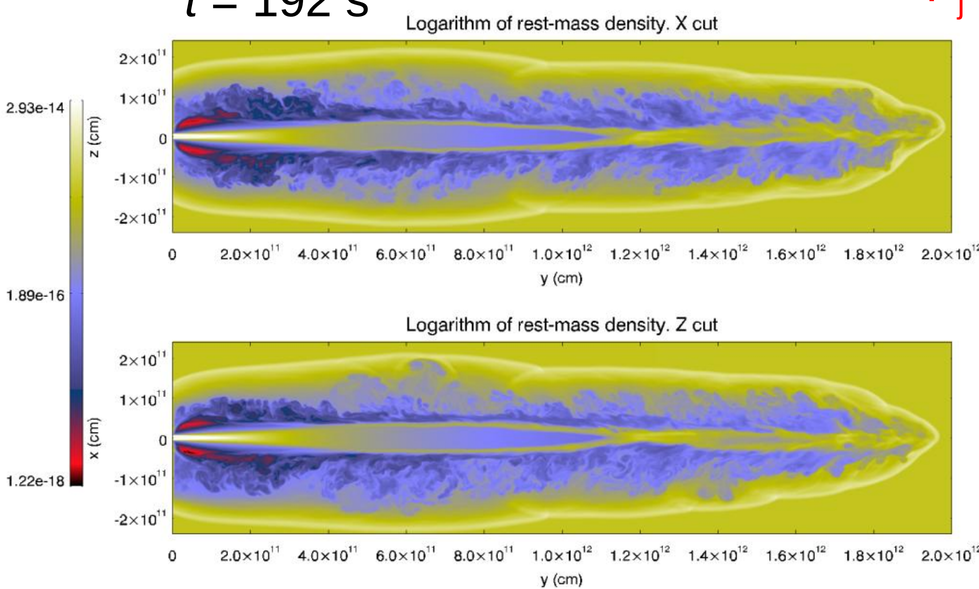

$P_j = 10^{37}$erg/s

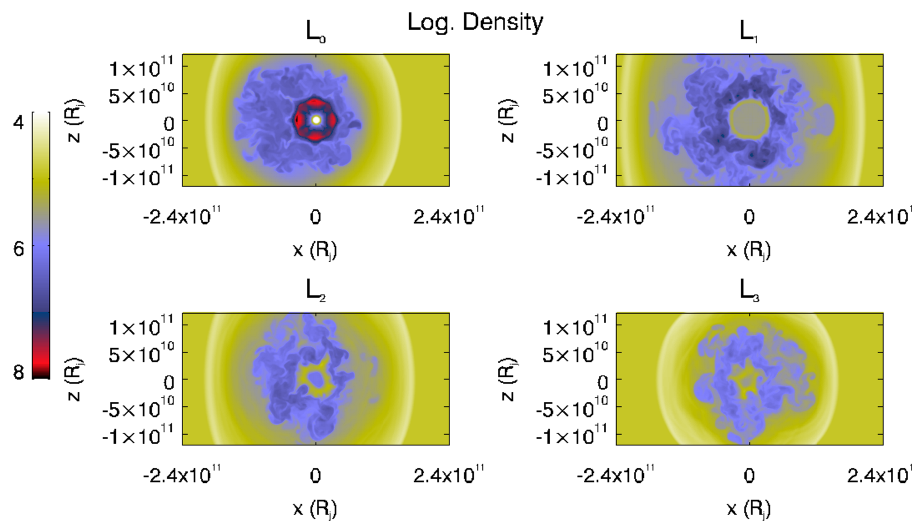

Non-linear effects

Wind-jet interaction in massive X-ray binaries: 3D simulations

Perucho & Bosch-Ramon, in preparation

Inhomogeneous wind. $P_j = 3\ 10^{36}$ erg/s

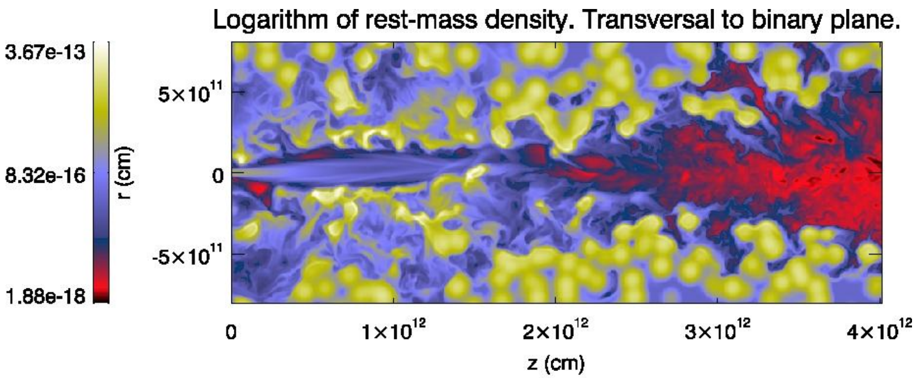

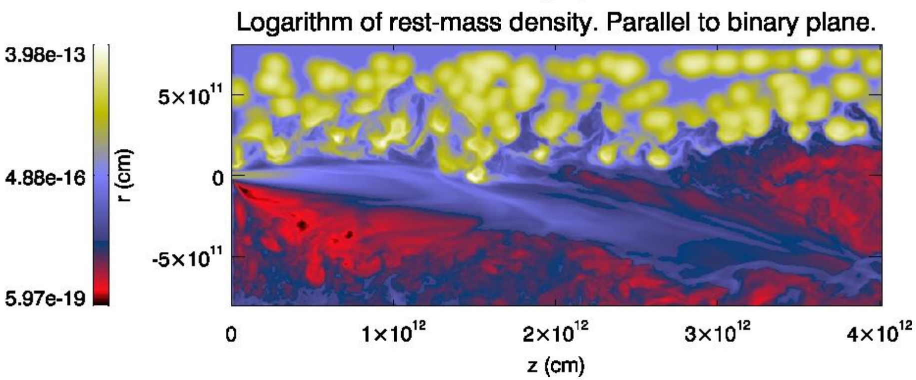

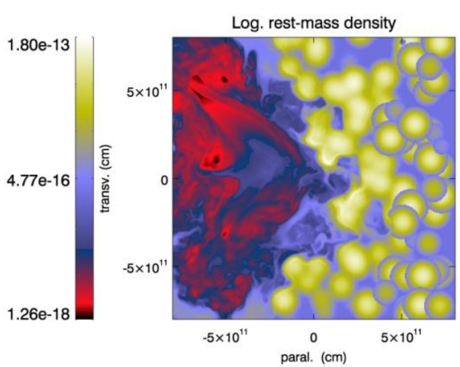

Inhomogeneous wind. $P_j = 10^{37}$ erg/s

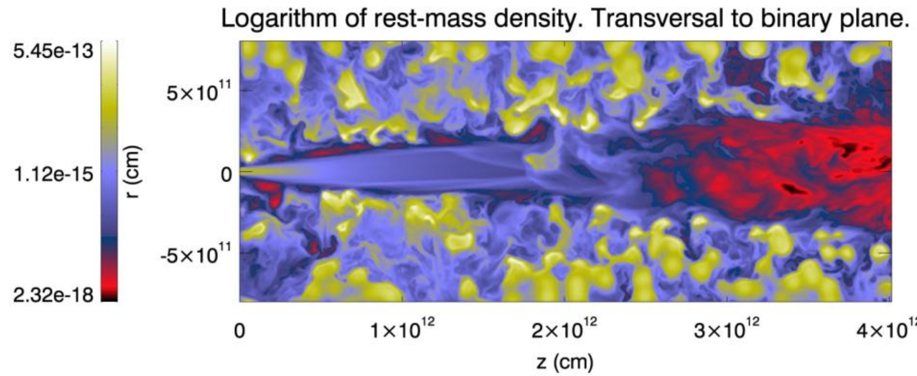

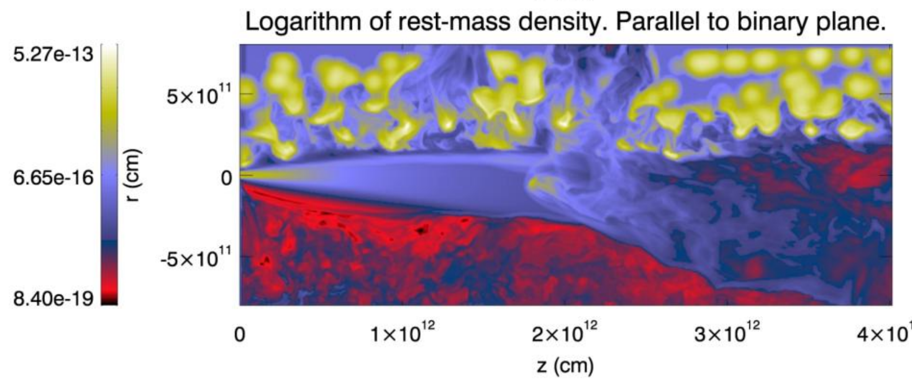

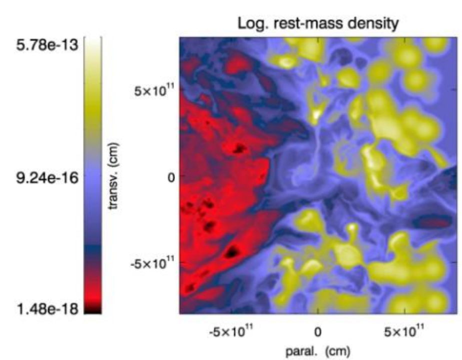

The largest scales: Energy deposition in the ambient

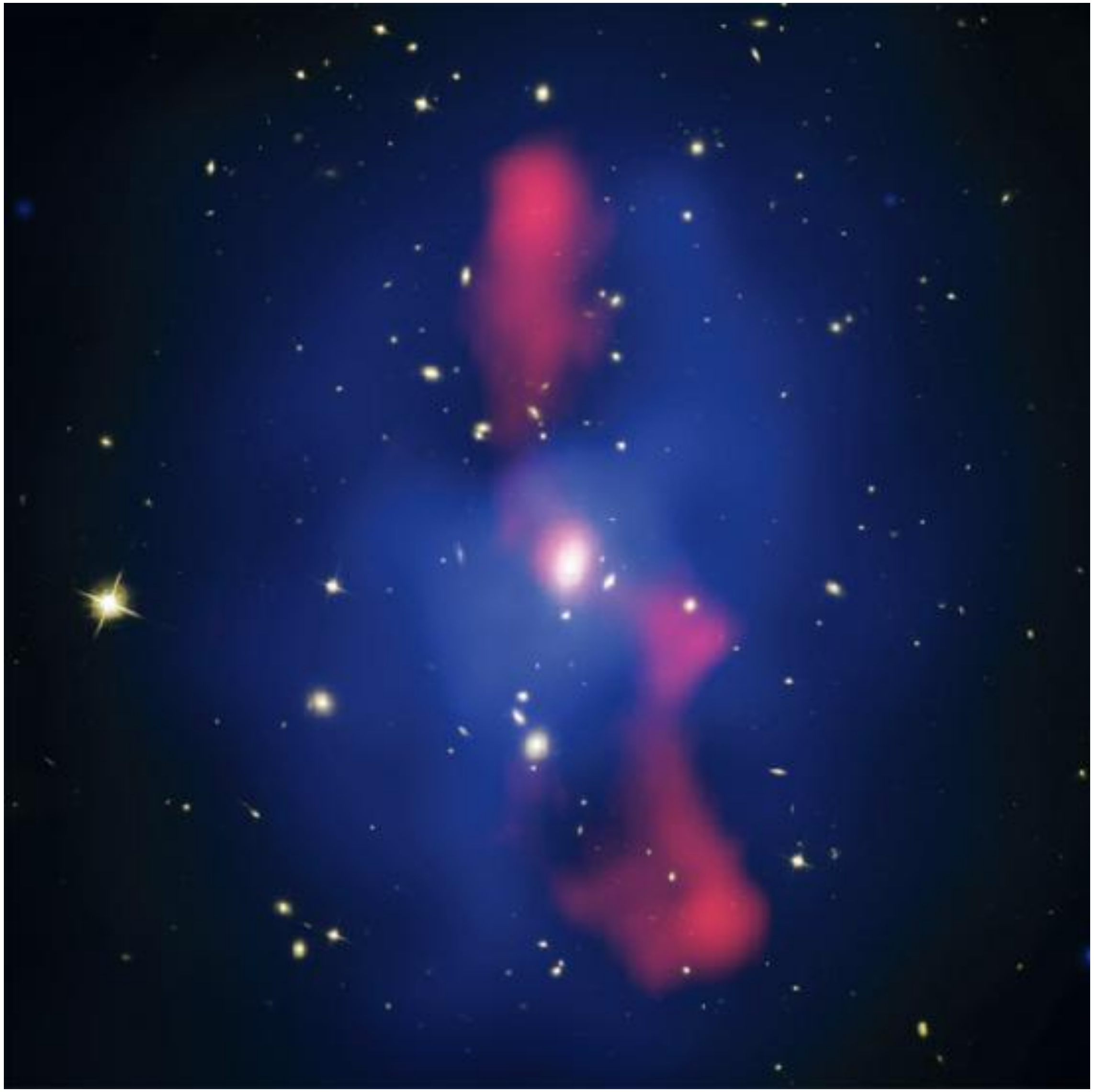

- MS0735+7421 (McNamara et al. 2005).
- 200 kpc diameter cavities.

- Shock-wave (M=1.4).

- $pV=10^{61}$ erg.
- $T=10^{8}$ yr.
- $P_s=1.7\ 10^{46}$ erg/s (from pV).

The largest scales: Energy deposition in the ambient

- **2D axisymmetric hydro simulations** with **RATPENAT** using up to 140 processors (added as the jet grows) during months... ≈10^6 computational hours for the whole project.

  - Jets **injected at 1 kpc** into a **King-profile for density** (Hardcastle et al. 2002, Perucho & Martí 2007) in hydrostatic.
    - Corresponding Dark Matter distribution of 10^{14} $M_\odot$ within 1 Mpc.

  - **Powers**: 10^{44} erg/s (**J3** - leptonic) – 10^{45} erg/s (**J1** –leptonic, **J4** - baryonic) – 10^{46} erg/s (**J2** - leptonic).
    - Jet radius: 100 pc. Jet velocity: 0.9 – 0.99 c

  - Injected during **16 to 50 Myr**. The simulations reproduce the jet evolution up to 200 Myr.

  - Resolution: 50x50 pc or 100x100 pc per cell in the central region (Total 16000x2000 cells, **800 /900 kpc x 500 kpc**).

The largest scales:
Energy deposition in the ambient

200 Myr

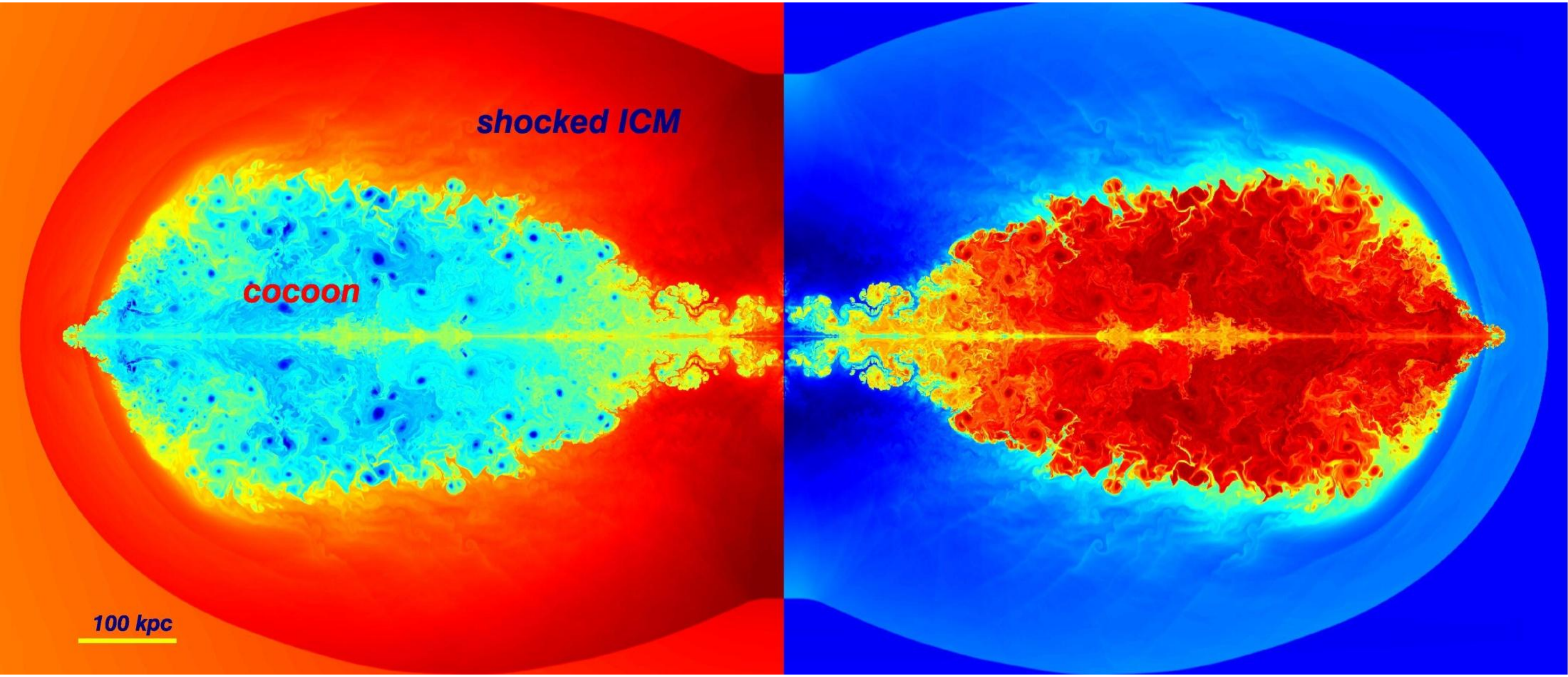

Perucho et al. 2011, submitted

10^{46} erg/s

X-ray morphology

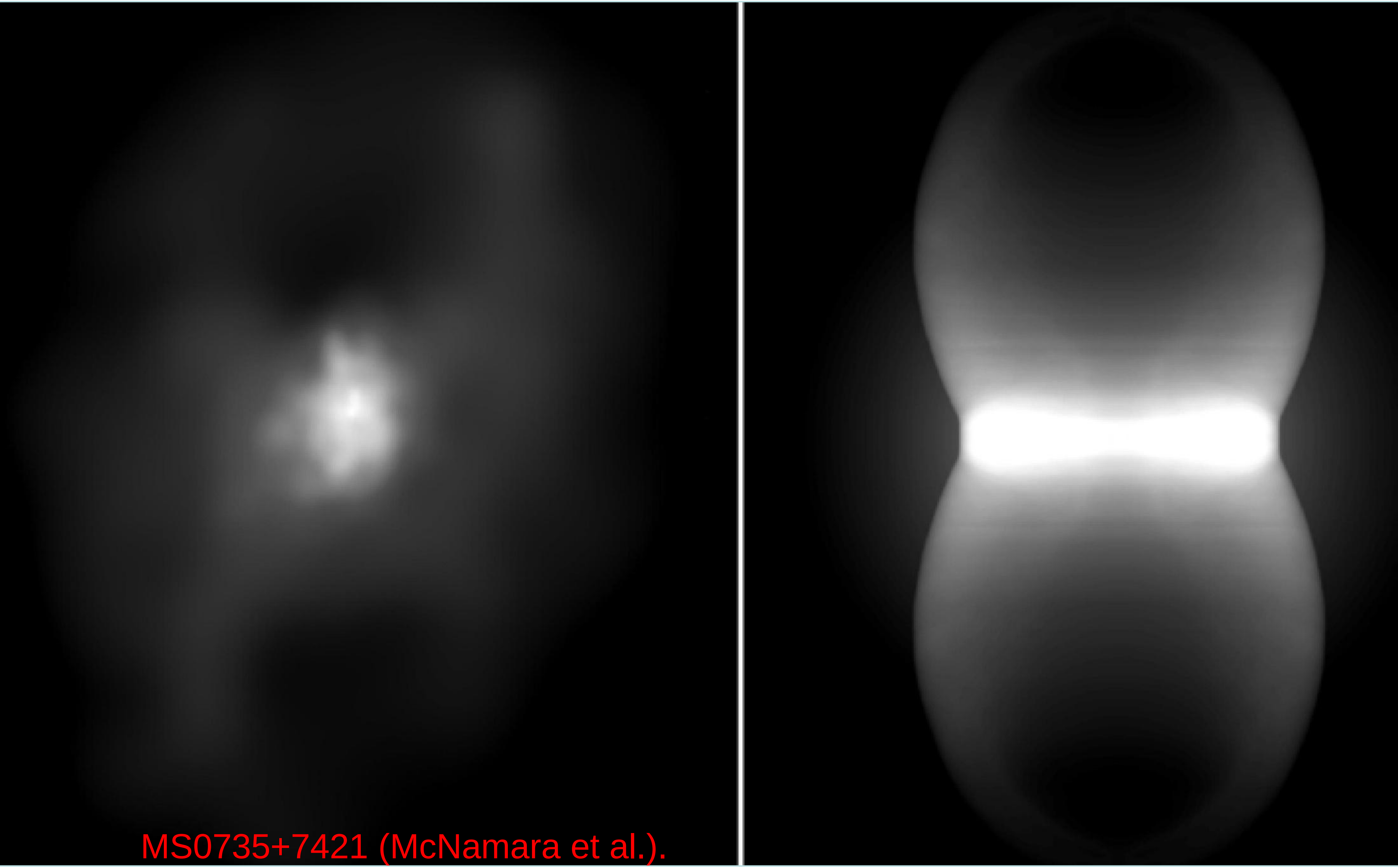

The largest scales:
Energy deposition in the ambient

Perucho et al. 2011, submitted

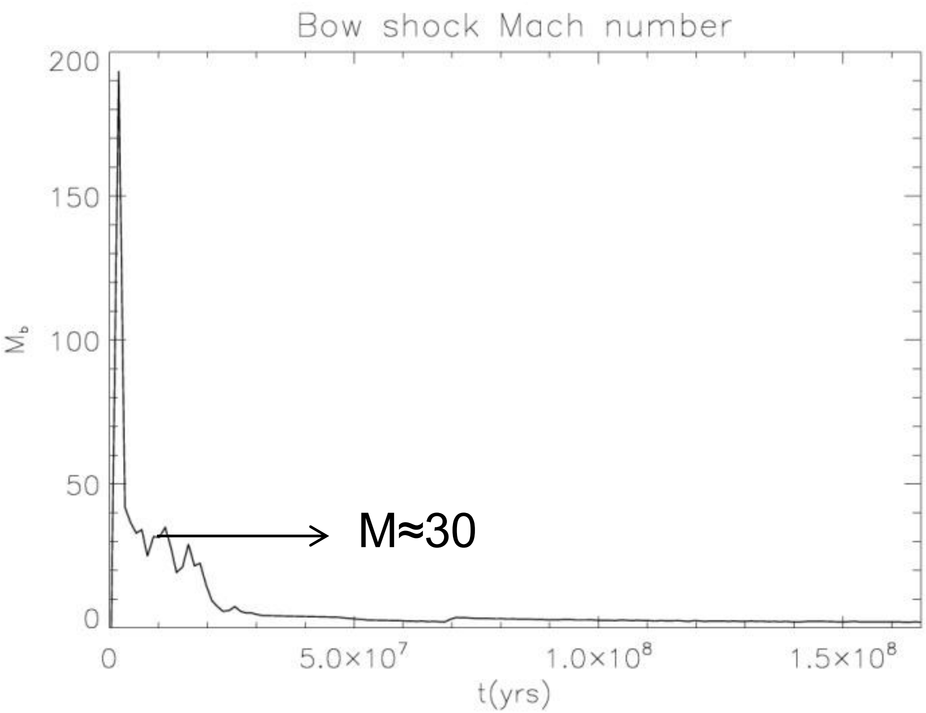

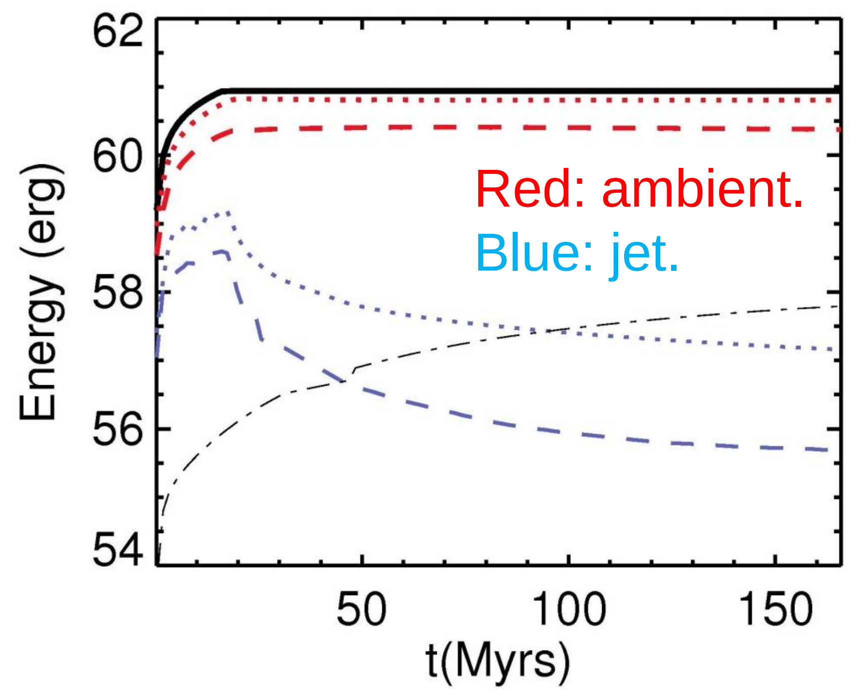

$>10^{11}\ M_{\odot}$ of shocked ambient gas.

$$V_j^R = \frac{\sqrt{\eta_R^*}}{1+\sqrt{\eta_R^*}}\, v_b\,,$$

Our parameters (consistent) → V_{bs} = 0.044 – 0.1 c, M_{bs} = 10 – 30

$$\eta_R^* = \eta_R W_b^2 \qquad \eta_R = \frac{\rho_b h_b}{\rho_m h_m}\,.$$

Martí et al. (1997)

$$V_j^N = \frac{\sqrt{\eta}}{1+\sqrt{\eta}}\, v_b$$

Usual parameters in newtonian simulations → V_{bs} = 0.009 – 0.015 c, M_{bs} = 3 – 5

$$\eta \equiv \rho_b/\rho_m$$

The largest scales:
Energy deposition in the ambient

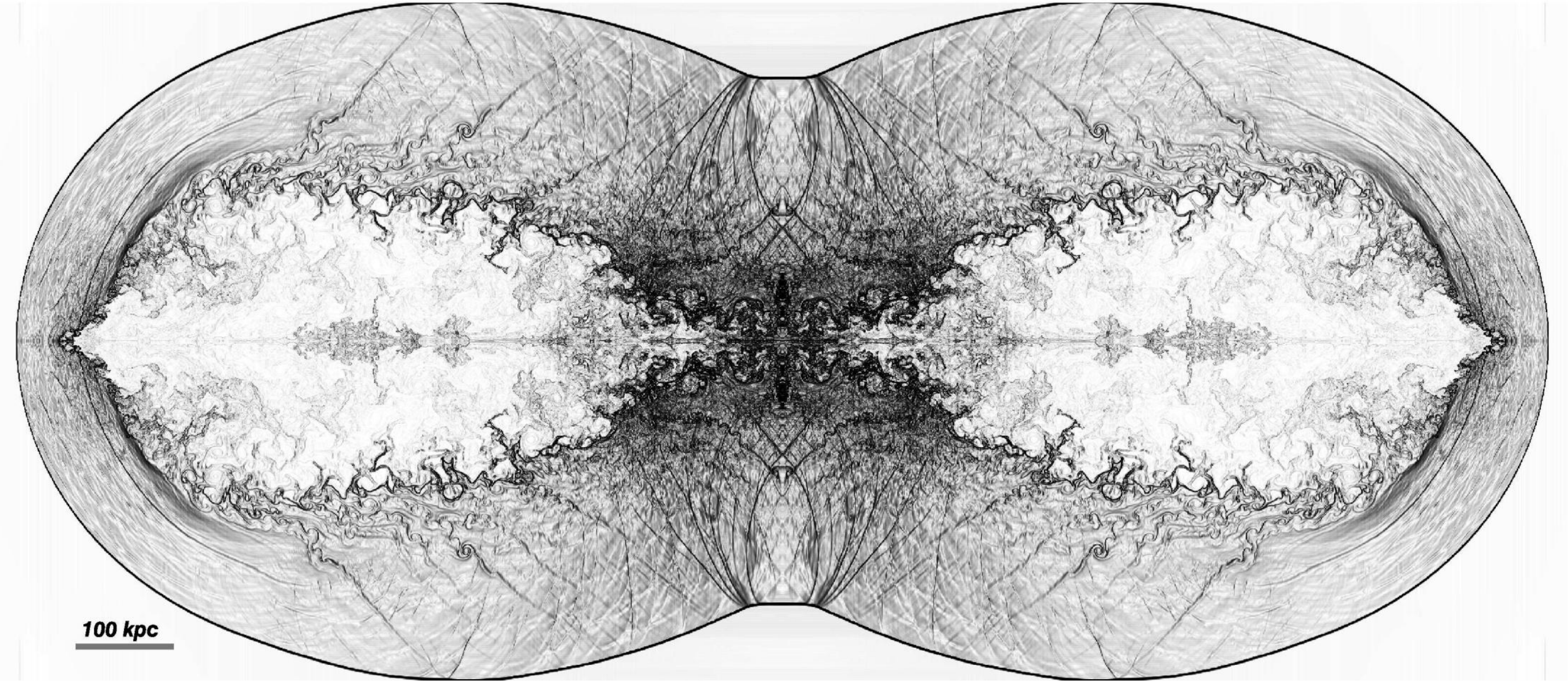

10^{46} erg/s

Schlieren plot: enhanced density gradients.

The largest scales:
Energy deposition in the ambient

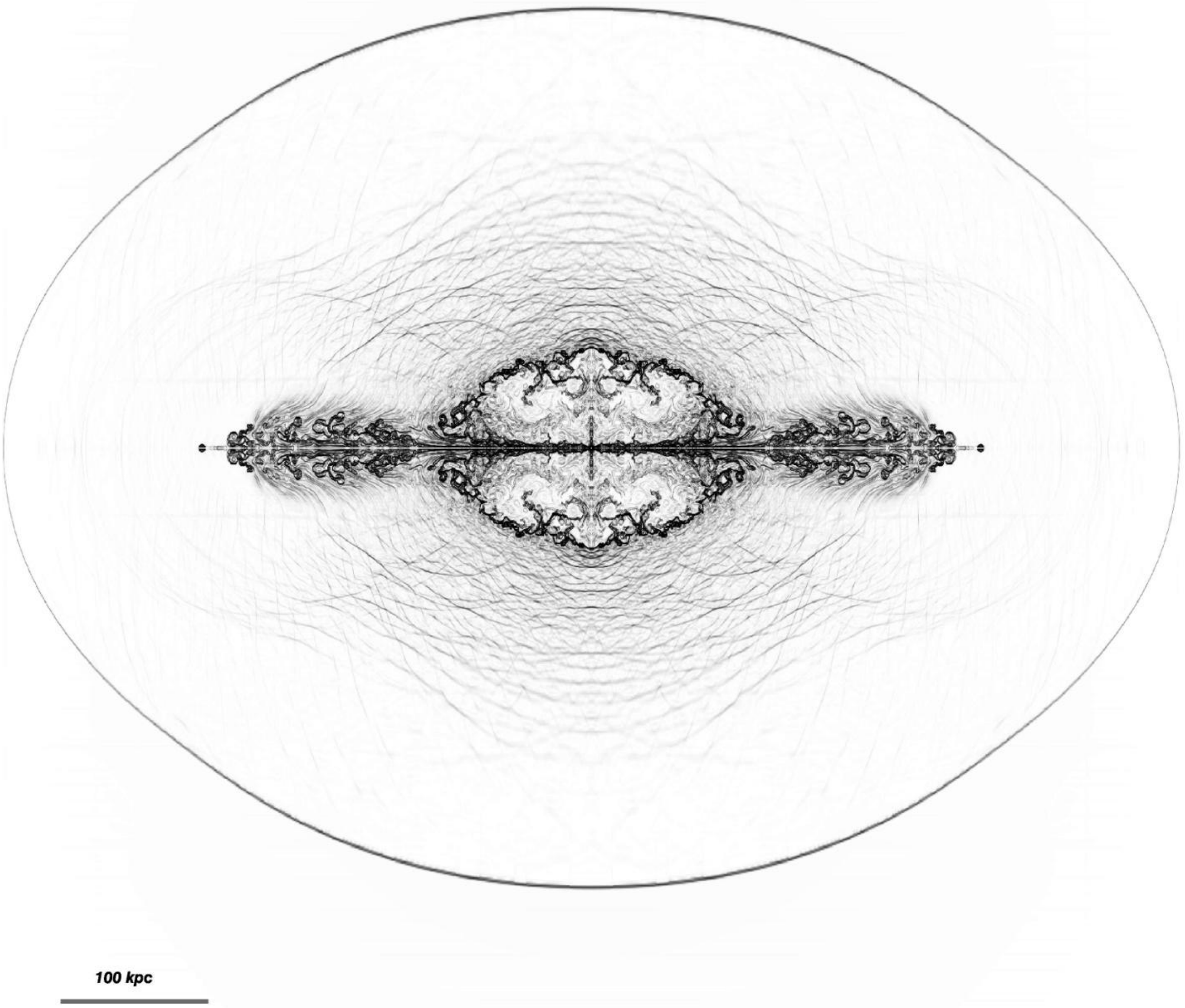

10^{44} erg/s

The largest scales: Energy deposition in the ambient

$v_c \propto t^{\alpha},\ \rho_a \propto r^{\beta}$

$R_c \propto t^{\frac{2-\alpha}{4+\beta}},\ P_c \propto t^{\frac{2(\alpha-2)-\alpha(4+\beta)}{4+\beta}}$

Active phase

$R_c \propto t^{\frac{1-\alpha}{4+\beta}},\ P_c \propto t^{\frac{2(\alpha-1)-(1+\alpha)(4+\beta)}{4+\beta}}$

Sedov phase

		1D phase				**2D phase**				**Sedov phase**			
		α	β	P_c	R_c	α	β	P_c	R_c	α	β	P_c	R_c
J1	Sim	0.07	-1.55	-1.58	0.75	-0.23	-0.52	-1.09	0.66	-0.74	-1.02	-1.70	0.90
	Model			-1.65	0.79			-1.05	0.64			-1.43	0.58
J2	Sim	0.27	-1.55	-1.67	0.67	-0.57	-0.52	-0.95	0.81	-0.83	-1.02	-1.67	0.72
	Model			-1.68	0.71			-0.91	0.74			-1.40	0.61
J3	Sim	0.13	-1.55	-1.55	0.67	-0.35	-0.52	-1.08	0.74	-0.60	-1.02	-2.16	1.00
	Model			-1.66	0.76			-1.00	0.68			-1.47	0.54